Title

Transcriptional manipulation of post-stroke axonal sprouting: A study of developmental transcription factors Ctip2 and Hhex

Author

Schweppe, Catherine

Publication Date

2020

Peer reviewed|Thesis/dissertation

UNIVERSITY OF CALIFORNIA

Los Angeles

Transcriptional manipulation of post-stroke axonal sprouting:

A study of developmental transcription factors Ctip2 and Hhex

A dissertation submitted in partial satisfaction of the requirements for the degree

Doctor of Philosophy in Neuroscience

by

Catherine Ann Schweppe

2020

ABSTRACT OF THE DISSERTATION

Transcriptional manipulation of post-stroke axonal sprouting:

A study of developmental transcription factors Ctip2 and Hhex

by

Catherine Ann Schweppe

Doctor of Philosophy in Neuroscience

University of California, Los Angeles, 2020

Professor S. Thomas Carmichael, Chair

The ability of the nervous system to repair itself following injury is a remarkable phenomenon, but central nervous system endogenous repair mechanisms are incomplete. Cortical ischemic stroke produces a limited process of neural repair, characterized by axonal sprouting and reorganization in the surviving tissue adjacent to the infarct. Changes in gene expression patterns have been observed in this peri-infarct region, in populations of neurons that specifically sprout new axons following stroke, and in neurons that have received delivery of growth factors following stroke, providing transcriptomic profiles of neuronal growth states post-stroke. Within these transcriptomic

data sets are a number of differentially regulated transcription factors that have been implicated in brain development.

Developmental transcription factors present an intriguing target for study due to their inherent ability to act as master regulators of genes responsible for neuronal growth. This thesis investigates a selection of these differentially regulated transcription factors for their ability to regulate axonal sprouting and functional recovery following stroke. Genes were screened for their ability to promote axonal growth in primary cortical neurons. From these studies, Hhex and Ctip2 emerged as candidates for further exploration. Overexpression of these genes following stroke revealed an ability of both Hhex and Ctip2 to promote long-distance axonal sprouting, but only Hhex to promote axonal sprouting in the peri-infarct region. Overexpression of Hhex or Ctip2 showed an ability to promote recovery of gait function following stroke to the forelimb motor cortex, but only overexpression of Hhex was associated with recovery of forelimb reach movements and fine motor manipulation.

Transcriptional profiling of neurons that have Ctip2 or Hhex overexpressed following stroke revealed that these transcription factors are driving different molecular pathways to achieve axonal growth and functional recovery. Ultimately, these studies implicate a role for these transcription factors in axonal growth in the adult brain and provide further evidence for unique intrinsic growth programs in neural repair processes.

The dissertation of Catherine Ann Schweppe is approved.

Bennett Novitch

Michael Sofroniew

Ye Zhang

S. Thomas Carmichael, Committee Chair

University of California, Los Angeles

2020

Table of Contents

List of Figures

Chapter 2

Chapter 3

Chapter 4

Chapter 5

List of Tables

Acknowledgements

No scientific progress can occur in isolation, and all of my accomplishments are truly a testament to the mentorship, collaboration, and support I have been fortunate to receive over the years. First and foremost, I would like to thank my advisor, Tom Carmichael, for providing a rich scientific environment in which I have had the opportunity to learn and grow. Under his mentorship, I have had the space to drive this project with a consistent cheerleader who believed in my abilities even when I myself had doubts.

I have been fortunate to share my years in the Carmichael lab with a number of incredible graduate students, postdoctoral fellows, staff scientists, and technicians who have been invaluable scientific collaborators as well as dear friends. Senior graduate students Esther, Andrew, and David helped guide me through my early years, and I have shared in the joys and frustrations of the graduate school journey with fellow students Sam, Natalie, Kiro, Thanh, Tiffani, Nora, and Jose. Postdocs in the lab have been both scientific and life mentors, particularly Irene, Amy, Teena, Qing, Alec, Luca, and Liang (just to name a few). The family I have found through my scientific journey is one that I will cherish throughout my life.

One of the great joys of my time as a graduate student has been the opportunity to work with a team of talented undergraduate students from UCLA and beyond. Isha, Andrew, Alejandra, Elle, and Joee have all played critical roles in this research process, and these experiments would not have happened without them.

Thank you to my committee members: Ben Novitch, Ye Zhang, and Michael Sofroniew. You all have provided welcome feedback throughout this project that has ultimately focused and guided this work to make it far stronger than it otherwise would have been. To my collaborators, Riki Kawaguchi and Yue Qin: thank you for your contribution to the bioinformatics analyses, the results of which have truly tied these studies together. Thank you to the UCLA core facilities, particularly

the UCLA Broad Stem Cell Research Center Flow Cytometry Core, the UCLA Neuroscience Genomics Core, and the UCLA Division of Laboratory Animal Medicine.

The community of fellow graduate students that I have found at UCLA has been the greatest gift one could ask for. The Neuroscience Interdepartmental PhD Program as well as the broader Graduate Programs in Biosciences at UCLA have fostered an environment of support and comradery that has far surpassed anything I could have hoped for. I am so grateful for the numerous friends I have made throughout this graduate school journey, they have made these years some of the greatest of my life.

None of this would have been possible without the love of my family. Thank you to my partner, Craig, for being right there with me in the highs and lows of the final years of graduate school. Your unwavering support has been such a lifeline. To Sarah and Thomas, who I am so grateful to call not only siblings but friends—thanks for keeping me humble and never failing to make me laugh. I'm so glad I've been able to share the city of Los Angeles with you both. Finally, thank you to my parents, who have always championed my intellectual curiosity and been a willing ear and source of support. I never would have believed that completing a PhD was something I could accomplish had you not believed in me first.

VITA

EDUCATION

University of California, Los Angeles (UCLA) **Los Angeles, CA**
Ph.D. in Neuroscience Expected 2020

University of Washington **Seattle, WA**
B.S. in Biology & Psychology 2012

RESEARCH

UCLA Department of Neurology **2014 – 2020**
Graduate Researcher, Principal Investigator Dr. S. Thomas Carmichael

National Institute on Drug Abuse, National Institutes of Health **2012 – 2014**
Postbaccalaureate Fellow, Principal Investigator Dr. Amy Newman

University of Washington, Division of Cardiology **2011 – 2012**
Research Assistant

Max Delbrück Center for Molecular Medicine **2011**
German Academic Exchange Services Research Fellow, Principal Investigator Dr. Michael Bader

University of Washington Memory Wellness Program **2010 – 2011**
Undergraduate Research Assistant, Principal Investigator Dr. Suzanne Craft

Pacific Northwest National Laboratory **2010**
DOE Science Undergraduate Laboratory Internship, Principal Investigator Dr. Aaron Wright

PUBLICATIONS

1. **Schweppe, C. A.**, Burzynski, C., Jayanthi, S., Ladenheim, B., Cadet, J. L., Gardner, E. L., Xi, Z.-X., Praag, H. van, Newman, A. H. & Keck, T. M. (2020). Neurochemical and behavioral comparisons of contingent and non-contingent methamphetamine exposure following binge or yoked long-access self-administration paradigms. *Psychopharmacology*, *237*(7), 1989–2005.
2. Carmichael, S. T., Kathirvelu, B., **Schweppe, C. A**. & Nie, E. H. (2017). Molecular, cellular and functional events in axonal sprouting after stroke. *Experimental Neurology*, *287*, 384–394.
3. Zou, M.-F., Keck, T. M., Kumar, V., Donthamsetti, P., Michino, M., Burzynski, C., **Schweppe, C.**, Bonifazi, A., Free, R. B., Sibley, D. R., Janowsky, A., Shi, L., Javitch, J. A. & Newman, A. H. (2016). Novel Analogues of (R)-5-(Methylamino)-5,6-dihydro-4 H -imidazo[4,5,1- ij

]quinolin-2(1 H)-one (Sumanirole) Provide Clues to Dopamine D 2 /D 3 Receptor Agonist Selectivity. *Journal of Medicinal Chemistry*, *59*(7), 2973–2988.

4. Boateng, C. A., **Schweppe, C. A.** & Newman, A. H. (2014). *Reference Module in Chemistry, Molecular Sciences and Chemical Engineering.*

SELECTED PRESENTATIONS

1. UCLA Brain Research Institute 30th Annual Neuroscience Poster Session. Los Angeles, CA. November 27, 2018. "Developmental transcription factors in post-stroke axonal sprouting." **Catherine A. Schweppe**, Andrew Wu, Isha Bagga, S. Thomas Carmichael.
2. Society for Neuroscience Annual Meeting. San Diego, CA. November 5, 2018. "Developmental transcription factors in post-stroke axonal sprouting." **Catherine A. Schweppe**, Andrew Wu, Isha Bagga, S. Thomas Carmichael.
3. UCLA Brain Research Institute 28th Annual Neuroscience Poster Session. Los Angeles, CA. November 29, 2016. "The role of developmental transcription factors in post-stroke axonal sprouting." **Catherine A. Schweppe**; Michal Machnicki; S. Thomas Carmichael.
4. Society for Neuroscience Annual Meeting. San Diego, CA. November 15, 2016. "The role of developmental transcription factors in post-stroke axonal sprouting." **Catherine A. Schweppe**; Michal Machnicki; S. Thomas Carmichael.
5. UCLA Brain Research Institute 27th Annual Neuroscience Poster Session. Los Angeles, CA. November 17, 2015. "Stroke transcriptome-driven analysis of axonal outgrowth mechanisms." **Catherine A. Schweppe**; Esther H. Nie; Songlin Li; S. Thomas Carmichael.
6. Society for Neuroscience Annual Meeting. Chicago, IL. October 19, 2015. "Stroke transcriptome-driven analysis of axonal outgrowth mechanisms." **Catherine A. Schweppe**; Esther H. Nie; Songlin Li; S. Thomas Carmichael.

HONORS & AWARDS

2020	Presidential Management Fellows Program Class of 2021 Finalist
2020	International Brain Research Organization Pan-European Regional Committee, The Brain Prize, and Federation of European Neuroscience Societies Stipend Award
2019	UCLA Grad Slam Semi-Finalist
2019	UCLA Graduate Programs in Biosciences AAAS Catalyzing Advocacy in Science & Engineering Fellowship
2016	UCLA Brain Research Institute/Semel Institute Neuroscience Graduate Travel Award
2012-2014	NIH Intramural Research Training Award, National Institute on Drug Abuse

Chapter 1

Introduction

1.1 Stroke: a growing clinical challenge

Stroke is a global health condition of tremendous concern. It is the second leading cause of death worldwide and a leading cause of adult disability (Benjamin et al., 2018). In the United States, stroke mortality is on the decline, falling from the third leading cause of death to the fifth leading cause of death in 2019 (Virani et al., 2020). This is a welcome progression, yet this increase in patients surviving the initial stroke event means that there is a growing population of individuals living with long-term speech, motor, or cognitive deficits due to stroke. Current chronic treatment options are limited in scope and efficacy, so there is an ever-growing need for increased understanding of how stroke impairs brain function, the brain's intrinsic capacity for repair, and how we can enhance the brain's intrinsic capacity for healing to develop therapies for those living with stroke-induced disability.

Current therapeutic options are restricted to the acute infarct window. Recombinant tissue plasminogen activator (tPA) is the only approved pharmacological therapy for stroke. This drug, which prevents cell death in stroke by promoting reperfusion of blood to the stroke penumbra, must be administered within the first 4.5 hours of stroke onset and is clinically only administered to <5% of stroke patients. Patients with acute ischemic stroke due to a large artery occlusion in the anterior circulation may also be treated with a mechanical thrombectomy, though this procedure must be administered within 24h of stroke onset. It is estimated that fewer than 10% of acute

ischemic stroke patients qualify for this treatment as presented clinically, and very few stroke centers currently have the resources to deliver this therapy (Chia et al., 2016).

A variety of factors influence how likely a patient is to recover from the neurological effects of stroke. These factors include patient age, comorbidities, stroke size and location, and clinical interventions. Common stroke-induced deficits include limb weakness, aphasia, dysphagia, and sensory loss. Following a stroke in the motor cortex specifically, movement deficits are common in the upper and/or lower limb contralateral to the injury. Deficits can include paralysis or weakness, abnormal muscle tone, abnormal posture, abnormal gait or movement synergies, and loss of coordination.

Most patients demonstrate a moderate degree of recovery from neurological symptoms within 12 hours to one week following ischemic stroke onset. The greatest amount of recovery occurs in the first 3-6 months following stroke, with some patients exhibiting further recovery within 18 months (Hankey et al., 2007). Physical and occupational therapies administered in the weeks and months following stroke can greatly improve patient outcomes, but neurological deficits such as hemiparesis and cognitive deficits persist in 40-50% of patients at six months following stroke, with up to 25% of patients requiring institutional care (Kelly-Hayes et al., 2003). As such, the development of novel therapeutics to accompany post-stroke rehabilitation is critical to ameliorate long-term disability in stroke survivors and improve quality of life.

1.2 The ischemic brain

Ischemic stroke occurs when there is an acute loss of blood flow to a region of the brain due to an embolus or local thrombosis. This loss of blood flow results in a cascade of damage directly affecting local neurons, astrocytes, endothelial and vascular cells, oligodendrocytes, oligodendrocyte precursor cells, and microglia. The mechanisms of this acute cellular damage are currently best understood in neurons. The loss of local blood supply causes neurons to lose the ability to maintain their most energetically expensive state: resting membrane potential. This results in rapid neuronal depolarization, causing neurons to release glutamate which further depolarizes neighboring neurons. This depolarization leads to a cytotoxic cascade as calcium subsequently pours in through voltage-gated calcium channels resulting in mitochondrial dysfunction, proteolysis, lipolysis, DNA degradation, and necrotic cell death. This initial neuronal death occurs in what is known as the infarct core and is largely irreversible (Carmichael, 2016).

Stroke does not only impact neurons, however. The cell types listed above are also susceptible to death from the stroke event, though this process may occur on a delayed timeline. In vitro data suggest that neurons are the cell type most susceptible to oxygen/glucose deprivation, followed by endothelial cells, astrocytes, and microglia (Redzic et al., 2013). Though stroke-induced cytotoxic processes differ between cell types, the ultimate effect is widespread cellular death throughout the infarct core within hours of stroke onset (Carmichael, 2016).

Given the irreversible nature of acute cellular death following stroke, the primary region of opportunity for intervention after stroke occurrence is the area immediately surrounding the core, commonly referred to as the peri-infarct region. In the days and weeks following stroke, the peri-infarct region undergoes dramatic reorganization. In cortical stroke, neurons lose afferent connections representing sensory, motor, or language stimuli. In human and animal studies, it is these surviving neurons in the peri-infarct cortex that have the greatest ability to undergo remodeling to re-map these functions onto surviving populations of cells (Murphy & Corbett, 2009; Buma et al., 2010; Carmichael, 2016). This cortical reorganization requires a number of signaling pathways, activating injury and growth-specific gene expression pathways to physically grow new axonal projections. This process of injury-induced axonal growth is referred to as axonal sprouting.

1.3 Axonal sprouting and cortical reorganization

1.3.1 Ipsilesional axonal sprouting

In cortical ischemic stroke, axonal sprouting is triggered most prominently in the cortical areas adjacent to or connected to the infarct. For example, in small somatosensory strokes in the rat, new projections form within three weeks in adjacent somatosensory cortex, significantly shifting the aggregate map of projections (Carmichael et al., 2001; 2017). In large motor or somatosensory strokes in the rodent, significant changes in axonal projections from the motor cortex are also observed. It has repeatedly been shown that these new projections connect motor cortex to

premotor cortex, primary somatosensory cortex, and secondary somatosensory cortex in these models of larger cortical ischemic stroke in rodents (Li et al., 2010, 2015; Overman et al., 2012; Clarkson et al., 2013). Anatomical tracing of cortical circuits can detect these sprouting patterns as early as three weeks after stroke, and robustly at one month post-stroke (Carmichael et al., 2017). Similar patterns of axonal sprouting have been observed in non-human primates (Dancause et al., 2005, Dancause 2006).

Following an initial stroke event, many patients show some degree of functional recovery throughout the subsequent weeks and months. Evidence from functional imaging and cortical stimulation/inactivation indicates that this functional recovery is correlated with reorganization of the anatomical representation of motor, sensory, language, and cognitive function. Specifically, reorganization of the ipsilesional peri-infarct cortex is most closely associated with recovery (Dancause 2006; Benowitz and Carmichael, 2010). Changes in axonal sprouting observed following stroke in rodents and non-human primates correlate with these changes in functional maps of motor function observed in human stroke patients, particularly in ipsilesional motor, premotor, and somatosensory cortex (Carmichael et al., 2017). Taken together, these findings demonstrate a potential role for these peri-infarct regions of plasticity in stroke recovery.

It has been previously shown that the stroke event itself induces a unique gene expression pattern in the peri-infarct cortex that includes upregulation of growth-promoting genes and downregulation of inhibitory molecules, defining a physical and temporal window of opportunity

for axonal sprouting following stroke. (Carmichael et al., 2005) An understanding of the molecular events that underlie this endogenous process of axonal sprouting and cortical reorganization will facilitate the development of therapies to stimulate recovery after stroke.

Indeed, progress has been made in the development of preclinical therapeutic strategies to further enhance this endogenous process of post-stroke axonal sprouting in service of functional recovery. Administration of growth and differentiation factor 10 (GDF10) (Li et al., 2015), inosine (Chen et al., 2002; Lindau et al., 2014), Nogo receptor-1 signaling antagonists (Lee et al., 2004; Li et al., 2010), or blockade of EphrinA5 signaling (Overman et al., 2012) have all been shown to promote axonal sprouting following stroke. It is clear that axonal sprouting in the post-stroke brain is a critical cellular process to harness for further development of therapeutics, but there remain a number of unexplored mechanisms for this endogenous action.

1.3.2 Contralesional axonal sprouting

Large cortical ischemic strokes can trigger axonal sprouting from neurons in the contralesional cortex in addition to peri-infarct regions (Carmichael, 2017). In mice, rats, and non-human primate models of stroke and cortical lesion, corticospinal neurons in the contralesional cortex can extend projections through the corticospinal tract to the side of the cervical spinal cord that has been denervated by the motor cortical stroke, ipsilateral to the somatic origin of these projection neurons. This contralesional sprouting is associated with somatotopic

reorganization of the contralesional motor cortex for potential recovery of lost ipsilesional motor function (Lindau et al., 2014). Indeed, when the specific projections from the contralesional cortex to their ipsilateral spinal cord are selectively inactivated, motor recovery is blocked (Wahl et al., 2014), indicating a causal role for contralesional corticospinal axonal sprouting in recovery of motor function in large volume stroke models.

1.3.3 Unbounded axonal sprouting

Though this process of cortical reorganization has been linked to motor recovery following stroke, there may be a limit to the benefits of post-stroke axonal growth. Unbounded axonal sprouting has been shown to occur when glial growth inhibitors are blocked in combination with stimulation of injured motor connections. This results in axonal sprouting throughout the ipsilesional hemisphere (Overman et al., 2012) or into aberrant and functionally unrelated regions of the cervical spinal cord (Wahl et al., 2014). In the latter study, these patterns of aberrant sprouting were associated with worsened recovery following stroke. However, it is yet to be determined if these patterns of aberrant sprouting are universally maladaptive. Further studies examining axonal sprouting patterns throughout the brain are essential to understanding the lesion-specific complexities of this process.

1.4 Extracellular mechanisms of post-stroke axonal sprouting

The extracellular environment following stroke is filled with signals that paradoxically both promote and inhibit axonal growth. Activated microglia, invading neutrophils, and macrophages release inflammatory cytokines that have the ability to impact post-stroke axonal sprouting (Carmichael, 2016). The transforming growth factor (TGF) superfamily of cytokines contains several molecules that contribute to post-stroke axonal sprouting. It has been previously shown in our lab that growth differentiation factor 10 (GDF10), a member of the TGF-β family, is upregulated in peri-infarct cortex after stroke and serves as a potent stimulant of axonal sprouting and functional recovery (Li et al., 2015). It has also been shown that bone morphogenic protein 7 stimulates dendritic growth in neurons and promotes functional recovery following stroke (Withers et al., 2000; Ren et al., 2000).

Though the release of inflammatory cytokines following stroke has the ability to promote axonal sprouting, it also has the ability to inhibit it. Inflammatory cytokines play a role in the activation of astrocytes, which then in turn secrete molecules that block axonal sprouting, including chondroitin sulfate proteoglycans or ephrin-A5. (Overman et al., 2012) It is important to note, however, that blockade or removal of extracellular inhibitory signals alone has shown limited efficacy in promoting axonal sprouting and regeneration (Alilain et al., 2011; Liu et al., 2011; Krucoff et al., 2019). Thus, it is the interplay between pro-growth and growth-inhibiting molecular systems that determines the pattern and extent of axonal sprouting and recovery.

In the early stages following cortical stroke, synchronized electrical activity sweeps through peri-infarct tissue. Within the first few days following stroke, peri-infarct tissue exhibits synchronized long-duration neuronal depolarizations that produce a significant metabolic demand on tissue, sometimes resulting in cell death—a transition of stroke penumbra to infarct core. These peri-infarct spreading depressions are followed by synchronized low-frequency neuronal discharges that span the peri-infarct cortex as well as more distant connected regions, including contralateral cortex. This spread of synchronized electrical activity across the brain serves as one of the first signals of damage to distant regions of the brain. It has been demonstrated that this peri-infarct synchronized neuronal activity serves as a trigger for axonal sprouting, promoting the formation of new connections after stroke (Carmichael and Chesselet, 2002). Furthermore, blocking these patterns of synchronized neuronal activity following cortical stroke blocks both peri-infarct and contralesional axonal sprouting (Gertz et al., 2012). This electrical stimulation phenomenon parallels activity patterns that occur in the formation of neuronal circuits during development of the retina, hippocampus, and cortex (Katz and Shatz, 1996; Stellwagen and Shatz 2002; Egorov and Draguhn, 2013).

1.5 Intrinsic mechanisms of post-stroke axonal sprouting

Gene transcription is a critical regulator of axon growth during development and in response to axonal injury. Dynamic regulation of transcriptional pathways correlates with the

ability of neurons to synthesize cytoskeletal elements, growth cone components, and key proteins involved in axon elongation (Tedeschi, 2012). In response to axonal injury in the peripheral nervous system (PNS), neurons mount a well-characterized transcriptional response by expressing a number of regeneration-associated genes that promote neurite outgrowth by modulating the intrinsic growth capacity of the cells, reverting neurons back to a development-like state to promote regeneration. Early activation of specific transcriptional pathways is one of the first steps required to initiate an intrinsic regenerative response. Neurons in the central nervous system (CNS), in contrast, show a significantly lower capacity for regenerative growth. This difference in regenerative capacity is so pronounced, that it is generally accepted in the field that PNS neurons can be considered to be "regeneration-competent," while CNS neurons are "regeneration-incompetent" (Liu et al., 2011).

This disparity is due in part to differences in the environment of the damaged cells: the CNS contains inhibitory factors secreted by myelinating oligodendrocytes and physical barriers such as a glial scar formed in response to injury by reactive astrocytes. (Doron-Mandel et al., 2015) However, experimental manipulations that attempt to minimize environmental inhibitors are not sufficient for robust axonal sprouting (Yang and Yang, 2012), indicating that an important consideration is the low intrinsic potential of most adult CNS neurons to extend axons. During the developmental transition from embryonic to adult neurons, cells' intrinsic growth programs are repressed to allow for proper synaptic development (Abe and Cavalli, 2008). Thus, enhancing cell-autonomous

regenerative signals, such as transcription regulators, may be a key factor in improving neural repair in the injured brain.

Spontaneous axonal sprouting after stroke represents a phenotypic response to a central injury that is otherwise not seen in healthy brain: adult neurons physically grow new connections within an environment that typically restricts this process. Axon injury leads to both rapid and delayed activation of signaling pathways that communicate post-injury cellular changes from the axon to the soma. In many cases, this process involves local generation and activation of transcription factors or epigenetic modifiers to convey this information (Mahar and Cavalli, 2018). In the peri-infarct cortex, the selective isolation and RNA profiling of neurons that engage in spontaneous axonal sprouting following stroke indicates differential expression of genes for growth factors, cytokines, cell surface receptors, and transcriptional and epigenetic regulators, indicating a "sprouting transcriptome" that provides molecular control of this function (Li et al., 2010) (discussed in further detail in Chapter 2). Unsurprisingly, the ability of neurons to respond to injury requires the induction of widespread transcriptional and epigenetic changes within injured cells.

A number of transcription factors have been implicated for a role in neurite growth and/or axonal regeneration, including p53, c-Jun, CREB, STAT3, Sox11, and the KLF family. Though these all act through different mechanisms, their commonality is an association with developmental stages of axonal growth. Generally speaking, pro-growth transcription factors tend to be upregulated during early development, when axons are growing to their targets (Moore and

Goldberg, 2011). Furthermore, these factors tend to be upregulated in neurons that demonstrate some capacity for regeneration but not in neurons that fail to regenerate.

1.6 Summary and motivation for the dissertation

Ischemic stroke elicits a degree of axonal sprouting and cortical reorganization that has been associated with restoration of function. This sprouting response occurs in response to both intracellular and extracellular signals, but requires profound changes in the intrinsic state of neurons controlled by transcriptional pathways. Changes in gene expression patterns have been observed in the peri-infarct region (Carmichael et al., 2005) and in populations of neurons that specifically sprout new axons following stroke (Li et al., 2010). These changes in axonal sprouting coupled with differential expression of genes canonically associated with brain development suggest a possible recapitulation of developmental processes to aid in cortical reorganization and functional recovery following stroke.

An understanding of the molecular events that underlie this endogenous process of axonal sprouting and cortical reorganization will facilitate the development of therapies to stimulate recovery after stroke. The proposed project will investigate intrinsic neuronal mechanisms of axonal sprouting and regeneration in the cerebral cortex through manipulation of transcription factors canonically associated with cortical development that have previously been linked to post-stroke axonal sprouting. The overarching goal of the studies that follow is to enrich

understanding of the developmentally-associated mechanisms of post-stroke axonal sprouting and assess the ability of these pathways to promote functional recovery. It is hoped that these studies will lead to a greater understanding of repair in CNS injury more broadly and provide promising targets for therapeutic intervention.

1.7 References

Abe N, Cavalli V (2008) Nerve injury signaling. Curr Opin Neurobiol 18:276–283.

Alilain WJ, Horn KP, Hu H, Dick TE, Silver J (2011) Functional regeneration of respiratory pathways after spinal cord injury. Nature 475:196–200.

Benjamin EJ et al. (2018) Heart Disease and Stroke Statistics—2018 Update. Circulation 137:e67–e492.

Buma FE, Lindeman E, Ramsey NF, Kwakkel G (2010) Review: Functional Neuroimaging Studies of Early Upper Limb Recovery After Stroke: A Systematic Review of the Literature. Neurorehab Neural Re 24:589–608.

Carmichael ST, Wei L, Rovainen CM, Woolsey TA (2001) New Patterns of Intracortical Projections after Focal Cortical Stroke. Neurobiol Dis 8:910–922.

Carmichael ST, Chesselet M-F (2002) Synchronous Neuronal Activity Is a Signal for Axonal Sprouting after Cortical Lesions in the Adult. J Neurosci 22:6062–6070.

Carmichael ST, Archibeque I, Luke L, Nolan T, Momiy J, Li S (2005) Growth-associated gene expression after stroke: evidence for a growth-promoting region in peri-infarct cortex. Experimental Neurology 193:291–311.

Carmichael ST (2016) The 3 Rs of Stroke Biology: Radial, Relayed, and Regenerative. Neurotherapeutics : the journal of the American Society for Experimental NeuroTherapeutics 13:348–359.

Carmichael ST, Kathirvelu B, Schweppe CA, Nie EH (2017) Molecular, cellular and functional events in axonal sprouting after stroke. Exp Neurol 287:384–394.

Chen P, Goldberg DE, Kolb B, Lanser M, Benowitz LI (2002) Inosine induces axonal rewiring and improves behavioral outcome after stroke. Proc National Acad Sci 99:9031 Available at: http://www.pnas.org/content/99/13/9031.abstract.

Chia NH, Leyden JM, Newbury J, Jannes J, Kleinig TJ (2016) Determining the Number of Ischemic Strokes Potentially Eligible for Endovascular Thrombectomy. Stroke 47:1377–1380.

Clarkson AN, López-Valdés HE, Overman JJ, Charles AC, Brennan K, Carmichael ST (2013) Multimodal Examination of Structural and Functional Remapping in the Mouse Photothrombotic Stroke Model. J Cereb Blood Flow Metabolism 33:716–723.

Dancause N, Barbay S, Frost SB, Plautz EJ, Chen D, Zoubina EV, Stowe AM, Nudo RJ (2005) Extensive Cortical Rewiring after Brain Injury. The Journal of Neuroscience 25:10167–10179.

Dancause N (2006) Vicarious Function of Remote Cortex following Stroke: Recent Evidence from Human and Animal Studies. Neurosci 12:489–499.

Doron-Mandel E, Fainzilber M, Terenzio M (2015) Growth control mechanisms in neuronal regeneration. Febs Lett 589:1669–1677.

Egorov AV, Draguhn A (2013) Development of coherent neuronal activity patterns in mammalian cortical networks: Common principles and local hetereogeneity. Mech Develop 130:412–423.

Gertz K, Kronenberg G, Kälin RE, Baldinger T, Werner C, Balkaya M, Eom GD, Hellmann-Regen J, Kröber J, Miller KR, Lindauer U, Laufs U, Dirnagl U, Heppner FL, Endres M (2012) Essential role of interleukin-6 in post-stroke angiogenesis. Brain 135:1964–1980.

Hankey GJ, Spiesser J, Hakimi Z, Bego G, Carita P, Gabriel S (2007) Rate, degree, and predictors of recovery from disability following ischemic stroke. Neurology 68:1583–1587.

Katz LC, Shatz CJ (1996) Synaptic Activity and the Construction of Cortical Circuits. Science 274:1133–1138.

Kelly-Hayes M, Beiser A, Kase CS, Scaramucci A, D'Agostino RB, Wolf PA (2003) The influence of gender and age on disability following ischemic stroke: the Framingham study. J Stroke Cerebrovasc Dis 12:119–126.

Krucoff MO, Miller JP, Saxena T, Bellamkonda R, Rahimpour S, Harward SC, Lad SP, Turner DA (2018) Toward Functional Restoration of the Central Nervous System: A Review of Translational Neuroscience Principles. Neurosurgery 84:30–40.

Li S, Overman JJ, Katsman D, Kozlov SV, Donnelly CJ, Twiss JL, Giger RJ, Coppola G, Geschwind DH, Carmichael ST (2010) An age-related sprouting transcriptome provides molecular control of axonal sprouting after stroke. Nat Neurosci 13:1496–1504.

Li S, Nie EH, Yin Y, Benowitz LI, Tung S, Vinters HV, Bahjat FR, Stenzel-Poore MP, Kawaguchi R, Coppola G, Carmichael ST (2015) GDF10 is a signal for axonal sprouting and functional recovery after stroke. Nature neuroscience 18:1737–1745.

Lindau NT, Bänninger BJ, Gullo M, Good NA, Bachmann LC, Starkey ML, Schwab ME (2014) Rewiring of the corticospinal tract in the adult rat after unilateral stroke and anti-Nogo-A therapy. Brain 137:739–756.

Liu K, Tedeschi A, Park KK, He Z (2011) Neuronal Intrinsic Mechanisms of Axon Regeneration. Annu Rev Neurosci 34:131–152.

Mahar M, Cavalli V (2018) Intrinsic mechanisms of neuronal axon regeneration. Nat Rev Neurosci 19:323–337.

Moore DL, Goldberg JL (2011) Multiple transcription factor families regulate axon growth and regeneration. Developmental neurobiology 71:1186–1211.

Morecraft RJ, Ge J, Stilwell-Morecraft KS, McNeal DW, Hynes SM, Pizzimenti MA, Rotella DL, Darling WG (2015) Frontal and frontoparietal injury differentially affect the ipsilateral corticospinal projection from the nonlesioned hemisphere in monkey (Macaca mulatta). J Comp Neurol 524:380–407.

Overman JJ, Clarkson AN, Wanner IB, Overman WT, Eckstein I, Maguire JL, Dinov ID, Toga AW, Carmichael ST (2012) A role for ephrin-A5 in axonal sprouting, recovery, and activity-dependent plasticity after stroke. Proc National Acad Sci 109:E2230–E2239.

Redzic ZB, Rabie T, Sutherland BA, Buchan AM (2013) Differential Effects of Paracrine Factors on the Survival of Cells of the Neurovascular Unit during Oxygen Glucose Deprivation. Int J Stroke 10:407–414.

Ren J, Kaplan PL, Charette MF, Speller H, Finklestein SP (2000) Time window of intracisternal osteogenic protein-1 in enhancing functional recovery after stroke. Neuropharmacology 39:860–865.

Stellwagen D, Shatz CJ (2002) An Instructive Role for Retinal Waves in the Development of Retinogeniculate Connectivity. Neuron 33:357–367.

Tedeschi A (2012) Tuning the Orchestra: Transcriptional Pathways Controlling Axon Regeneration. Frontiers in Molecular Neuroscience 4.

Virani SS et al. (n.d.) Heart Disease and Stroke Statistics—2020 Update. Circulation 141:e139–e596.

Wahl AS, Omlor W, Rubio JC, Chen JL, Zheng H, Schröter A, Gullo M, Weinmann O, Kobayashi K, Helmchen F, Ommer B, Schwab ME (2014) Asynchronous therapy restores motor control by rewiring of the rat corticospinal tract after stroke. Science 344:1250–1255.

Withers GS, Higgins D, Charette M, Banker G (2000) Bone morphogenetic protein-7 enhances dendritic growth and receptivity to innervation in cultured hippocampal neurons. Eur J Neurosci 12:106–116.

Yang P, Yang Z (2012) Enhancing intrinsic growth capacity promotes adult CNS regeneration. Journal of the Neurological Sciences 312:1–6.

Chapter 2

A screen to assess impact of candidate genes on axonal growth *in vitro*

2.1 Introduction

2.1.1 Transcriptomic profiles of stroke-induced axonal growth states

Cortical ischemic stroke elicits a degree of reorganization of motor, sensory and language functions in the spared ipsilesional tissue that is closely correlated with functional recovery. (Carmichael, 2006) This cortical reorganization relies upon axonal sprouting and the formation of new neuronal connections in the peri-infarct region. (Carmichael et al., 2001; Dancause et al., 2005; Brown et al., 2009) Previously our lab sought to better understand the molecular mechanisms underlying this sprouting response in peri-infarct neurons, with the aim of elucidating the intrinsic growth state of these cells. In this previous study, neurons that showed an endogenous sprouting response following cortical stroke were selectively isolated via laser capture microdissection and total RNA was captured for cDNA microarray. Of the >41,000 genes represented in this microarray, 558 were differentially and significantly regulated in sprouting neurons vs. non-sprouting neurons at 7 days post-stroke, providing a "sprouting transcriptome" for further investigation. (Li et al., 2010)

From this study, growth and differentiation factor 10 (GDF10) emerged as one of the most highly upregulated genes in the initiation of axonal sprouting in peri-infarct cortical neurons in the aged brain. GDF10 was of particular interest due to its established role as a secreted growth factor active in the developing brain (Söderström and Ebendal, 1999; Zhao et al., 1999). Upon further

investigation, GDF10 upregulation following stroke was found to be conserved across rodents, non-human primates, and humans. In order to characterize the ability of GDF10 to promote axonal sprouting and enhance functional recovery, Li and Nie et al. (2015) administered the growth factor directly to the infarct core via hydrogel. GDF10 was shown to promote axonal sprouting in the peri-infarct cortex and promote functional recovery. RNA-seq of peri-infarct neurons subject to GDF10 treatment revealed that GDF10 regulates several signaling pathways to induce a unique growth state distinct from other reported developmental or injury-associated mechanisms. This study provided an additional transcriptome dataset associated with axonal sprouting.

Taken together, these foundational studies from our lab provide two unique transcriptomic datasets representing neuronal growth states within the context of ischemic stroke. Both of these datasets provide insight into the transcriptional pathways that may be playing a role in post-stroke axonal sprouting. Of particular interest within these datasets are those differentially regulated transcription factors that have a reported role in brain development. Targeted manipulation of these developmentally associated transcriptional pathways may reveal novel regenerative pathways that recapitulate developmental periods of plasticity.

This chapter details the identification of developmentally associated transcription factors that have been implicated in post-stroke axonal sprouting. An *in vitro* screening platform of postnatal murine primary cortical neurons is utilized to identify candidate transcription factors that have an ability to promote axon growth upon overexpression. The aim of the studies in this chapter

is to identify novel genes for further investigation that may promote axonal sprouting and functional recovery following cortical ischemic stroke.

2.1.2 Primary neuronal cultures as a model system for axon growth

Primary neuronal culture systems can provide a large amount of data about cellular features under various conditions, allowing analysis of effects on neurite number, branching, and length. This approach provides researchers with the ability to efficiently evaluate numerous candidate perturbagens for their ability to influence axon growth. An important consideration in the development of these *in vitro* assays is the source of neuronal tissue: both the region of the brain and the age of the animal from which the tissue is harvested. Both of these factors can dramatically impact how cultures respond to manipulation by genes or pharmacological compounds. Hippocampal neurons derived from embryonic rodents are a well-established and widely-used culture model, as these cells show high survival and readily extend quantifiable axons and dendrites. However, it is the robust innate ability of these neurons to grow *in vitro* that makes their response to perturbagens less translatable to the regeneration of adult CNS neurons in the context of ischemic injury. Embryonic cortical neurons are also frequently used for screening for similar reasons, but they too differ from mature neurons in their endogenous molecular cues that navigate migration, cell division, and differentiation. In order to model axon growth in the adult brain, mature neurons that do not migrate or undergo cell division are more appropriate.

Postnatal cortical neuronal cultures are an ideal model system because these cells have undergone the developmental changes in gene expression that reduce their innate ability to extend or regenerate axons. (Motti et al., 2018) The screening assays detailed in this chapter utilized primary cortical neurons derived from early postnatal (postnatal day 3, P3) and late postnatal (postnatal day 12, P12) mice. The goal of these experiments was to develop a strategy to best model the adult injured brain *in vitro* to best identify transcription factors that may play a role in promoting axonal growth following cortical stroke.

2.2 Methods

2.2.1 Selection of genes for *in vitro* study

The sprouting transcriptome and GDF10 datasets were filtered through a p-value threshold of <0.05 and a minimum log2-transformed fold-change of 0.2 and 1.5, respectively. The GDF10 dataset was additionally subjected to an FDR cutoff of 0.1. Ingenuity Pathway Analysis (Qiagen) was used to identify those genes classified as "transcriptional regulators," and of those significantly regulated TFs, 23 genes were identified by IPA as being associated with brain development. From this list of differentially regulated developmental TFs, initial targets were selected based upon their degree of up- or downregulation and their known function in cortical development and axonal sprouting.

2.2.2 Development of viral vectors

Primary neurons are not amenable to chemical transfection (Ding and Kilpatrick, 2013; Geraerts et al., 2006), therefore lentiviruses were selected as the delivery vector for gene overexpression. The pCDH-CMV plasmid was a gift from Kazuhiro Oka (Addgene plasmid # 72265 ; http://n2t.net/addgene:72265 ; RRID:Addgene_72265) and used as a backbone for lentiviral vector development. For these studies, the CMV promoter was replaced with the EFS promoter, a truncated version of the constitutive EF1-alpha promoter, and open reading frames were obtained commercially for genes of interest (see **Table 2-1**), PCR amplified, and inserted downstream of EFS and upstream of a 2A-copGFP sequence, for protein level cleavage of the fluorophore from the gene of interest (**Figure 2-1**). Lentiviral constructs yielded expression of the fluorophore within 3 days following transduction of primary neurons.

2.2.3 Lentivirus Packaging

As illustrated in **Figure 2-2**, third-generation lentiviruses were packaged according to an established lab protocol based on published techniques (Dull et al., 1998). Briefly, HEK 293T/17 cells (ATCC CRL-11268) were cultured in DMEM + 10% FBS media at 37°C and 3% CO2. Packaging plasmids pMDLg/pRRE (Addgene 12251), pRSV-Rev (Addgene 12253), and pMD2.G (Addgene 12259) along with transfer vectors were transfected into cells using calcium phosphate transfection protocols with BES buffer prepared according to a standard recipe (CSH protocols, 2x

BBS). At 18 hours after transfection, cells were treated with fresh media containing 10 mM sodium butyrate and incubated another 24 hours. Media containing viral particles was collected and centrifuged at 1,500 x g for 10 min. Viruses were purified from the supernatant with a 2.5 hour, 20,000 rpm spin in a Beckson ultracentrifuge, followed by a 2.5 hour 32,000 rpm through 20% sucrose. The resulting pellet was resuspended in PBS and purified with a final spin at 7,000 x g for 5 min, and viral particles were collected from the supernatant.

2.2.4 P3 Primary neuron cultures

Primary mouse cortical neurons were prepared from P3 C57/BL6 mice (**Figure 2-3**). Briefly, mouse pups were euthanized on ice and a midline incision of the scalp and underlying translucent skull revealed the brain for removal. Under a dissecting microscope, meninges were carefully detached from the surface of the brain, cortices were separated from underlying white matter, and hippocampal formations were removed. The sensorimotor cortex was isolated, quartered, and collected in 4°C HBSS (calcium and magnesium-free). After dissections, cortical tissue pieces were transferred to a dissociation solution of preheated 37°C HBSS + 0.2% w/v papain solution (Worthington Biochemical) and digested for 12 min with intermittent inversion. DNase I and FBS were added after dissociation to minimize the presence of free-floating DNA fragments and clumping of tissue and to stop the papain reaction, respectively. The resulting cell suspension was passed through a 70 μm cell strainer and counted. Cells were plated into NbActiv4 medium

(BrainBits) at 30,000 cells/well in a 96-well plate (Ibidi) coated with poly-l-lysine (Sigma), for a total media volume of 200 μL/well. All conditions were tested in triple replicates.

2.2.5 P12 Primary neuron cultures

Primary mouse cortical neurons were prepared from P12 C57/BL6 mice, following a modified protocol utilizing the Adult Brain Dissociation Kit (Miltenyi Biotec). Mouse pups were euthanized on ice followed by decapitation. A midline incision of the scalp revealed the underlying skull which was carefully removed with forceps to allow access to the brain. The brain was quickly rinsed with ice-cold D-PBS (with added calcium and magnesium) and transferred to a petri dish for dissection in D-PBS. Cortices were separated from underlying white matter, hippocampal formations were removed, and tissue was divided into 500 μm coronal slices and collected in tubes containing D-PBS and proprietary dissociation enzymes (Miltenyi Biotec). Tissue was dissociated for 30 minutes at 37°C with heat and agitation provided by a GentleMACS Octo Dissociator with Heaters (Miltenyi Biotec). Following dissociation, tissue suspension was passed through a 70 μm cell strainer into a 50 mL conical tube with an additional 10 mL D-PBS and centrifuged at 300 x g for 10 min at 4°C. The supernatant was aspirated completely, and the cell pellet was rinsed with 3100 μL D-PBS. 900 μL proprietary Debris Removal Solution (Miltenyi Biotec) was added, and an additional 4 mL cold D-PBS was carefully overlayed on cell suspension. Cells were centrifuged at 3000 x g for 10 min at 4°C, forming three distinct phases. The top two phases were aspirated, and ~11 mL cold D-PBS was added to the remaining bottom phase for a total volume of 15 mL. The cell

suspension was inverted 3-5 times then centrifuged at 1000 x g for 10 min at 4°C. The supernatant was discarded, and the pellet was resuspended in 1 mL Red Blood Cell Removal Solution (Miltenyi Biotec), incubated for 10 min at 4°C, then centrifuged at 300 x g for 10 min at 4°C. The supernatant was discarded, the cell pellet was resuspended in NbActiv4 medium, and viable cells were counted. Cells were plated into NbActiv4 medium at 30 K/well in a 96-well plate coated with poly-l-lysine, for a total media volume of 200 μL/well. All conditions were tested in triple replicates.

2.2.6 Transduction and culture of cortical neurons

For all primary cortical neuron assays, cells were cultured for 24 h at 37°C and 5% CO2 prior to viral treatment. At 24 h following plating, half of the media (100 μL) was removed, and media containing lentivirus (1 μL/mL) was carefully added to cells so as to not disrupt adherence to the bottom of the well. Cells were returned to the incubator to allow for viral transduction. Neurons isolated from P3 mice were cultured for a total of 4 days *in vitro* (DIV). Neurons isolated from P12 mice were fed with additional growth medium at 4 DIV and fixed at 6 DIV.

2.2.7 Immunocytochemistry

Neurons were fixed after 4 or 6 days *in vitro* in 4% paraformaldehyde and washed in 0.02 M KPBS. Cells were immunolabeled with primary antibodies for axons (mouse anti tuj-1/βIII Tubulin, Promega, G7121) and neuronal cell bodies (chicken anti NeuN, Synaptic Systems, 266-006) and viral fluorophore amplification (rabbit anti copGFP, Invitrogen, PA5-22688). Donkey secondary

antibodies (JacksonImmuno, PA) against Mouse (cy3), Chicken (cy5), and Rabbit (cy2) were used at 1:500 for fluorescent conjugation. After the last wash, cells were left in cold KPBS for in-well confocal imaging.

2.2.8 Imaging and quantification of axon growth

Images of immunostained cultures were captured using a Nikon C2 confocal microscope collecting 10 images per well in a 96-well plate at 20X magnification. Automated unbiased analysis of images was conducted using Nikon Elements with High Content Analysis to remove fluorescence from cellular debris, skeletonize tuj-1 signal, measure total neurite length of segments longer than 12 um, and normalize by number of NeuN+ cell bodies that have a sprouting neurite >12um to give average tuj-1+ neurite length per image.

2.2.9 Statistics

Average neurite length for all images was assessed for outliers using the ROUT method with Q set to 1%, and outlier images were removed. Average neurite lengths for all images within each well were pooled to determine the average neurite length per well, which became the data points assessed across treatment groups. One-way ANOVA with Dunnett's post-hoc test for multiple comparisons was used to compare the effects of treatment conditions on neurite growth.

For assessment of differences between P3 and P12 growth, well averages from each condition were compared with an unpaired t-test.

2.3 Results

2.3.1 Selection of genes for *in vitro* study

From the list of differentially regulated developmental TFs generated from the sprouting transcriptome and the GDF10 dataset, eight initial targets were selected based upon their degree of up- or downregulation and their known function in cortical development and axonal sprouting. They are B-cell lymphoma/leukemia 11A (BCL11A, commonly known as CTIP1), B-cell lymphoma/leukemia 11B (BCL11B/CTIP2), cut-like homeobox 2 (CUX2), empty spiracles homeobox 1 (EMX1), Forkhead box protein P2 (FoxP2), Hematopoietically Expressed Homeobox (HHEX), Kruppel-Like Factor 7 (KLF7), and Onecut homeobox 2 (Onecut2).

2.3.2 Optimization of primary cortical neuron culture assay

The *in vitro* platform used for initial experiments was murine P3 primary cortical neurons cultured for 4 days. Gene overexpression was induced via lentivirus at 1 DIV, with TFs of interest expressed downstream of the EFS promoter, a truncated version of the constitutive EF1-alpha promoter, and tagged with a copGFP fluorophore. Lentiviral constructs yielded expression of fluorophore 3 days following transduction. A medium-throughput screening platform was

employed to culture primary neurons in 96-well plates with automated image capture and analysis, enabling studies of single and combinatorial effects of gain- or loss-of-function of multiple gene targets in parallel.

In order to further assess the ability of genes that showed promising results in the initial assay, a new approach was desired using P12 primary neurons. This approach was initially sought due to concerns about a potential ceiling effect of neurite growth in early postnatal cultures. P3 cells show a far greater intrinsic growth ability compared to cells obtained from P12 tissue, as the ability of developing neurons to extend new axons rapidly diminishes with postnatal age. After consultation with members of Dr. Mark Tuszynski's lab as well as with scientists and representatives at Miltenyi Biotec, a modified protocol was developed using the Miltenyi Adult Brain Dissociation Kit (methods section). It was hoped that these neurons obtained from P12 tissue would demonstrate a decreased capacity for growth compared to neurons from P3 tissue, and as the results in **Figure 2-4** show, that is indeed what was observed. P12 neurons show significantly shorter average axon length at 6 DIV compared to P3 neurons at only 4 DIV ($p = 0.0004$, unpaired t-test).

2.3.3 Effect of candidate gene overexpression on neurite outgrowth

Lentiviruses were used to overexpress genes of interest in primary cortical neurons, and effect on neurite length was evaluated after 4-6 days in vitro. The results of these assays are

presented in **Figure 2-5**. In early postnatal cultures (P3), overexpression of transcription factors Ctip2 and Hhex was associated with modest increased neurite length, measured by tuj-1 length after 4 DIV (**Figure 2-5, top panel**). Ctip2 overexpression was associated with an 8% increase in neurite length ($p = 0.0451$, one-way ANOVA followed by Dunnett's multiple comparisons test), while Hhex overexpression was associated with a 10% increase in neurite length ($p = 0.0068$, one-way ANOVA followed by Dunnett's multiple comparisons test).

Late postnatal cultures were obtained from P12 mice. Cultures were transduced with lentiviruses overexpressing genes of interest after 24 hours in vitro, and neurite length was evaluated after a total of 6 DIV (**Figure 2-5, bottom panel**). In this assay, Ctip2 overexpression did not show a significant effect on neurite length. However, the effect of Hhex overexpression observed in P3 cultures was amplified in P12 cultures. Hhex overexpression was associated with a 40% increase in neurite length ($p = 0.0331$, one-way ANOVA followed by Dunnett's multiple comparisons test).

2.4 Discussion

Transcription factors that have an implicated role in cortical development were selected from our lab's previously generated post-stroke sprouting transcriptomes were selected for initial in vitro study. Ctip1, Ctip2, and Foxp2 have been shown to play a critical role in the development of layer V/VI projection neurons, Ctip1 and Foxp2 directing callosal and thalamic projections

(Hisaoka et al., 2010; Woodworth et al., 2016) and Ctip2 directing corticospinal motor neuron projection. (Arlotta et al., 2005) Emx1 has a known role in early embryonic neural development and the formation of the corpus callosum. (Qiu et al., 1996) In both mice and humans, Cux2 defines upper layer cortical neurons and has been shown to play a critical role in layer II/III synapse formation. (Cubelos et al., 2010) Klf7, Hhex, and Onecut2 have less-defined roles in cortical development specifically, but there is evidence for their respective roles in the regulation of neural development. (Caiazzo et al., 2010; Simpson et al., 2015; Villaescusa et al., 2016) Though these transcription factors have been investigated for their role in cortical development, little is known of their potential role in response to neuronal injury and repair.

Neuronal cultures derived from both P3 and P12 mice were used for this screen. Data from initial P3 *in vitro* assays indicate a potential ability of the transcription factors Ctip2 and Hhex to promote axonal outgrowth. P3 primary neurons transduced with lentivirus overexpressing Ctip2 or Hhex show significantly increased axon length 3 days following transduction (4 DIV).

One key issue that arose in the quantification of axon length from P3 neurons at 4 DIV was the potential for a ceiling effect. P3 neurons cultured over a permissive substrate show robust neurite growth over the length of time it takes for lentiviral expression. By the time we are able to assess the impacts of gene overexpression itself, a significant amount of endogenous neurite growth has already occurred, potentially masking the effects of the overexpression. It was for this reason,

coupled with the desire to better recapitulate the state of an adult mouse brain, that a second assay using P12 neurons was employed.

The results of the P12 assay differ slightly from those of the P3 assay, but it is this difference that enables the refinement of scope moving forward. P12 primary neurons transduced with lentivirus overexpressing only Hhex show significantly increased axon length 5 days following transduction (6 DIV). This difference between P3 and P12 assays is not surprising, as the latter employs cells from a more developmentally mature state, with greater intrinsic growth inhibition already in place. This can be seen directly from the significant difference in neurite length at P3 at 4DIV versus P12 at 6DIV (**Figure 2-4**). It is due to this developmental difference that we hypothesize that the effects observed in the P12 assay will have greater *in vivo* reproducibility than the P3 assay.

These studies, combined with our previous studies identifying Hhex as one of the most significantly upregulated genes in neurons treated with the growth-inducing GDF10 following cortical stroke (Li et al., 2015), indicate Hhex as a promising target for *in vivo* study of post-stroke axonal sprouting. Given the promising result of Ctip2 in the initial P3 assay (especially its potential to induce growth over inhibitory substrates)

As with any culture system, there are notable limitations of these in vitro methods. The use of early to late postnatal tissue as the source of primary culture is inherently imperfect, given that

we are hoping to model axonal growth mechanisms occurring in the adult brain. Furthermore, we are attempting to capture neuronal intrinsic mechanisms of axonal growth with a predominantly neuronal culture system, but the brain contains a multitude of cell types that are constantly interacting with one another. It is impossible to capture the complexity of this system in a simple screen like the one developed for these studies. However, these results do point us in the direction of further exploration and *in vivo* validation that will be explored in the following chapters.

2.5 Figures

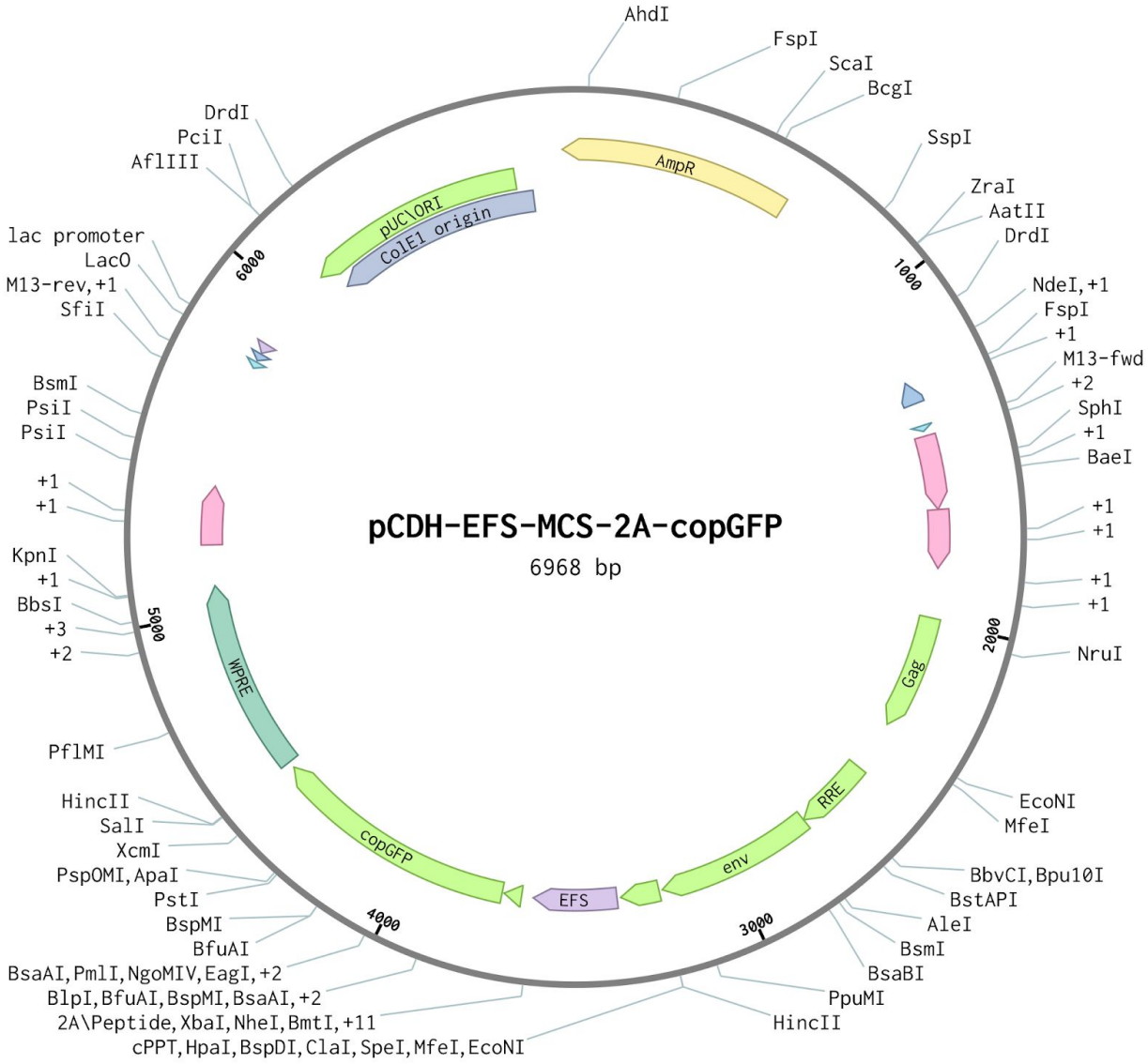

Figure 2-1. Control lentiviral construct for *in vitro* applications. EFS promoter, a truncated version of the constitutive EF1-alpha promoter, was used to drive expression of genes of interest upstream of a 2A-copGFP sequence, for protein level cleavage of the fluorophore. Genes of interest were cloned downstream of the EFS promoter. Created with Benchling.com.

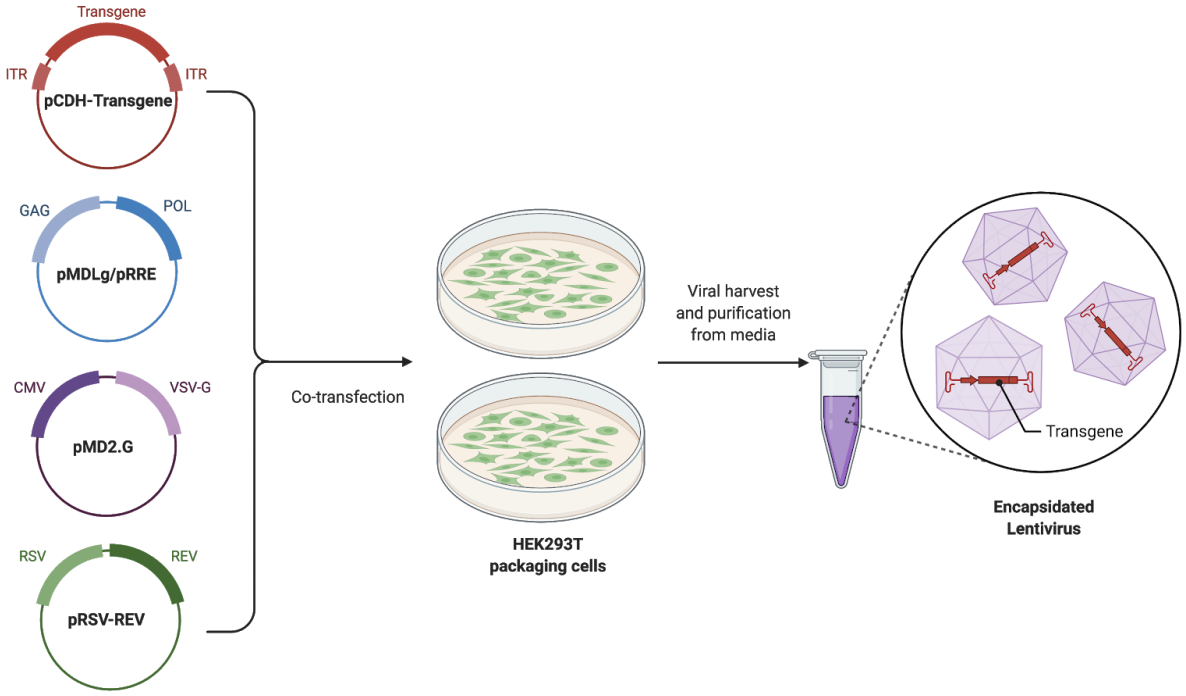

Figure 2-2. Third generation lentivirus packaging. HEK 293T/17 cells were cultured in DMEM + 10% FBS media at 37°C and 3% CO2. Packaging plasmids pMDLg/pRRE, pRSV-Rev, and pMD2.G along with pCDH transfer vector were transfected into cells using a calcium phosphate transfection protocol. Media containing viral particles was collected and viruses were purified from the supernatant with serial high speed centrifugation. Created with BioRender.com.

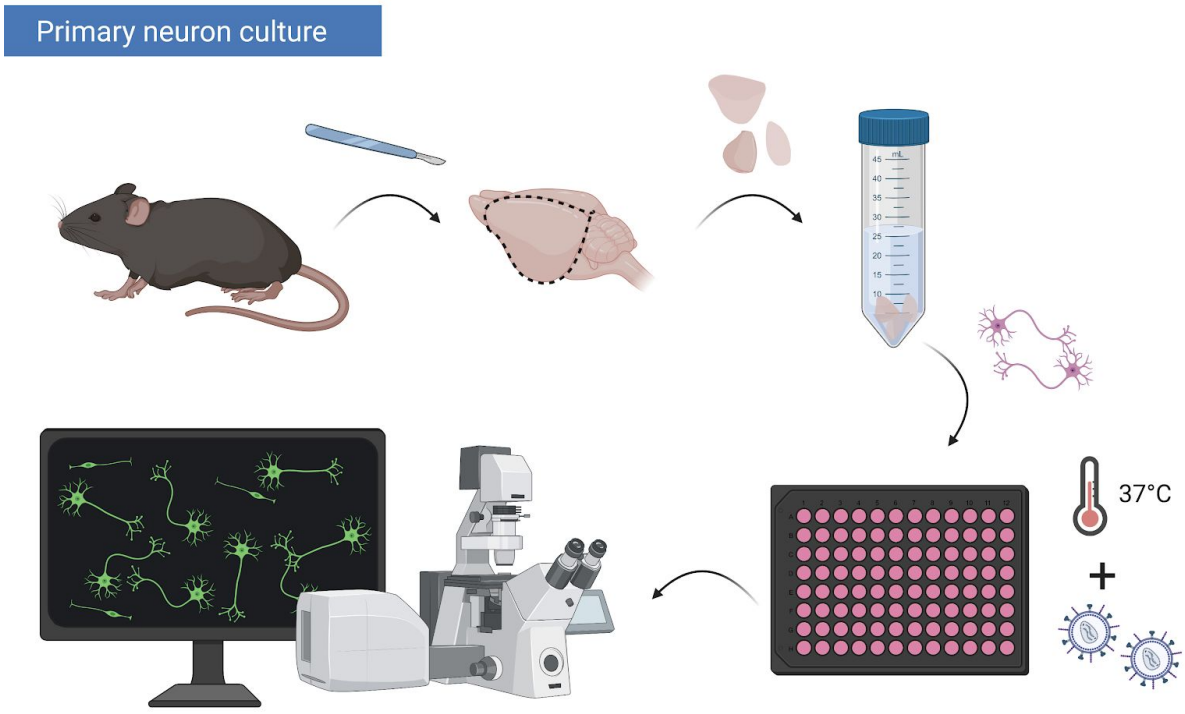

Figure 2-3. Primary neuron screening platform. Primary cortical neurons are obtained from C57/Bl6 mice 3 or 12 days postnatal. Brains are removed and cortices are carefully dissected. Tissue is enzymatically dissociated to form a single cell suspension, and resulting cells are plated in 96-well plates with neuronally enriched medium. After one day in vitro, cells are transduced with lentivirus expressing genes of interest or empty control vectors. After 4 or 6 days in vitro, cells are fixed, immunostained, and imaged on a confocal microscope. Neurite length is quantified to identify effects of gene delivery on axon growth.

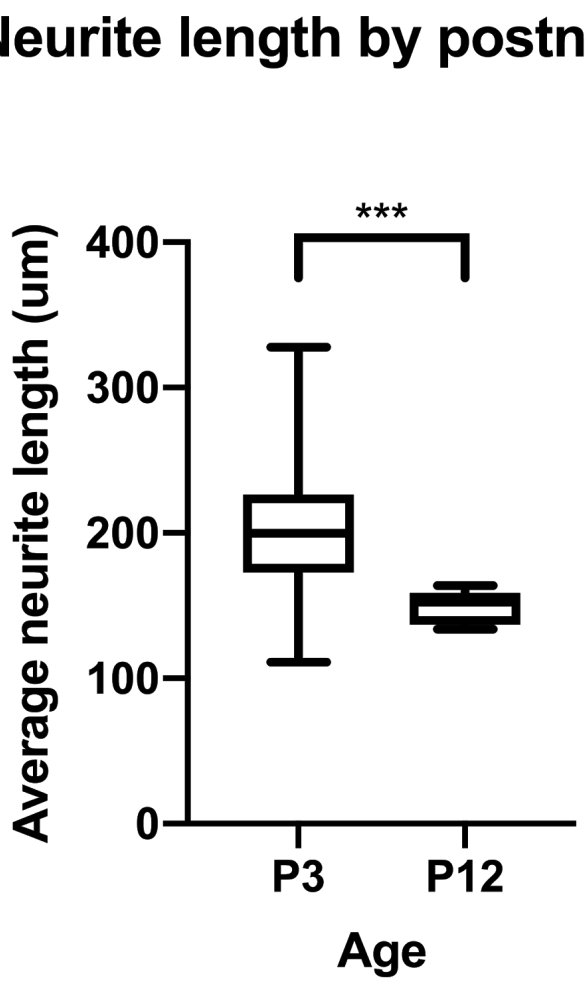

Figure 2-4. Comparison of neurite length between P3 and P12 cultures. P12 neurons show significantly shorter average axon length at 6 DIV compared to P3 neurons at only 4 DIV ($p = 0.0004$, unpaired t-test).

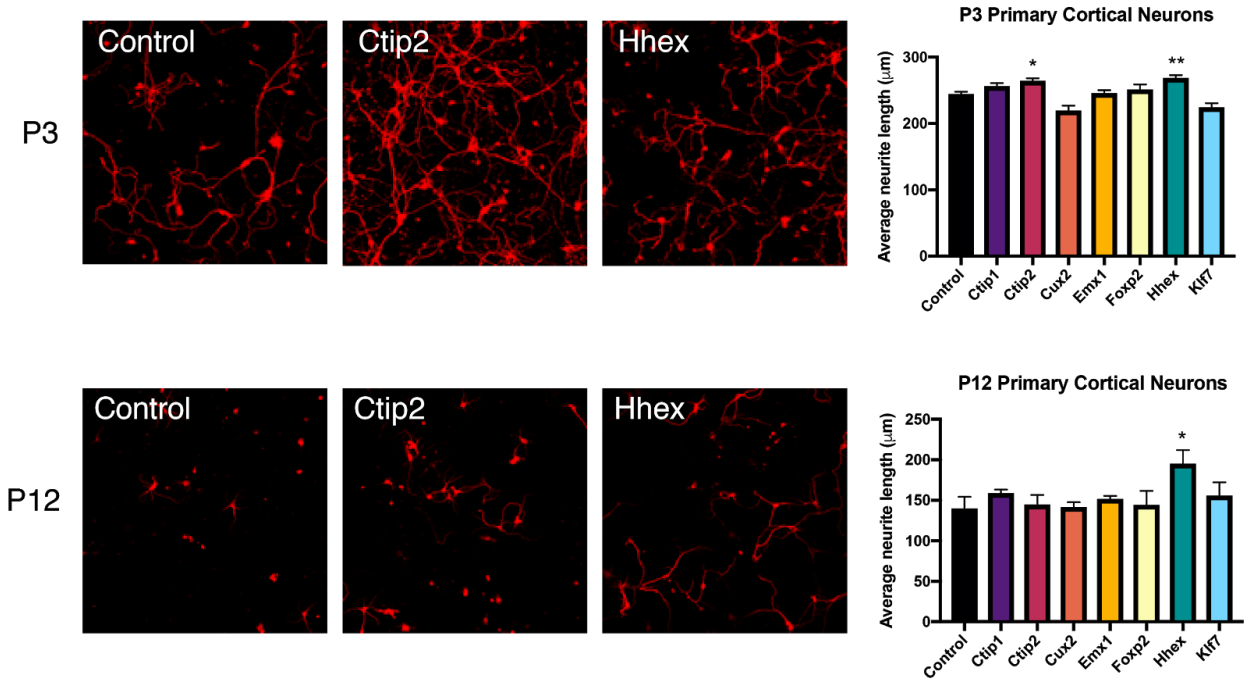

Figure 2-5. Impact of genes of interest on neurite growth in primary neurons. Lentiviruses were used to overexpress genes of interest in primary cortical neurons, and effect on neurite length was evaluated after 4-6 days in vitro. In early postnatal cultures (P3), overexpression of transcription factors Ctip2 and Hhex was associated with modest increased neurite length, measured by tuj-1 length after 4 DIV (top). Ctip2 overexpression was associated with an 8% increase in neurite length ($p = 0.0451$, one-way ANOVA followed by Dunnett's multiple comparisons test), while Hhex overexpression was associated with a 10% increase in neurite length ($p = 0.0068$, one-way ANOVA followed by Dunnett's multiple comparisons test). Late postnatal cultures were obtained from P12 mice, and neurite length was evaluated after a total of 6 DIV (bottom). In this assay, Hhex overexpression was associated with a 40% increase in neurite length ($p = 0.0331$). All statistics one-way ANOVA followed by Dunnett's multiple comparisons test. * $p < 0.5$; ** $p < 0.01$; *** $p < 0.001$.

Gene	Source
Ctip1	Origene ORF Clone #MR207799
Ctip2	Addgene Plasmid pmCTIP2-N174 #60858
Cux2	Dharmacon cDNA #MMM1013-202858453
Emx1	Origene ORF Clone #MR222943
Foxp2	Origene ORF Clone #MR203607
Hhex	Origene ORF Clone #MR210221
Klf7	Origene ORF Clone #MR204201
Onecut2	Origene ORF Clone #MR227438

Table 2-1. DNA sources for lentivirus plasmid cloning. pmCTIP2-N174 was a gift from Andrew Yoo (Addgene plasmid # 60858 ; http://n2t.net/addgene:60858 ; RRID:Addgene_60858).

2.6 References

Arlotta P, Molyneaux BJ, Chen J, Inoue J, Kominami R, Macklis JD (2005) Neuronal Subtype-Specific Genes that Control Corticospinal Motor Neuron Development In Vivo. Neuron 45:207–221.

Brown CE, Aminoltejari K, Erb H, Winship IR, Murphy TH (2009) In Vivo Voltage-Sensitive Dye Imaging in Adult Mice Reveals That Somatosensory Maps Lost to Stroke Are Replaced over Weeks by New Structural and Functional Circuits with Prolonged Modes of Activation within Both the Peri-Infarct Zone and Distant Sites. J Neurosci 29:1719–1734.

Caiazzo M, Colucci-D'Amato L, Esposito MT, Parisi S, Stifani S, Ramirez F, Porzio U di (2010) Transcription factor KLF7 regulates differentiation of neuroectodermal and mesodermal cell lineages. Exp Cell Res 316:2365–2376.

Carmichael ST, Wei L, Rovainen CM, Woolsey TA (2001) New Patterns of Intracortical Projections after Focal Cortical Stroke. Neurobiol Dis 8:910–922.

Carmichael ST (2006) Cellular and molecular mechanisms of neural repair after stroke: Making waves. Ann Neurol 59:735–742.

Cubelos B, Sebastián-Serrano A, Beccari L, Calcagnotto M, Cisneros E, Kim S, Dopazo A, Alvarez-Dolado M, Redondo J, Bovolenta P, Walsh CA, Nieto M (2010) Cux1 and Cux2 Regulate Dendritic Branching, Spine Morphology, and Synapses of the Upper Layer Neurons of the Cortex. Neuron 66:523–535.

Dancause N, Barbay S, Frost SB, Plautz EJ, Chen D, Zoubina EV, Stowe AM, Nudo RJ (2005) Extensive Cortical Rewiring after Brain Injury. The Journal of Neuroscience 25:10167–10179.

Ding B, Kilpatrick DL (2013) Neural Development, Methods and Protocols. Methods Mol Biology Clifton N J 1018:119–131.

Dull T, Zufferey R, Kelly M, Mandel RJ, Nguyen M, Trono D, Naldini L (1998) A Third-Generation Lentivirus Vector with a Conditional Packaging System. J Virol 72:8463–8471.

Geraerts M, Willems S, Baekelandt V, Debyser Z, Gijsbers R (2006) Comparison of lentiviral vector titration methods. Bmc Biotechnol 6:34.

Hisaoka T, Nakamura Y, Senba E, Morikawa Y (2010) The forkhead transcription factors, Foxp1 and Foxp2, identify different subpopulations of projection neurons in the mouse cerebral cortex. Neuroscience 166:551–563.

Li S, Overman JJ, Katsman D, Kozlov SV, Donnelly CJ, Twiss JL, Giger RJ, Coppola G, Geschwind DH, Carmichael ST (2010) An age-related sprouting transcriptome provides molecular control of axonal sprouting after stroke. Nat Neurosci 13:1496–1504.

Li S, Nie EH, Yin Y, Benowitz LI, Tung S, Vinters HV, Bahjat FR, Stenzel-Poore MP, Kawaguchi R, Coppola G, Carmichael ST (2015) GDF10 is a signal for axonal sprouting and functional recovery after stroke. Nature neuroscience 18:1737–1745.

Motti D, Blackmore M, Bixby JL, Lemmon VP (2018) High Content Screening, A Powerful Approach to Systems Cell Biology and Phenotypic Drug Discovery. Methods Mol Biology Clifton N J 1683:293–304.

Qiu M, Anderson S, Chen S, Meneses JJ, Hevner R, Kuwana E, Pedersen RA, Rubenstein JLR (1996) Mutation of theEmx-1Homeobox Gene Disrupts the Corpus Callosum. Developmental Biology 178:174–178.

Simpson MT, Venkatesh I, Callif BL, Thiel LK, Coley DM, Winsor KN, Wang Z, Kramer AA, Lerch JK, Blackmore MG (2015) The tumor suppressor HHEX inhibits axon growth when prematurely expressed in developing central nervous system neurons. Molecular and cellular neurosciences 68:272–283.

Söderström S, Ebendal T (1999) Localized expression of BMP and GDF mRNA in the rodent brain. J Neurosci Res 56:482–492.

Victor MB, Richner M, Hermanstyne TO, Ransdell JL, Sobieski C, Deng P-Y, Klyachko VA, Nerbonne JM, Yoo AS (2014) Generation of Human Striatal Neurons by MicroRNA-Dependent Direct Conversion of Fibroblasts. Neuron 84:311–323.

Villaescusa JC, Li B, Toledo EM, Cervo PR di V, Yang S, Stott SR, Kaiser K, Islam S, Gyllborg D, Laguna-Goya R, Landreh M, Lönnerberg P, Falk A, Bergman T, Barker RA, Linnarsson S, Selleri L, Arenas E (2016) A PBX1 transcriptional network controls dopaminergic neuron development and is impaired in Parkinson's disease. Embo J 35:1963–1978.

Woodworth MB, Greig LC, Liu KX, Ippolito GC, Tucker HO, Macklis JD (2016) Ctip1 Regulates the Balance between Specification of Distinct Projection Neuron Subtypes in Deep Cortical Layers. Cell Reports 15:999–1012.

Zhao R, Lawler AM, Lee S-J (1999) Characterization of GDF-10 Expression Patterns and Null Mice. Dev Biol 212:68–79.

Chapter 3

Investigating the ability of candidate genes to enhance post-stroke axonal sprouting

3.1 Introduction

In the previous set of experiments, candidate developmentally-associated transcription factors were screened for their ability to promote axon growth in a simplified in vitro system. The goal of this approach was to prioritize genes for further study in vivo, to examine effects within the context of cortical ischemic stroke. The current chapter focuses on these studies.

Previous work in our lab has shown that factors that promote axonal growth in primary neuronal cultures have the potential to promote axonal sprouting in the adult brain following ischemic stroke. (Clarkson et al., 2010; Li et al., 2015; Overman et al., 2012) Furthermore, axonal sprouting and cortical remodeling in the peri-infarct region, specifically in the circuit from motor to premotor cortex, is one of the best predictors of functional recovery following experimental ischemia. (Carmichael, 2006) Thus, the experiments detailed in this chapter evaluated the ability of peri-infarct transcription factor overexpression to enhance axonal sprouting in the ipsilesional cortex, contralesional cortex, and subcerebral structures. The top two individual gene candidates identified in Chapter 2, Ctip2 and Hhex, were selected for further study in vivo. These transcription factors were virally overexpressed in the anterior peri-infarct premotor cortex following focal ischemia to the forelimb motor cortex. The aim of the studies that follow was to evaluate the potential for these transcription factors to activate a neuronal growth program in motor circuits that enhances functional recovery.

3.1.1 Ctip2

Coup-TF interacting protein 2 (Ctip2), also referred to as B cell leukemia 11b (BCL11b), is a Kruppel-like C2H2 zinc finger protein transcription factor with a number of identified functions within populations of neuronal and non-neuronal cells. Broadly, Ctip2, like many transcription factors, acts as both a transcriptional activator and a repressor of a multiplicity of genes. It acts directly by binding to promoter regions, or indirectly by binding to other transcription factors that are in turn bound to promoter regions. (Cismasiu et al., 2005) Notably, CHIP-seq studies of Ctip2 activity in cultured striatal cell lines have implicated a role for the transcription factor in the regulation of a number of genes in the Brain-Derived Neurotrophic Factor (BDNF) signaling pathway. (Tang et al., 2011)

Ctip2 expression throughout murine development has been characterized by Leid et al (2004), who found Ctip2 expressed diffusely throughout the embryo at E10.5, localized within the CNS to cortical layers IV/V, basal ganglia, CA1/2 regions of the hippocampus, and olfactory bulb at E12.5 and E14.5, and this pattern of expression in cortex and limbic structures remained from E18.5 through adulthood. Ctip2 has been best characterized in its distribution to corticospinal motor neurons (CSMNs) of cortical layer V, where it plays a critical role in directing axon development and pathfinding in these cells. (Chen et al., 2004) In the absence of Ctip2, corticospinal motor neurons fail to project axons to the spinal cord. (Arlotta et al., 2005) In adult mice, Ctip2 is highly

expressed in layer V CSMNs but is absent from cortico-cortical neurons, which are characterized by expression of the transcription factor Satb2 (Fame et al., 2011).

Neuronal subtype identity is highly correlated with the brain's developmental timeline. Subcerebral projection neurons are born around E12.5-E13.5 in mice, while most callosal projection neurons are born between E14.5 and E15.5. (Woodworth et al., 2016). This timeline coincides with the sequential expression of Ctip2 and Satb2 in the developing cortex (Hatanaka et al., 2016). This apparent specificity of Ctip2 and correlation with subcerebral projectional neuron development led to the general acceptance of Ctip2 as a marker of layer IV/V subcerebral projection neurons.

However, Ctip2 has since been identified at high levels not only in deep layer excitatory neurons but also in the majority of GABAergic interneurons throughout the cortex. When looking at the distribution of Ctip2+ cells in layers I-IV, nearly all are GABAergic interneurons, and nearly 40% of Ctip2+ cells in layer V were actually GABAergic interneurons (Nikouei et al., 2016). Given the established role of Ctip2 in promoting axonal projection in excitatory cortical neurons, its role in regulating BDNF signaling pathways, and its presence in cortical GABAergic interneurons, there may be a broader function of Ctip2 in the promotion of axon extension in a diversity of neuronal subtypes. The results of the primary neuronal screens detailed in the previous chapter indicate a potential role for Ctip2 to promote axonal growth, though this effect may be dependent on the age of the neurons in question. The understanding of its role in cortical development coupled with the

results of my preliminary in vitro screens led to the selection of Ctip2 as one of two target genes for in vivo investigation for its ability to promote post-stroke axonal sprouting.

3.1.2 Hhex

Hematopoietically-expressed homeobox protein (Hhex) is a highly conserved homeobox protein transcription factor. As does Ctip2, Hhex acts as a context-dependent transcription factor, activating or repressing transcription depending on its target DNA sequence. Hhex's N-terminal proline-rich domain is highly conserved between mouse and human gene sequences and is responsible for much of the gene's repressive activity (Tanaka et al., 1999), while its C-terminal domain is largely responsible for its transactivating properties (Kasamatsu et al., 2004). Hhex is a homooligomer-forming transcription factor that binds DNA through homeodomains for direct regulation or forms protein-protein interactions with other transcription factors for indirect transcriptional modulation (Jang et al., 2019).

Hhex has reported roles in developmental processes for a variety of organs and cell types. It perhaps has been best characterized for its role in vascular development; overexpression of Hhex in the Xenopus embryo causes disorganization of vascular structures and an increase in the number of vascular endothelial cells (Newman et al., 1997). Noy and colleagues (2010) showed that Hhex is a regulator of the Vegf signaling pathway through direct repression of the *Vegf* gene as well as the *Vegfr-1* and *Vegfr-2* genes. This repression generally involves the recruitment of additional Groucho/TLE corepressor proteins. This study further showed that Hhex activity decreases cell

survival through DNA binding and recruitment of TLE, and this effect on cell survival is due at least in part to HHex's regulation of the Vegf signaling pathway.

Perhaps paradoxical to its reported inhibitory function in the Vegf signaling pathway, Hhex has been identified as an early-phase promoter of somatic cell reprogramming towards human induced pluripotent stem cells (iPSCs). Hhex overexpression enhanced early-phase reprogramming but acted as an inhibitor of pluripotency maintenance through later phase induction of differentiation (Yamakawa et al., 2016).

Though Hhex has been studied in relation to its role in development and the vascular system, a number of discrepancies and questions remain about how its function changes throughout developmental stages and organ type. Hhex's role in the brain has been investigated in a limited capacity. Hhex is detected in the Human Protein Atlas with low regional specificity within the brain (Uhlén et al., 2015), but detected robustly across regions via the Allen Brain Atlas mouse brain ISH dataset (Lein et al., 2007). Simpson et al. (2015) report neuronally-specific expression of Hhex throughout the adult mouse cortex, but no expression at P3.

In 2014, Buga et al. classified Hhex as a "pro-angiogenetic transcription factor" and a "new-for-stroke" gene, as they found it to be significantly upregulated in the brains of both young and aged mice at 3 and 14 days post middle cerebral artery occlusion, a time in which post-stroke angiogenesis is taking place. This study failed to associate Hhex upregulation with a particular

cellular population, as the gene expression analysis was conducted via whole-tissue microarray. Notably, an inhibitory role has been implicated for Hhex in axonogenesis and sprouting when overexpressed in developing CNS neurons (Simpson et al., 2015), but it remains to be seen if this is relevant in the adult mouse as well as in the context of cortical ischemic injury. The studies in this chapter seek to further evaluate the ability of Hhex to promote axonal growth in the peri-infarct region following ischemic stroke.

3.1.3 Evaluation of axonal sprouting

The experiments detailed in this chapter evaluate axonal sprouting from the peri-infarct motor cortex to regions throughout the brain. This approach was selected because it has been most robustly demonstrated that cortical reorganization originating from this region best correlates with recovery of function lost to stroke. Post-stroke axonal sprouting has additionally been reported to occur in the contralesional cortex, projecting from the contralesional cortex through its ipsilateral corticospinal tract to the cervical spinal cord denervated by the stroke (Chen et al., 2002; Zai et al., 2009, Carmichael et al., 2017). This form of axonal sprouting has also been associated with remapping of the limb representation damaged by stroke. However, given that the foundational work (Li et al., 2010, Li et al., 2015) leading to the identification of the genes of interest for these studies was in the context of axonal sprouting originating in the peri-infarct region, the scope of the axonal sprouting evaluated in this chapter was limited to that originating from the peri-infarct region and extending throughout the brain.

3.2 Methods

3.2.1 Mice

All animals used for the studies described in this chapter were Ai9 strain male mice (Madisen et al., 2010) aged 2-4 months at the time of surgery (n=9/group). Mice were obtained from the Jackson Laboratory (JAX stock #007909). Mice were randomly assigned to treatment groups. All experiments were performed in accordance with the National Institutes of Health animal protection guidelines and were approved by the University of California, Los Angeles Animal Research Committee (protocol #00-159).

3.2.2 Development of viral vectors

The lentiviral vectors used for these studies were modified from the EFS-driven vectors developed for the studies detailed in Chapter 2. For these in vivo studies, the EFS promoter was replaced with the neuronal-specific human synapsin promoter (hSyn), and the copGFP fluorophore was replaced with a Cre recombinase open reading frame. The purpose of these modifications was twofold to achieve precise targeting of neurons for gene overexpression, and the Cre recombinase is used in conjunction with the Ai9 mouse to achieve robust expression of the tdTomato fluorophore throughout neuronal cell bodies and processes.

3.2.3 Lentivirus packaging

Lentiviruses were packaged according to the methods described in Chapter 2.

3.2.4 Photothrombotic stroke and lentivirus injection

Ischemic stroke was produced in 2-4-month-old male Ai9 mice using a photothrombotic approach. Anesthesia was induced with 4% isoflurane supplied with 100% O_2 and maintained at 2% isoflurane for the duration of the procedure. Body temperature was maintained at 37.0 °C +/-0.5°C by homeothermic heating pads. Under isoflurane anesthesia, mice were placed in a stereotactic apparatus (Model 900, Kopf Instruments) with the skull exposed through a midline incision, cleared of connective tissue, and dried. The photosensitive dye Rose Bengal (100 mg/kg in sterile PBS) was injected intraperitoneally (concentration 10 mg/ml) to enter the bloodstream. After 5 minutes, the skull was revealed and 520 nm wavelength laser light (laser light source CLD1010LP, ThorLabs; laser diode LP520-MF100, ThorLabs) at 10.5 mW output was targeted to the forelimb motor cortex (coordinates from Bregma: 1.5 mm medial, 0.0 mm anterior/posterior) for 10 minutes to activate the photosensitive dye and induce focal ischemia. When activated by light targeted through the skull to a precise area of the cortex, endothelial damage with platelet activation and thrombosis is induced, resulting in local blood flow disruption. This technique allows for precise targeting of ischemic infarct to the forelimb motor cortex. Immediately following stroke induction, mice received injections in the anterior intact peri-infarct forelimb motor cortex (coordinates from Bregma: 1.75 medial, 1.5 mm anterior, 0.7 mm ventral) with 500 nl lentivirus overexpressing Hhex or Ctip2, or control virus. A dental drill was used to create a small hole in the skull to allow for needle access, through which a 33-gauge Hamilton needle attached to a 25 μl syringe was lowered into the cortex. Virus was infused into the brain at 0.1 μl/min. After intracranial injection, the

needle was allowed to remain in the brain for an additional 5 minutes, after which the needle was slowly removed from the brain, the wound was closed with Vetbond tissue adhesive (3M), and animals were returned to their home cage for recovery. All subsequent analyses were performed by individuals blinded to condition.

3.2.5 Tissue collection

Following stroke, animals were allowed to recover in their home cages for four weeks, a critical period during which new neural connections are formed after stroke (Carmichael et al., 2005). 28 days following stroke, animals were sacrificed via transcardial perfusion with cold saline followed by 4% PFA. Brains were post-fixed in 4% PFA at 4°C overnight and cryoprotected in 30% sucrose at 4°C for 24h prior to coronal sectioning on a cryostat (Leica CM 0530). 40 μm sections were collected and stored in a 50% glycerol antifreeze solution at –20°C until staining or mounting.

3.2.6 Immunohistochemistry

Immunohistochemistry for synaptic quantification was prepared according to a lab protocol. Briefly, sections were removed from 50% glycerol solution and washed three times in 0.02M KPBS for 5 minutes. Sections were incubated in pre-heated 1% SDS in 1x PBS for 5 minutes at 90°C, and washed again three times in 0.02M KPBS for 5 minutes. Tissues were blocked in a solution of 5% normal donkey serum (NDS), 0.1% Triton-X in KPBS for 1h at room temperature. Sections were then incubated in primary antibody solution of anti-Homer (1:000, rabbit, Synaptic Systems 160-003) and anti-Synaptophysin (1:200, guinea pig, Frontier Institute Syn-GP-Af300) prepared in

2% NDS, 0.1% Triton-X in KPBS for 2 days at 4°C. Following primary incubation, sections were washed three times in KPBS, and then incubated in a secondary antibody solution of anti-guinea pig 488 (1:500, JAX), anti-rabbit 647 (1:500 JAX), and DAPI (1:1000 from 250 μg/ml stock) in 2% NDS, 0.1% Triton-X in KPBS for 3h at room temperature. Tissues were washed 3 times in KBPS for 10 minutes before mounting on triple-subbed slides. Slides were dehydrated with ethanol washes 50-100% (1 min each) and xylene washes(2 min, 5 min) prior to coverslip application with DPX mounting media. All tissues were protected from light for the entirety of the immunohistochemical protocol.

3.2.7 Imaging and analysis of axonal sprouting

For contralesional and subcortical analysis, whole-brain sections from each animal representing every 240 μm were acquired at 20x using a Nikon epifluorescent microscope and Stereo Investigator software (MBF Bioscience). Images were subsequently analyzed in ImageJ. Individual sections were mapped to their corresponding position within the Paxinos Mouse Brain Atlas, and anatomical regions of interest were traced according to the atlas. Axonal sprouting was quantified via relative fluorescence intensity in 30 anatomically-defined cortical and subcortical areas to determine region-specific effects on axonal growth (**Table 3-1**).

The above approach of fluorescence intensity measurement was not appropriate for evaluating peri-infarct axonal sprouting, as the infarct and injection regions exhibited a significant amount of fluorescence from transduced neuronal cell bodies. To overcome this issue, peri-infarct

and peri-injection sections were imaged at 20x with a Nikon confocal microscope and processed using Bitplane Imaris software. Fluorescent cell bodies were masked and removed from images prior to fluorescence intensity analysis in ImageJ as described above.

3.2.8 Synaptic density quantification

Synapses were labeled according to the immunohistochemical protocol above, and regions of interest were identified based on the results of the axonal sprouting quantification. Tissue was imaged at 60x with a 2x optical zoom using a Nikon confocal microscope. Images were analyzed using Bitplane Imaris software according to a previously established protocol (Liang et al., 2019). Briefly, surface rendering was applied to generate the surface of tdTomato+ axons (Imaris, Bitplane). Presynaptic synaptophysin and postsynaptic Homer1 puncta were detected using the spot detection function in this system. The identification of presynaptic markers located inside tdTomato+ axons was achieved by detecting all synaptophysin puncta within 0.5 um of the tdTomato surface. Synapses were identified as colocalized pre- and post-synaptic puncta. The spot colocalization distance was set at 0.75 μm, which corresponded to the average sum of the radius from the Synaptophysin and Homer1 puncta. To normalize the number of colocalized synapses per cell surface, the number of colocalized spots was divided by the surface area of tdTomato+ axons.

3.2.9 Statistics

Sample sizes were assessed by power analysis using a significance level of a = 0.05 with 80% power to detect differences in ANOVA. For quantification of axonal sprouting, relative tdTomato

fluorescence intensity in regions of interest was assessed for outliers using the ROUT method with Q set to 1%, and outlier data points were removed. One-way ANOVA followed by Holm Sidak's multiple comparisons test was then used to evaluate cleaned data. Synapses were quantified using ordinary one-way ANOVA followed by Dunnett's multiple comparisons test. Statistical analysis and graph generation was conducted using GraphPad Prism software (version 8.4.3)

3.3 Results

3.3.1 Viral design for in vivo gene expression

In order to more precisely assess the roles of neuronal Ctip2 and Hhex overexpression in the context of stroke recovery, it was necessary to revisit lentiviral construct design for in vivo applications. Two distinct changes were made from those constructs discussed in Chapter 2.

First, overexpression needed to be neuronal-specific. The EFS promoter used in previous studies was constitutive. This was not a significant issue when working with neuronally-enriched cultures, but when probing the heterogeneous cell population of the mouse brain a more refined approach is necessary. To this end, the EFS promoter was removed via restriction digest and replaced with the neuronal-specific human Synapsin promoter, amplified from pAAV-hSyn-EGFP, a gift from Bryan Roth (Addgene plasmid # 50465 ; http://n2t.net/addgene:50465 ; RRID:Addgene_50465).

Second, virally transduced neurons needed to be robustly labeled throughout all processes in order to evaluate changes in post-stroke axonal sprouting. The constructs used in Chapter 2 provided sufficient labeling of the cell body with the copGFP fluorophore, but when injected into the mouse brain did not show clear labeling throughout axonal projections. To overcome this, Ai9 Cre reporter strain mice were selected for the experiments outlined in this chapter. Ai9 mice have a loxP-flanked STOP cassette preventing transcription of a CAG promoter-driven tdTomato fluorophore inserted into the Gt(ROSA)26Sor locus. Ai9 mice express robust tdTomato fluorescence following Cre-mediated recombination. Lentiviral constructs were designed for use with this strain, further modifying the constructs used previously by replacing the copGFP fluorophore with a Cre recombinase open reading frame amplified from pCAG-Cre, a gift from Connie Cepko (Addgene plasmid # 13775 ; http://n2t.net/addgene:13775 ; RRID:Addgene_13775).

The resulting constructs used for studies in this chapter are illustrated in **Figure 3-1**. Each contained a pCDH backbone, a human Synapsin promoter driving expression of Hhex, Ctip2, or an empty reading frame control, and a 2A-Cre directly downstream of the gene of interest for protein level cleavage of the recombinase. The resulting viral expression when injected into Ai9 mice is presented in **Figure 3-2**. These vectors induce overexpression of genes of interest while providing robust expression of the tdTomato fluorophore throughout axonal projections.

3.3.2 Effects of Hhex and Ctip2 on post-stroke axonal sprouting

In order to determine if either Hhex or Ctip2 has an ability to promote axonal sprouting following stroke, each transcription factor was virally overexpressed in the brains of mice immediately after undergoing ischemia. Ischemic stroke was induced in the forelimb motor cortex of 2-4-month-old male Ai9 mice. The forelimb motor cortex was selected as a model system for this study for two critical reasons: first, previous studies utilizing a forelimb motor stroke model have established a critical role of axonal sprouting in the peri-infarct cortex, specifically the formation of new connections from motor cortex to premotor cortex and primary and secondary somatosensory cortex, in recovery from ischemia (Carmichael et al., 2017); second, it reliably produces motor deficits that have been quantified in previous behavioral studies and thus serves as an ideal model for evaluating targets to promote functional behavioral recovery (Clarkson et al., 2010; Li et al., 2015; Overman et al., 2012). Immediately following stroke, mice received 500nl injections in the anterior intact peri-infarct forelimb motor cortex with lentivirus(es) overexpressing Hhex or Ctip2, or control MCS under the human Synapsin promoter. Each virus also contained a Cre recombinase open reading frame downstream of the hSyn promoter and gene of interest, so that expression of Cre in transduced cells of the Ai9 mouse brain would induce robust expression of the tdTomato fluorophore within those cell body and throughout all processes. This timepoint of viral injection was selected to ensure that gene manipulation via lentivirus expression would be occurring by roughly 7 days post-stroke, a sub-acute period identified as a time in which axons are initiating

sprouting (Carmichael, 2006). After 28 days, animals were euthanized, brains were extracted and histologically examined for changes in patterns of axonal sprouting.

Axonal sprouting was evaluated in 30 anatomically-defined regions (indicated in **Table 3-1**) through quantification of tdTomato+ signal relative to background for each individual section. Regions of interest were selected in ipsilesional cortex, contralesional cortex, and subcortical structures. Of all regions evaluated, 8 showed significant increases in axonal sprouting patterns with treatment of Ctip2 and/or Hhex. Results from ipsilesional regions of interest are present in **Figure 3-4**. Analysis of peri-infarct regions revealed that overexpression of Hhex, but not Ctip2, was associated with increased axonal sprouting in ipsilesional primary motor cortex (Stroke Hhex vs. Stroke Control $p = 0.0111$), ipsilesional secondary motor cortex (Stroke Hhex vs. Stroke Control $p = 0.0268$), and ipsilesional primary somatosensory cortex (Stroke Hhex vs. Stroke Control $p = 0.0069$). This is of particular interest, as sprouting in these regions has been previously shown to be associated with functional recovery following cortical stroke. As illustrated in **Figure 3-5**, both Ctip2 and Hhex showed an ability to promote axonal sprouting in contralesional primary somatosensory and secondary somatosensory cortex compared to Stroke Control (contralesional primary somatosensory cortex: Stroke Ctip2 vs. Stroke Control $p < 0.05$; Stoke Hhex vs Stroke Control $p < 0.05$); contralesional secondary somatosensory cortex: Stroke Ctip2 vs. Stroke Control $p < 0.01$, Stroke Hhex vs. Stroke Control $p < 0.001$). The subcortical regions evaluated that showed significant differences in axonal sprouting patterns were the contralesional striatum, which showed

a significant effect of both Ctip2 and Hhex (Stroke Ctip2 vs. Stroke Control $p < 0.001$; Stroke Hhex vs. Stroke Control $p < 0.001$), and the ipsilesional ventral posterolateral thalamic nucleus, which showed a significant ($p < 0.05$) effect associated with Ctip2 overexpression (**Figure 3-6**).

3.2.3 Assessment of synaptic density in regions of increased axonal sprouting

An ever-important question in the study of axonal sprouting and regeneration is whether or not these new axons are successfully forming new functional connections with synaptic targets. In order to begin to answer this question, we looked for evidence of changes in synaptic density in select regions of the brain that exhibited increased axonal sprouting, as reported above. We hypothesized that increased synaptic density could indicate an increase in aberrant synapses as a result of axonal sprouting, while decreased synaptic density could indicate a lack of functional connectivity occurring with these new axons. If there was no change in synaptic density with these new axons, this could suggest that functional connections were being established and maintained.

Synaptic density was quantified in regions of significant axonal sprouting, including ipsilesional and contralesional primary motor cortex, ipsilesional secondary motor cortex, ipsilesional and contralesional primary somatosensory cortex, and contralesional striatum. Synapses were identified via immunohistochemical colocalization of Synaptophysin (presynaptic marker), Homer1 (postsynaptic marker), and tdTomato (axonal label of virally transduced cells) in tissue collected 28 days post cortical motor photothrombotic stroke and pre-motor virus administration. As indicated in **Figure 3-7**, no decreases in synaptic density with either Hhex or Ctip2 treatment

were observed compared to control virus across all regions evaluated. These findings suggest that in these regions, Hhex- or Ctip2-induced axonal sprouting is accompanied by comparable increases in synapse formation.

3.4 Discussion

In this study, two transcription factors, Hhex and Ctip2, were selected for further study given their established roles in embryonic and brain development, their differential regulation in sprouting neurons after stroke, and their ability to promote axonal growth in vitro (Chapter 2). Hhex and Ctip2 were evaluated for their ability to promote axonal sprouting following cortical ischemic stroke. Genes were virally overexpressed in the peri-infarct cortex, and the degree of axonal sprouting was assessed in 30 anatomically-defined regions 28 days following stroke.

The axonal sprouting quantification approach selected for this study was of particular note in that it differs from previous approaches employed by our research group. Typically, a quantitative connectional mapping approach is applied to images obtained from horizontal sections of flattened cortex. This approach involves mapping of axonal projections to Cartesian coordinates in relation to the injection site, allowing for visualization and analysis of the average sprouting patterns observed within and between experimental treatment groups. However, this approach comes with limitations that were particularly relevant to this chapter's study. First, this approach is best employed for assessing directionality and changes in patterns of sprouting but does not provide insight into the relative density of axonal projections in a given area. Most importantly, this

measurement is only designed for cortico-cortical projections. Given the known role of Ctip2 in promoting subcortical axonal projections during development, it was necessary for this study to assess subcortical axonal sprouting.

To achieve the goal of assessing the relative density of axonal sprouting in pre-defined regions of interest including subcortical brain structures, coronal sections were hand-segmented into regions of interest as defined by the Paxinos Mouse Brain Atlas. Relative fluorescence intensity emitted by the virally-induced axonal label was measured across regions, revealing different patterns of post-stroke axonal sprouting following Hhex or Ctip2 overexpression.

Both Ctip2 and Hhex showed an ability to promote axonal sprouting in contralesional primary and secondary somatosensory cortex and contralesional striatum. Post-stroke axonal sprouting originating from the ipsilesional cortex and projecting to the contralesional cortex has not been definitively characterized as beneficial or detrimental to recovery, so the functional implications of this pattern of sprouting induced by Hhex and Ctip2 remain to be determined.

Analysis of axonal sprouting within the ipsilesional cortex revealed that Hhex overexpression, but not Ctip2 overexpression, led to increased sprouting in the ipsilesional primary motor cortex, secondary motor cortex, and primary somatosensory cortex. This is of particular interest, as sprouting in these regions has been previously shown to be associated with functional recovery following cortical stroke. Given these results, we would predict that this pattern of axonal

reorganization induced by Hhex would be more likely to induce motor recovery following cortical stroke than Ctip2. This hypothesis will be tested in the following chapter.

3.2.1 Limitations of this study

A persistent challenge in the study of axonal reorganization and sprouting following stroke is the specific labeling of only those axons that have formed following the infarct injury. Sequential retrograde labeling approaches have been employed to evaluate these neurons in a sparsely-labeled capacity (Li et al 2010), but this approach is impractical to employ in a higher-throughput anterograde manner due to limitations in the ability to parse out individual axons labeled throughout the brain when robustly labeled. Given this, it is not possible to determine with certainty that the increased axonal projections observed in this study are truly newly-formed axons. We can infer this due to differences compared to the control level of axonal labeling, but it should be acknowledged that this is indeed an inference.

An additional limitation of this approach is that it is not possible to determine precisely where these labeled axons are terminating. The analysis of synaptic density in regions of increased sprouting revealed that there are no discernible differences in synaptic density between treatment and control across these regions. The face-value explanation of this finding is that though we are increasing axonal projections, we are also increasing synaptic connections in this region, and these new projections are integrating into the brain architecture and forming functional connections.

However, there is the possibility that we are not capturing the location of the axon terminus and we cannot make any clear inferences about the nature of the projections' synaptic formation.

Furthermore, it is not possible from this study alone to determine whether or not these increased axonal projections represent reactive, reparative, or unbounded axonal sprouting. In order to begin to assess this question, the next chapter will detail a study of functional recovery following overexpression of either Ctip2 or Hhex following ischemic stroke in the forelimb motor cortex.

3.5 Figures

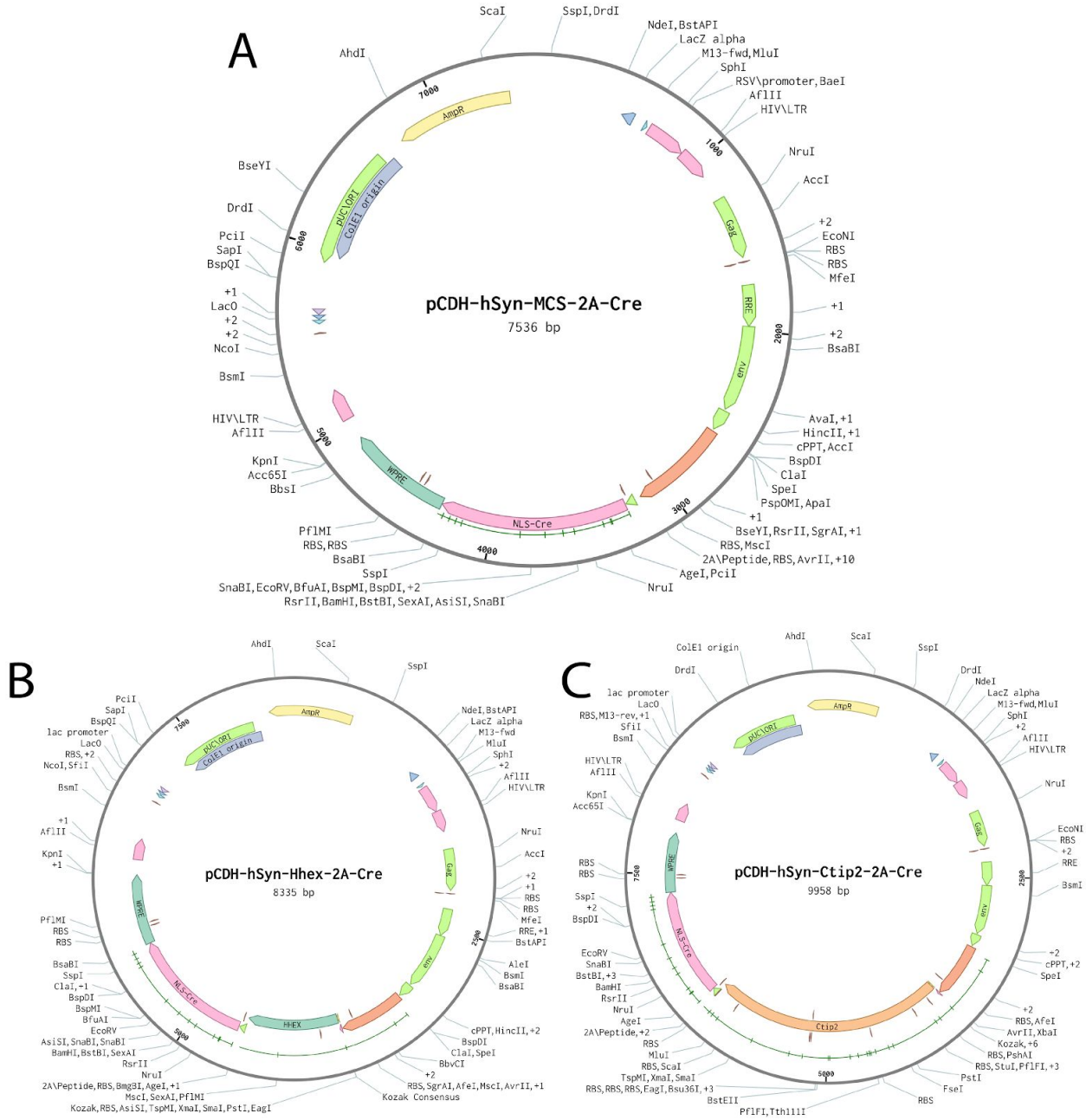

Figure 3-1. Lentiviral constructs for in vivo application. (A) Map of control viral construct containing a multiple cloning site (MCS) in place of genes of interest. (B) and (C) map the designed Hhex and Ctip2 overexpression vectors containing genes of interest and Cre driven by a human synapsin promoter. Created with Benchling.com.

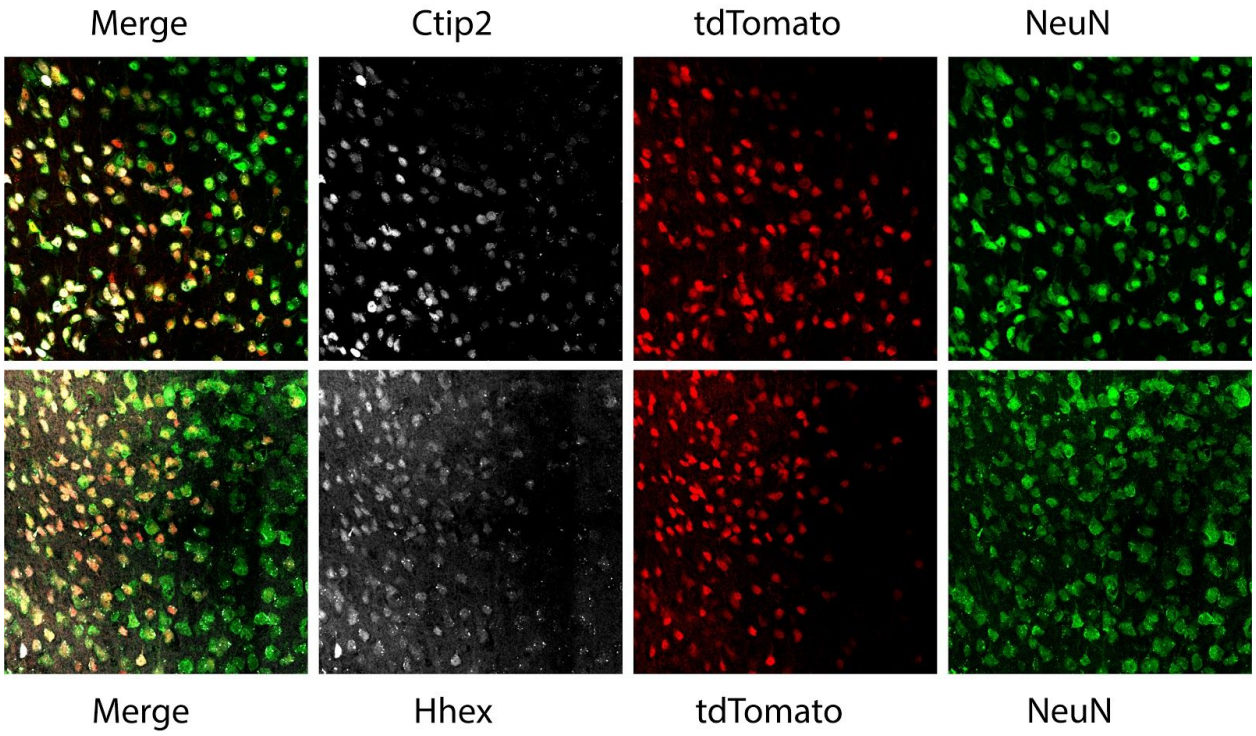

Figure 3-2. Viral expression in Ai9 mouse cortex. The top panel is a representative pane of the Ctip2-overexpressing lentivirus, while the bottom panel is representative of the Hhex-overexpressing lentivirus. TdTomato signal is induced in all cells that receive Cre-containing lentivirus, and shows overlap with NeuN expression. TdTomato signal also overlaps with increased expression of Ctip2 (top) or Hhex (bottom).

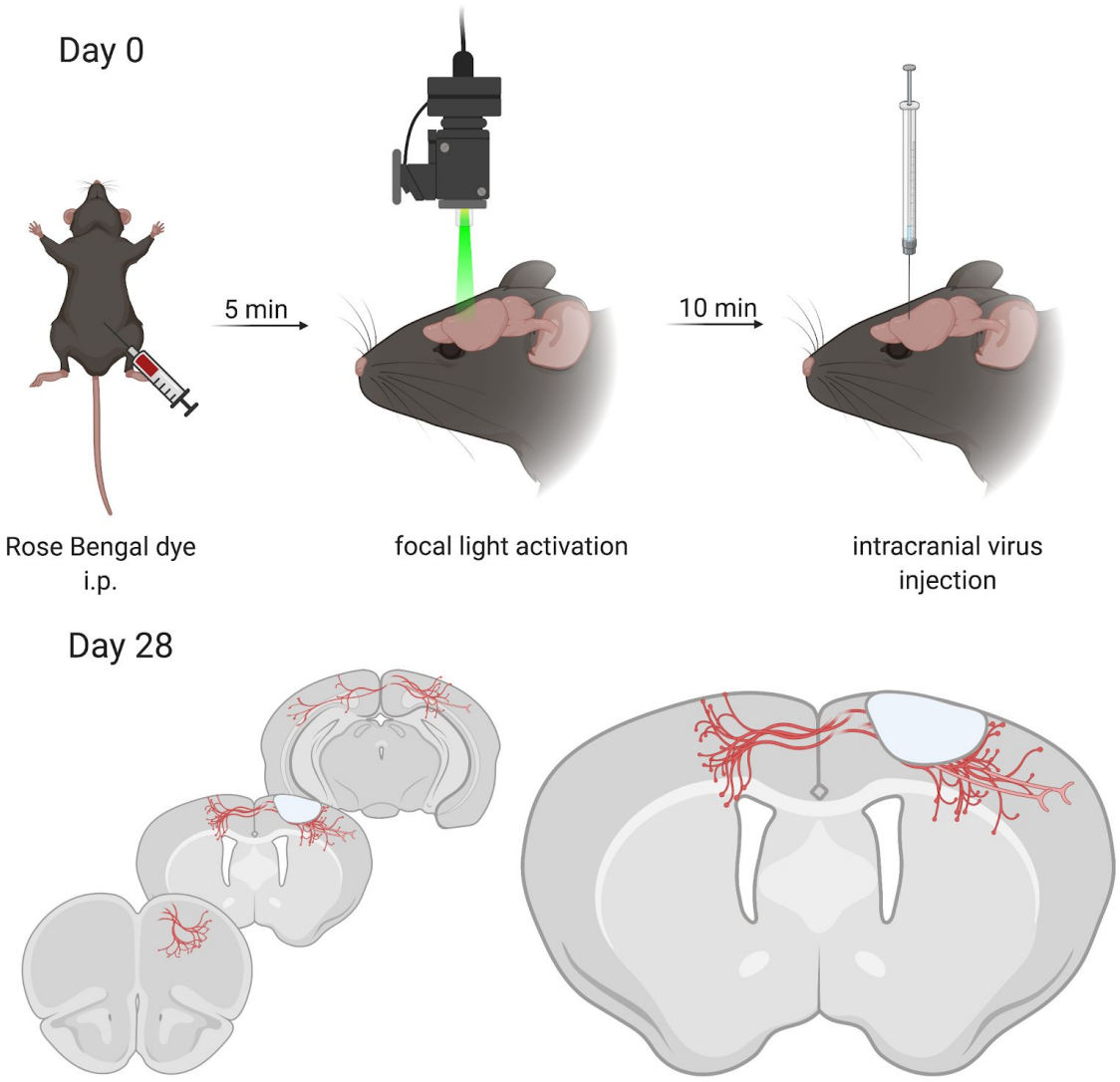

Figure 3-3. Experimental overview of in vivo axonal sprouting. At day 0, stroke is induced in the forelimb motor cortex of Ai9 mice via photothrombosis, and lentiviruses carrying Cre plus expression vectors for genes of interest Hhex or Ctip2 or empty control vectors are infused into the anterior per-infarct premotor cortex. On day 28, animals are sacrificed and axonal sprouting is visualized throughout the brain via Cre-induced tdTomato signal. Created with BioRender.com

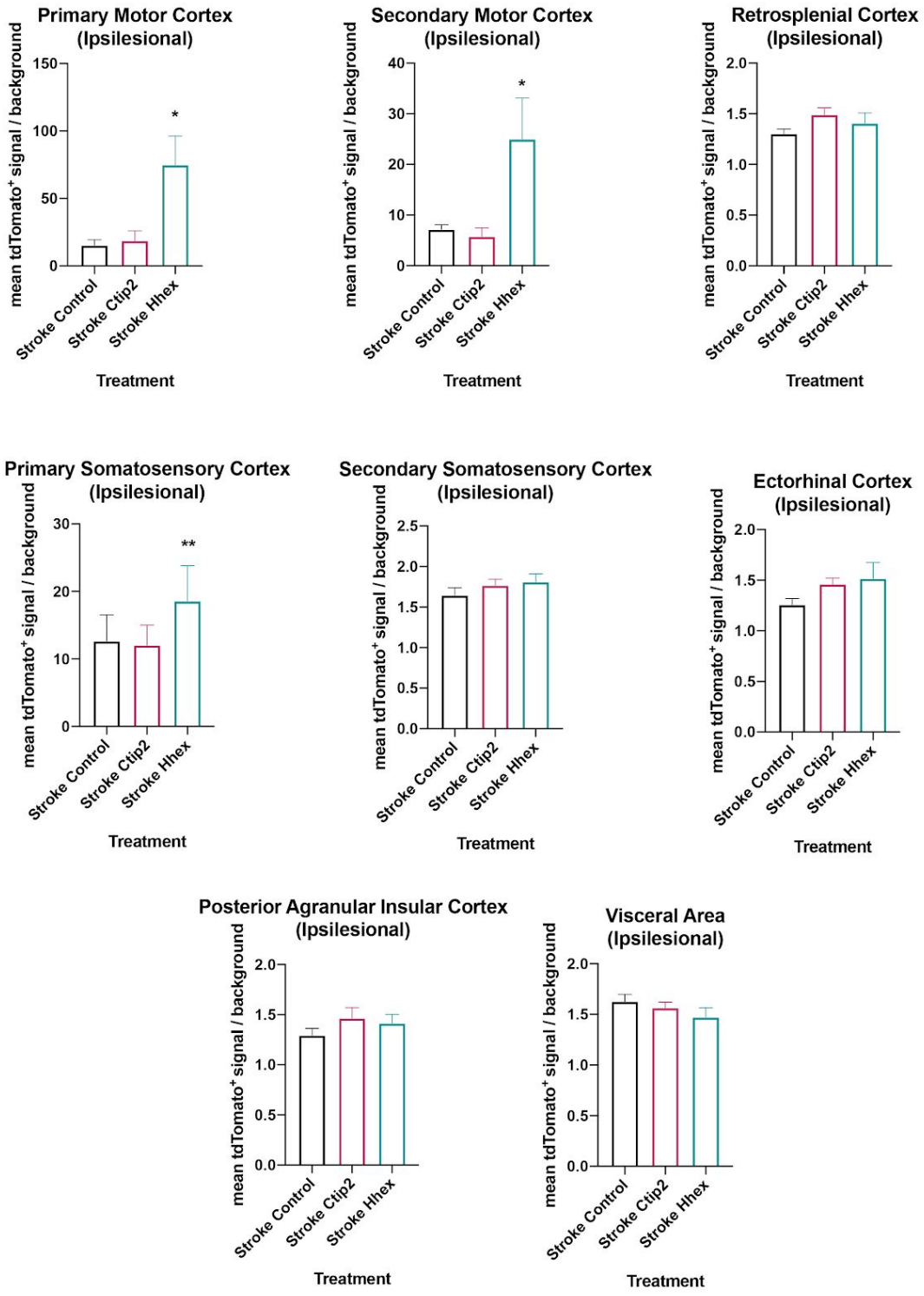

Figure 3-4. Ipsilesional cortical sprouting. Hhex, but not Ctip2, is associated with increased axonal sprouting in ipsilesional primary motor cortex (Stroke Hhex vs. Stroke Control p = 0.0111),

ipsilesional secondary motor cortex (Stroke Hhex vs. Stroke Control $p = 0.0268$), and ipsilesional primary somatosensory cortex (Stroke Hhex vs. Stroke Control $p = 0.0069$). One-way ANOVA followed by Dunnett's multiple comparisons test. * $p < 0.5$; ** $p < 0.01$; *** $p < 0.001$.

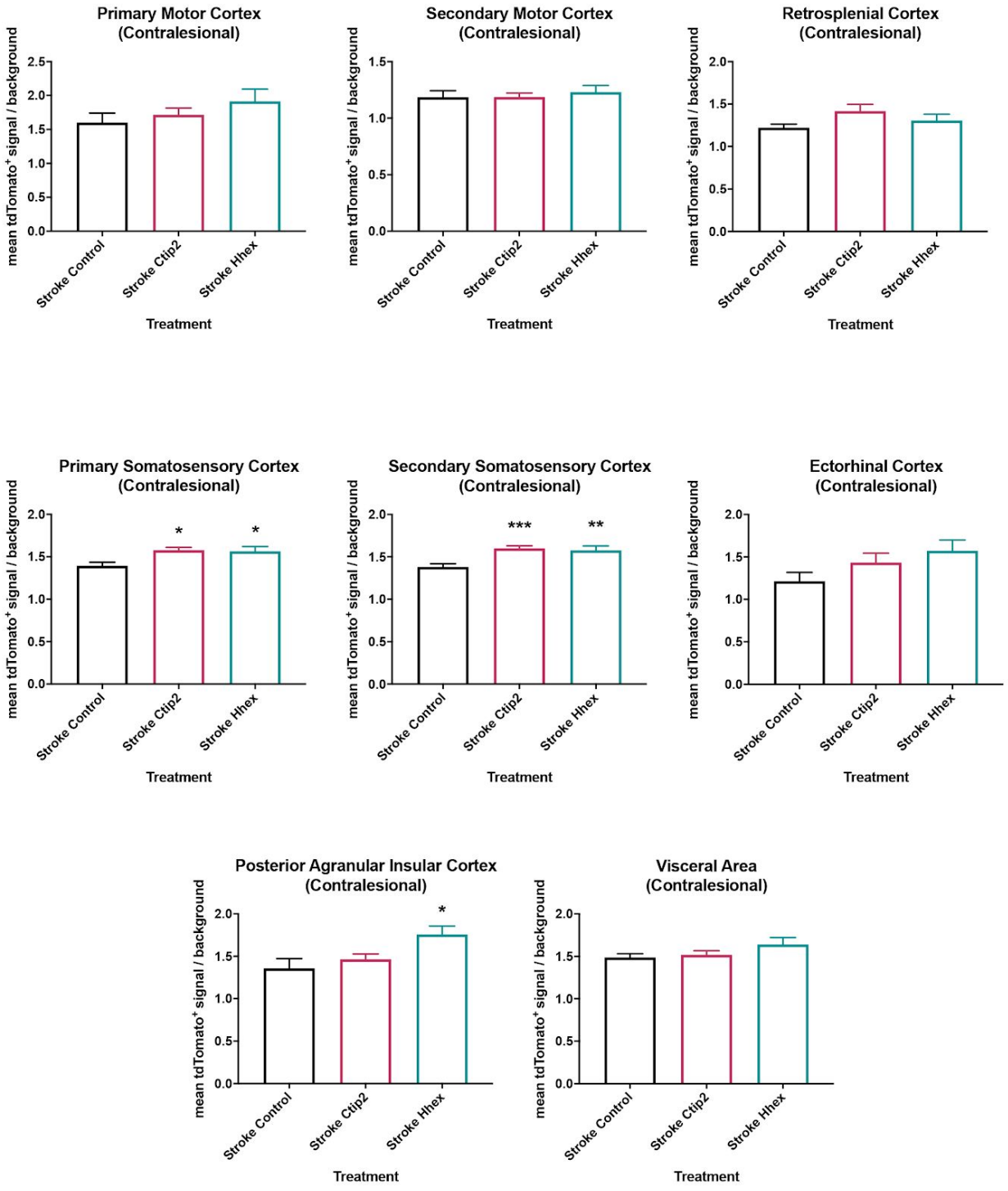

Figure 3-5. Contralesional cortical sprouting. Ctip2 and Hhex show an ability to promote axonal sprouting in contralesional primary somatosensory and secondary somatosensory cortex compared to Stroke Control (contralesional primary somatosensory cortex: Stroke Ctip2 vs. Stroke Control $p < 0.05$; Stoke Hhex vs Stroke Control $p < 0.05$; contralesional secondary somatosensory cortex:

Stroke Ctip2 vs. Stroke Control $p < 0.01$, Stroke Hhex vs. Stroke Control $p < 0.001$). One-way ANOVA followed by Holk-Sidak's multiple comparisons test. * $p < 0.5$; ** $p < 0.01$; *** $p < 0.001$.

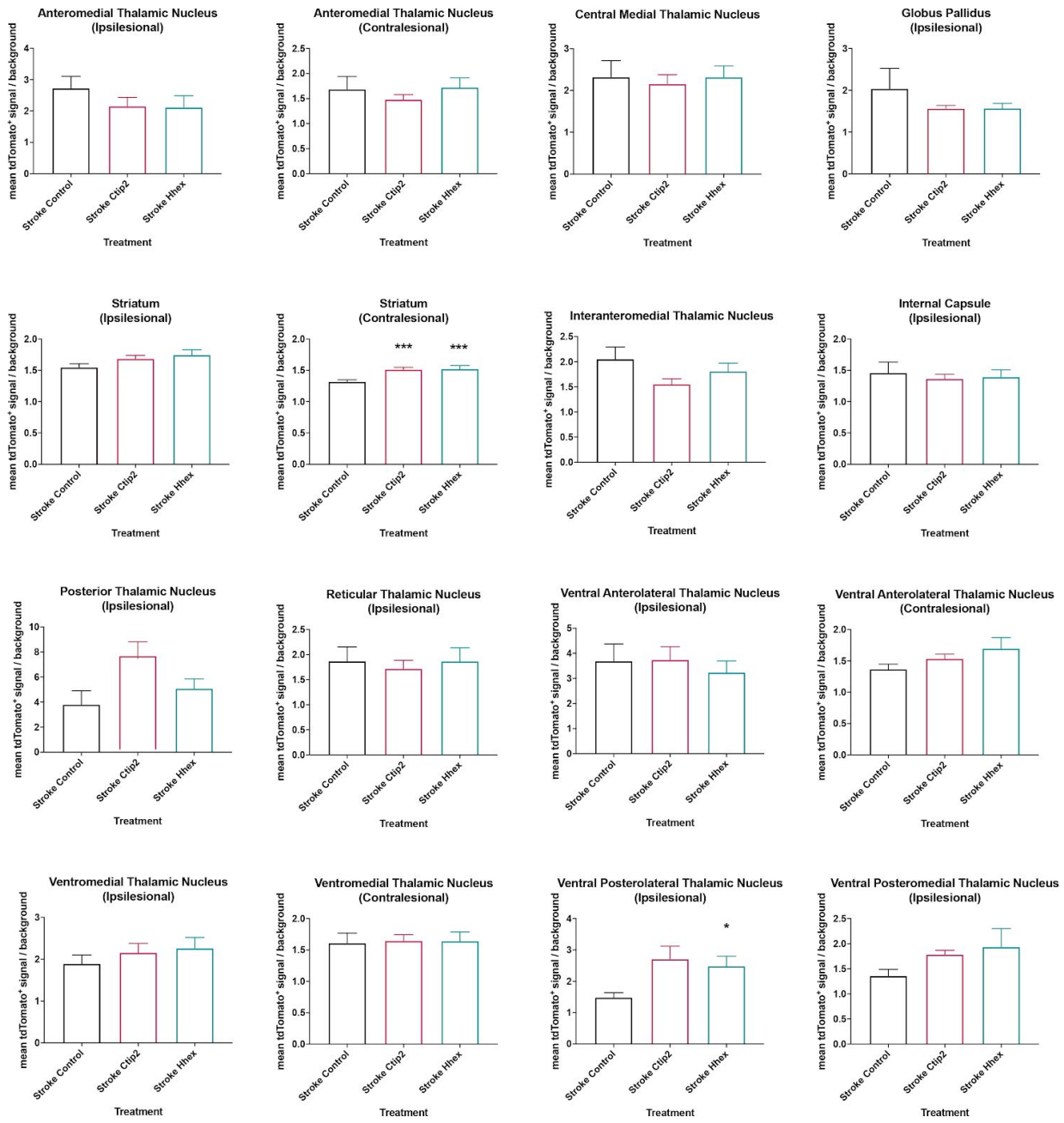

Figure 3-6. Subcortical axonal sprouting. The subcortical regions evaluated that showed significant differences in axonal sprouting patterns were the contralesional striatum, which showed a significant effect of both Ctip2 and Hhex (Stroke Ctip2 vs. Stroke Control $p < 0.001$; Stroke Hhex vs. Stroke Control $p < 0.001$), and the ipsilesional ventral posterolateral thalamic nucleus, which showed a significant ($p < 0.05$) effect associated with Ctip2 overexpression. One-way ANOVA followed by Holk-Sidak's multiple comparisons test. * $p < 0.5$; ** $p < 0.01$; *** $p < 0.001$.

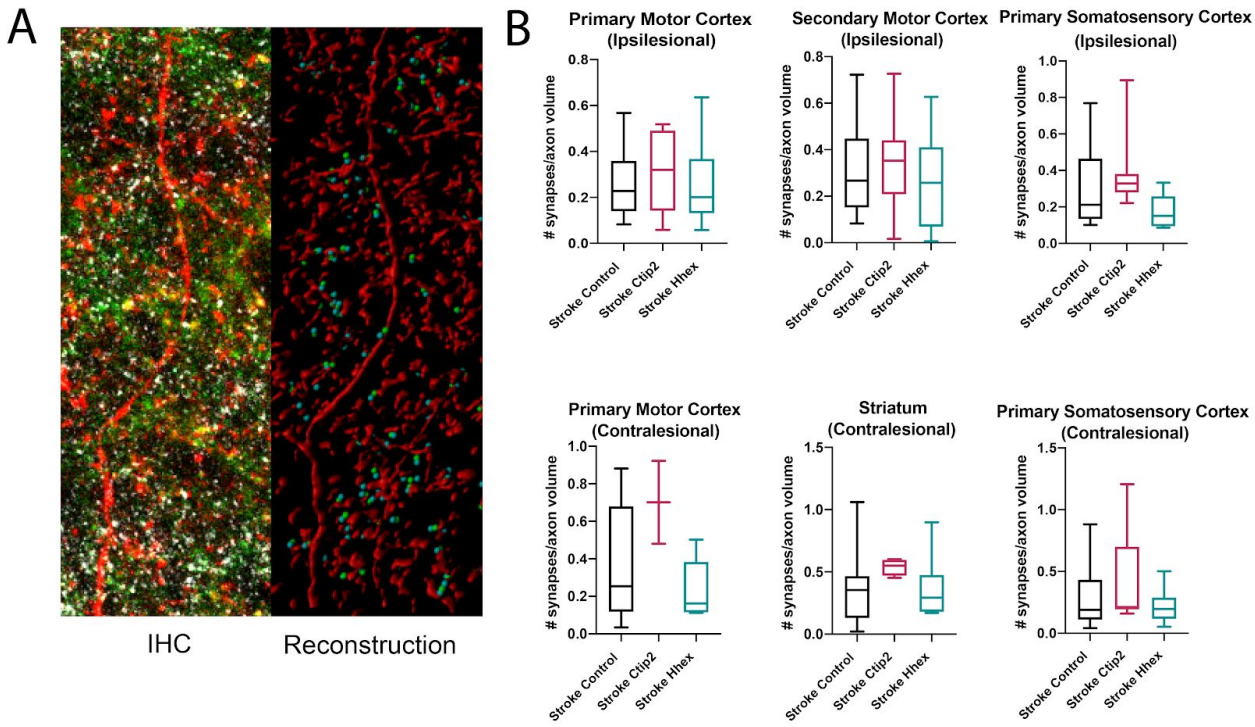

Figure 3-7. Synaptic density quantification. (A) Synapses were identified via immunohistochemical colocalization of Synaptophysin (green, presynaptic marker), Homer1 (white, postsynaptic marker), and tdTomato (red, axonal label of virally transduced cells) in tissue collected 28 days post cortical motor photothrombotic stroke and pre-motor virus administration. Surface rendering was applied to generate the surface of tdTomato+ axons (Imaris, Bitplane). Synaptophysin and Homer1 puncta were detected using the spot detection function in this system. Presynaptic puncta were identified as synaptophysin+ spots within 0.5 μm of the tdTomato surface. Synapses were identified as

colocalized pre- and post-synaptic puncta. The spot colocalization distance was set at 0.75 μm, which corresponded to the average sum of the radius from the Synaptophysin and Homer1 puncta. (B) No decreases in synaptic density with either Hhex or Ctip2 treatment were observed compared to control virus across all regions evaluated. To normalize the number of colocalized synapses per cell surface, the number of colocalized spots was divided by the surface area of tdTomato+ axons.

Cortical regions	Subcortical regions
Ectorhinal Cortex (Contralesional)	Anteromedial Thalamic Nucleus (Contralesional)
Ectorhinal Cortex (Ipsilesional)	Anteromedial Thalamic Nucleus (Ipsilesional)
Posterior Agranular Insular Cortex (Contralesional)	Central Thalamic Nucleus
Posterior Agranular Insular Cortex (Ipsilesional)	Globus Pallidus (Ipsilesional)
Primary Motor Cortex (Contralesional)	Interanteromedial Thalamic Nucleus
Primary Motor Cortex (Ipsilesional)	Internal Capsule (Ipsilesional)
Primary Somatosensory Cortex (Contralesional)	Posterior Thalamic Nucleus (Ipsilesional)
Primary Somatosensory Cortex (Ipsilesional)	Reticular Thalamic Nucleus (Ipsilesional)
Retrosplenial Cortex (Contralesional)	Striatum (Contralesional)
Retrosplenial Cortex (Ipsilesional)	Striatum (Ipsilesional)
Secondary Motor Cortex (Contralesional)	Ventral Anterolateral Thalamic Nucleus (Contralesional)
Secondary Motor Cortex (Ipsilesional)	Ventral Anterolateral Thalamic Nucleus (Ipsilesional)
Secondary Somatosensory Cortex (Contralesional)	Ventral Posterolateral Thalamic Nucleus (Ipsilesional)
Secondary Somatosensory Cortex (Ipsilesional)	Ventral Posteromedial Thalamic Nucleus (Ipsilesional)
Visceral Area (Contralesional)	Ventromedial Thalamic Nucleus (Contralesional)
Visceral Area (Ipsilesional)	Ventromedial Thalamic Nucleus (Ipsilesional)

Table 3-1. Anatomical regions of interest.

3.6 References

Arlotta P, Molyneaux B, Chen J, Inoue J, Kominami R, Macklis J (2005) Neuronal Subtype-Specific Genes that Control Corticospinal Motor Neuron Development In Vivo. Neuron 45:207–221.

Buga AM, Margaritescu C, Scholz CJ, Radu E, Zelenak C, Popa-Wagner A (2014) Transcriptomics of Post-Stroke Angiogenesis in the Aged Brain. Frontiers in Aging Neuroscience 6:44.

Carmichael ST, Kathirvelu B, Schweppe CA, Nie EH (2017) Molecular, cellular and functional events in axonal sprouting after stroke. Exp Neurol 287:384–394.

Chen P, Goldberg DE, Kolb B, Lanser M, Benowitz LI (2002) Inosine induces axonal rewiring and improves behavioral outcome after stroke. Proc National Acad Sci 99:9031 Available at: http://www.pnas.org/content/99/13/9031.abstract.

Chen J, Magavi SS, Macklis JD (2004) Neurogenesis of corticospinal motor neurons extending spinal projections in adult mice. Proc Natl Acad Sci USA 101:16357–16362.

Cismasiu VB, Adamo K, Gecewicz J, Duque J, Lin Q, Avram D (2005) BCL11B functionally associates with the NuRD complex in T lymphocytes to repress targeted promoter. Oncogene 24:6753–6764.

Fame RM, MacDonald JL, Macklis JD (2011) Development, specification, and diversity of callosal projection neurons. Trends Neurosci 34:41–50.

Hatanaka Y, Namikawa T, Yamauchi K, Kawaguchi Y (2016) Cortical Divergent Projections in Mice Originate from Two Sequentially Generated, Distinct Populations of Excitatory Cortical Neurons with Different Initial Axonal Outgrowth Characteristics. Cerebral Cortex 26:2257–2270.

Jang SW, Hwang SS, Kim HS, Kim MK, Lee WH, Hwang SU, Gwak J, Yew SK, Flavell RA, Lee GR (2019) Homeobox protein Hhex negatively regulates Treg cells by inhibiting Foxp3 expression and function. Proc National Acad Sci 116:25790–25799.

Kasamatsu S, Sato A, Yamamoto T, Keng VW, Yoshida H, Yamazaki Y, Shimoda M, Miyazaki J -i, Noguchi T (2004) Identification of the Transactivating Region of the Homeodomain Protein, Hex. J Biochem 135:217–223.

Leid M, Ishmael JE, Avram D, Shepherd D, Fraulob V, Dollé P (2004) Ctip1 and Ctip2 are differentially expressed during mouse embryogenesis. Gene Expr Patterns 4:733–739.

Lein ES et al. (2007) Genome-wide atlas of gene expression in the adult mouse brain. Nature 445:168–176.

Madisen L; Zwingman TA; Sunkin SM; Oh SW; Zariwala HA; Gu H; Ng LL; Palmiter RD; Hawrylycz MJ; Jones AR; Lein ES; Zeng H. 2010. A robust and high-throughput Cre reporting and characterization system for the whole mouse brain. Nat Neurosci 13(1):133-40PubMed: 20023653MGI: J:155793

Newman CS, Chia F, Krieg PA (1997) The XHex homeobox gene is expressed during development of the vascular endothelium: overexpression leads to an increase in vascular endothelial cell number. Mechanisms of Development 66:83–89.

Nikouei K, Muñoz-Manchado AB, Hjerling-Leffler J (2016) BCL11B/Ctip2 is highly expressed in GABAergic interneurons of the mouse somatosensory cortex. J Chem Neuroanat 71:1–5.

Noy P, Williams H, Sawasdichai A, Gaston K, Jayaraman P-S (2010) PRH/Hhex Controls Cell Survival through Coordinate Transcriptional Regulation of Vascular Endothelial Growth Factor Signaling. Mol Cell Biol 30:2120–2134.

Simpson MT, Venkatesh I, Callif BL, Thiel LK, Coley DM, Winsor KN, Wang Z, Kramer AA, Lerch JK, Blackmore MG (2015) The tumor suppressor HHEX inhibits axon growth when prematurely expressed in developing central nervous system neurons. Molecular and cellular neurosciences 68:272–283.

Tanaka T, Inazu T, Yamada K, Myint Z, Keng VW, Inoue Y, Taniguchi N, Noguchi T (1999) cDNA cloning and expression of rat homeobox gene, Hex, and functional characterization of the protein. Biochem J 339:111–117.

Tang B, Lena P, Schaffer L, Head S, Baldi P, Thomas E (2011) Genome-Wide Identification of Bcl11b Gene Targets Reveals Role in Brain-Derived Neurotrophic Factor Signaling. Plos One 6:e23691.

Uhlén M et al. (2015) Tissue-based map of the human proteome. Science 347:1260419.

Woodworth M, Greig L, Liu K, Ippolito G, Tucker H, Macklis J (2016) Ctip1 Regulates the Balance between Specification of Distinct Projection Neuron Subtypes in Deep Cortical Layers. Cell Reports 15:999–1012.

Yamakawa T, Sato Y, Matsumura Y, Kobayashi Y, Kawamura Y, Goshima N, Yamanaka S, Okita K (2016) Screening of Human cDNA Library Reveals Two Differentiation-related Genes, HHEX and HLX, as Promoters of Early Phase Reprogramming Toward Pluripotency. Stem cells (Dayton, Ohio) 34:2661–2669.

Zai L, Ferrari C, Subbaiah S, Havton LA, Coppola G, Strittmatter S, Irwin N, Geschwind D, Benowitz LI (2009) Inosine Alters Gene Expression and Axonal Projections in Neurons Contralateral to a Cortical Infarct and Improves Skilled Use of the Impaired Limb. J Neurosci 29:8187–8197.

Chapter 4

Evaluation of candidate gene ability to enhance functional recovery following stroke

4.1 Introduction

Axonal sprouting and cortical remodeling in the peri-infarct region have been associated with functional recovery following experimental cortical stroke. To explore if the identified developmental TFs showing a capacity to promote axonal growth can thereby promote functional recovery, motor skills were evaluated in mice via behavioral tasks requiring forelimb motor cortex use. This chapter details the implementation of three well-established behavioral tasks to assess recovery of forelimb motor function in the weeks and months following induction of ischemia in the forelimb motor cortex.

4.1.1 In vivo study of Hhex and Ctip2 to promote post-stroke motor recovery

Given the ability of both Hhex and Ctip2 to promote post-stroke axonal sprouting accompanied by relative synaptic density, a study of the ability of these transcription factors to promote motor recovery following stroke in forelimb motor cortex was assessed. Forelimb motor performance was evaluated using two behavioral tasks: gridwalk and pasta matrix. In the gridwalk task, gait is assessed as animals walk across a metal grid, and errors in stepping are identified as limbs falling through the grid. Following injury to the forelimb motor cortex, animals show a greater number of errors in stepping with the affected limb (Baskin et al., 2003). In the pasta matrix task, mice are trained to reach through a plexiglass chamber for pieces of capellini pasta, and reach performance and recovery is assessed following insult (Ballerman et al., 2001). These tests are

well-validated in this stroke model and thoroughly assess forelimb motor control, with both proximal and less precise motor movements (gait, reach) and precise distal limb movements (pasta manipulation).

Baseline behavior is assessed 1-3 days prior to stroke. As with axonal sprouting, ischemia is produced in mice via photothrombosis, and lentivirus overexpressing either Ctip2 or Hhex (or empty control) under a human synapsin promoter is injected in the peri-infarct region at the time of stroke. Acute behavioral deficits induced by ischemia are assessed 7 days post-stroke. Behavior continues to be assessed at weeks 4 and 8 for grid walking and weeks 3, 5, 7, and 9 for pasta matrix to determine the impact of Ctip2 and Hhex intervention on functional recovery.

4.1.2 Interpretations and potential limitations

As it has been previously shown that axonal sprouting in the peri-infarct region is associated with post-stroke motor improvement, it is hypothesized that those genes that showed an ability to promote axonal growth in Chapters 2 and 3 will promote recovery of forelimb motor function when overexpressed following focal cortical stroke. Though it is also expected that increased axonal sprouting will be correlated with behavioral recovery, it is possible that stimulating axonal sprouting will not promote motor recovery or even inhibit it. This would also be an important finding because it would indicate a role for the target TF in aberrant axonal sprouting that is ultimately detrimental to recovery. Similarly, if behavioral recovery is observed in the

absence of peri-infarct axonal sprouting (i.e. following overexpression of Ctip2), this would indicate a potential mechanism of the target gene in post-stroke neural repair that would be worthy of future study. Either of these alternative outcomes would be interesting and would provide a basis for future mechanistic studies.

4.2 Methods

4.2.1 Mice

All animals used for the studies described in this chapter were C57BL/6J strain male mice aged 2-4 months at the time of surgery (n = 12/group). Mice were obtained from the Jackson Laboratory (JAX stock #000664). Mice were randomly assigned to treatment groups. All experiments were performed in accordance with the National Institutes of Health animal protection guidelines and were approved by the University of California, Los Angeles Animal Research Committee (protocol #00-159).

4.2.2 Photothrombotic stroke and lentivirus injection

Ischemic stroke was produced in 2-4-month-old male mice using a photothrombotic approach as described in Chapter 3. Immediately following stroke, mice received 500nl injections in the anterior intact peri-infarct forelimb motor cortex with lentivirus(es) overexpressing Hhex

(n=12) or Ctip2 (n=12), or control virus (n=12, sham + control virus n=12). AAV9 pCAG-FLEX-EGFP-WPRE was a gift from Hongkui Zeng (Addgene viral prep # 51502-AAV9 ; http://n2t.net/addgene:51502 ; RRID:Addgene_51502) and injected as well to enable visualization of the Cre-expressing lentiviruses. All subsequent assays were performed by investigators blinded to condition.

4.2.3 Gridwalk

The gridwalk task was administered as previously described by our lab. (Baskin et al., 2003; Overman et al., 2012) Baseline behavior was assessed 1-3 days prior to stroke. Acute behavioral deficits induced by ischemia were assessed 7 days post-stroke, and gait was further assessed 4 and 8 weeks following stroke (**Figure 4-1**). The grid-walking apparatus was built using 12-mm square wire mesh with a grid area of 32 cm/20 cm/50 cm (length/width/height). A mirror was placed below the grid to facilitate video capture of the animals' gait and stepping errors ("footfaults") One trial was run per animal per testing day at approximately the same time each day. Each mouse was placed individually on the wire grid and allowed to walk freely for a period of 5 minutes while steps were video recorded.

Videos were scored by the investigator blinded to the condition. The number of total steps was counted, as defined as a forward movement incorporating a step from all four limbs. The number of footfaults was counted for the right forelimb, the stroke-affected limb. A forelimb step

was considered a footfault if the limb was not supporting the animal above the grid, leading to the forepaw slipping through the hole in the grid. The percentage of footfaults was calculated as [(number of footfaults / number of total steps) x 100]. A percentage of footfaults among total steps was employed to account for differences in the degree of locomotion between animals and trials.

4.3.3 Pasta matrix

The pasta matrix task was adapted from Ballermann et al. (2001). In this task, mice are placed in a plexiglass chamber and reach through a narrow window to retrieve small pieces of pasta (3.2 cm in length and 1 mm diameter) that have been vertically oriented in a matrix in front of the window. 2-3-month-old food-deprived mice were subjected to three weeks of training (6 days/week) prior to baseline assessment. Each mouse received one training session/day, during which they were placed in the plexiglass chamber and allowed to freely retrieve pieces of pasta. The total number of pasta pieces broken in a 15-minute session was recorded. Mice who did not reach a threshold of >3 breaks after three weeks of training were excluded from this analysis. Baseline behavior was assessed 1-3 days prior to stroke. Acute behavioral deficits induced by ischemia were assessed 7 days post-stroke, and behavior was further assessed at 3, 5, 7, and 9 weeks post-stroke (**Figure 4-1**).

4.3.4 Tissue collection

Following the completion of behavioral assessment nine weeks following stroke, animals were sacrificed via transcardial perfusion with cold saline followed by 4% PFA. Brains were post-fixed in 4% PFA at 4°C overnight and cryoprotected in 30% sucrose at 4°C for 24h prior to coronal sectioning on a cryostat (Leica CM 0530). 40 μm sections were collected and stored in a 50% glycerol antifreeze solution at –20°C until immunohistochemical staining.

4.3.5 Immunohistochemistry

Immunohistochemistry for infarct size analysis was prepared according to a lab protocol. Briefly, sections were removed from 50% glycerol solution and washed three times in 0.02M KPBS for 5 minutes. Tissues were blocked in a solution of 5% normal donkey serum (NDS), 0.1% Triton-X in KPBS for 1h at room temperature. Sections were then incubated in primary antibody solution of anti-NeuN (1:000, rabbit, Abcam ab177487) and anti-GFAP (1:500, rat, Thermo Fisher 13-0300) prepared in 2% NDS, 0.1% Triton-X in KPBS overnight at 4°C. Following primary incubation, sections were washed three times in KPBS, and then incubated in a secondary antibody solution of anti-rabbit 488 (1:500, JAX), anti-rat 647 (1:500 JAX), and DAPI (1:1000 from 250 ug/ml stock) in 2% NDS, 0.1% Triton-X in KPBS for 1h at room temperature. Tissues were washed 3 times in KBPS for 5 minutes before mounting on triple-subbed slides. Slides were dehydrated with ethanol washes 50-100% (1 min each) and xylene washes (2 min, 5 min) prior to coverslip

application with DPX mounting media. All tissues were protected from light for the entirety of the immunohistochemical protocol.

4.3.6 Infarct size analysis

Coronal sections representing every 240 μm were stained with GFAP and DAPI as described above and acquired at 4x using a Nikon confocal microscope and Nikon Elements software. Images were subsequently analyzed in ImageJ. The infarct border was defined by the GFAP+ astrocytic scar which was traced for area measurements in ImageJ. The section with the greatest infarct area measurement was selected as representative for each animal, and average infarct size was calculated for each treatment group.

4.3.6 Statistics

Sample sizes were assessed by power analysis using a significance level of a = 0.05 with 80% power to detect differences in ANOVA. Behavioral data were analyzed using a two-way ANOVA followed by Dunnett's multiple comparisons test. Infarct size data were analyzed using ordinary one-way ANOVA followed by Dunnett's multiple comparisons test. Mice assigned to stroke groups were excluded from behavioral analysis if they did not show signs of stroke when assessed for infarct size. Statistical analysis and graph generation was conducted using GraphPad Prism software (version 8.4.3)

4.3 Results

4.3.1 Overexpression of Hhex or Ctip2 is associated with accelerated recovery in gridwalk task

All mice were assessed for baseline gait performance in the gridwalk task 1-3 days prior to stroke and peri-infarct viral administration (**Figure 4-1**). Across all groups, animals consistently averaged about 10% footfaults (relative to total number of steps) at baseline (**Figure 4-2**). One week following surgery, all stroke groups nearly doubled their average percentage of footfaults, demonstrating a significant impairment in gait compared to pre-stroke performance (Baseline vs. 1 Week: Stroke Control $p = 0.0004$; Stroke Ctip2 $p = 0.0007$; Stroke Hhex $p = 0.0009$; two-way ANOVA followed by Dunnett's multiple comparisons test) and compared to performance of sham mice at one week (1 Week: Stroke Control vs Sham Control $p = 0.0124$; Stroke Ctip2 vs. Sham Control $p = 0.0207$; Stroke Hhex vs. Sham Control $p = 0.0128$; two-way ANOVA followed by Dunnett's multiple comparisons test). One month post stroke, mice that received a stroke with control virus continue to show impairment (avg. 20.2% footfaults) compared to Sham Control ($p = 0.0018$), but those mice that received a stroke with Hhex or Ctip2 viral overexpression have accelerated improvement. At one month post-stroke, Hhex and Ctip2 treated mice show reduced footfaults that are not statistically different from sham control (4 Weeks: Stroke Ctip2 vs. Sham Control $p = 0.1077$; Stroke Hhex vs. Sham Control $p = 0.1701$; two-way ANOVA followed by

Dunnett's multiple comparisons test). By two months post-stroke, all stroke animals demonstrated a degree of gait recovery. At this time point, all stroke groups return to performance that is statistically similar to sham control (8 Weeks: Stroke Control vs Sham Control p = 0.6980; Stroke Ctip2 vs. Sham Control p = 0.2487; Stroke Hhex vs. Sham Control p = 0.4998; two-way ANOVA followed by Dunnett's multiple comparisons test) (**Figure 4-2**).

4.3.2 Hhex-treated mice show elevated performance in pasta matrix task

All mice were assessed for baseline performance in the pasta matrix task 1-3 days prior to stroke. One week following stroke, all mice showed some degree of impairment in performance in this task, with the stroke control group showing the greatest decline in performance (**Figure 4-3**). Two-way ANOVA followed by Dunnett's multiple comparisons test revealed that Hhex-treated animals showed a statistically significant (p = 0.0030) elevation in overall performance compared to stroke control over the course of the study. Ctip2 treatment did not show as clear of an effect on performance in the task. However, when a two-way ANOVA followed by Dunnett's multiple comparisons test is employed to evaluate performance compared to sham control, mice in the stroke control group performed significantly worse than the sham group throughout the course of the study (p = 0.0482), while performances of Ctip2 and Hhex groups are not significantly different from sham control (p = 0.8736 and p = 0.5159, respectively).

4.3.3 Functional recovery is not correlated with infarct size

Mice were sacrificed after completion of their final behavioral assessment at nine weeks following stroke, after which stroke size was measured via tracing of GFAP+ infarct border. As indicated in **Figure 4-4**, no significant differences in infarct size were observed across treatment groups. This suggests that differences in functional recovery observed across experimental groups are not directly related to changes in infarct size.

4.4 Discussion

Chapter 3 detailed the impact of Hhex or Ctip2 overexpression on post-stroke axonal sprouting. Given the established correlation between cortical reorganization and functional recovery following stroke (Carmichael et al., 2017), the studies in this chapter sought to evaluate the ability of Hhex and Ctip2 to enhance recovery of gait and reach function following stroke to the forelimb motor cortex.

In the gridwalk task, all animals that received a stroke show a significant degree of impairment one week following insult, as measured by the percentage of total steps that included a footfault. By one month following stroke, however, both Ctip2 and Hhex treated mice show improved gait performance compared to stroke control mice. The percentage of footfaults recorded by Hhex- and Ctip2-treated mice at this timepoint was not statistically different from that of sham

mice. By two months following stroke, all stroke mice showed recovery of gait function such that there was no significant difference in percentage of footfaults between stroke groups and sham mice. These findings indicate that there is an ability of either Hhex or Ctip2 to accelate motor recovery following a stroke to the forelimb motor cortex. This is particularly interesting because Hhex and Ctip2 induced different patterns of axonal sprouting at one month following stroke: Hhex promoted widespread axonal growth within the peri-infarct cortex and in contralesional structures, while Ctip2 primarily increased axonal sprouting from the peri-infarct region to the contralesional cortex. The patterns of sprouting observed with Hhex treatment have previously been associated with functional recovery (Overman et al., 2012; Li et al., 2015; Carmichael et al., 2017), but the patterns of sprouting observed with Ctip2 overexpression have been less definitively characterized. These findings suggest that these longer-distance patterns of axonal growth may also be associated with functional recovery and peri-infarct sprouting may not be necessary for recovery for all forms of motor function following stroke to the forelimb motor region.

There are a few limitations to this experiment that beg further study. First, it is not yet clear which motor circuits are primarily responsible for this accelerated recovery of motor function. Selected inactivation of these circuits following stroke and gene overexpression may reveal a role for specific circuitry in accelerating recovery. Additionally, further study of the roles of Ctip2 and Hhex in motor recovery using the gridwalk task as a read of gait function would benefit from more frequent testing. In this experiment, mice were evaluated at baseline, one week, one month, and

two months post stroke, but there was a significant degree of spontaneous recovery that occurred during the second month. This is to be expected: as with humans, mice also show some level of spontaneous recovery in the days, months, and years following stroke (Carmichael et al., 2017). When scaled to a human lifespan, this two-month timeline of recovery in the adult mouse would represent roughly two decades of human life (Dutta and Sengupta, 2015). Given this, future studies would benefit from weekly or bi-weekly testing to more precisely evaluate the timeline of accelerated recovery with Hhex or Ctip2 manipulation.

The pasta matrix task was used to evaluate recovery of stroke-induced impairment in both reach and fine motor manipulation. In this task, all animals showed some degree of impairment at one week post stroke, however even at this timepoint Hhex- and Ctip2-treated animals demonstrated performance that was not statistically different from sham animals, a trend that continued throughout the course of the study. This indicates that both Hhex and Ctip2 overexpression have a degree of positive effect on functional recovery following stroke. That being said, the Hhex-treated group alone reached a threshold of significantly elevated performance throughout the course of this study compared to the stroke control group. This suggests that Hhex manipulation, and perhaps the peri-infarct axonal sprouting that is seen with Hhex overexpression but not Ctip2 overexpression, has greater potential to promote recovery of reach and fine motor function following ischemic motor stroke.

Interestingly, animals did not show the same degree of spontaneous recovery in the pasta matrix task as observed in the gridwalk test. Stroke control animals continued to show a significant deficit in this task throughout all 9 weeks of study, whereas spontaneous recovery was observed in the gridwalk test by 8 weeks post-stroke. There are a few explanations for why this could be occurring. First, it is possible that the mice do not show spontaneous recovery as quickly in the pasta matrix task because they don't have the opportunity to practice their specific reach skills for this task beyond the initial training period (prior to baseline testing). This task is administered daily during the training period leading up to baseline testing, one week after the stroke, and every two weeks thereafter. It may take longer to recover a specific motor function that is not frequently engaged or required of the animal. In contrast, the gridwalk test is a measure of gait function, something that the mice are able to engage frequently through ad-lib walking in their home cage. Additionally, the pasta matrix task relies primarily on the function of the impaired limb for success. Though the gridwalk test does measure disability of the impaired limb, simply walking in the grid engages the uninjured limbs which may be having a compensatory effect on overall performance.

Ultimately, the differences in outcomes between the gridwalk task and the pasta matrix task are not surprising: each task measures unique elements of motor function that rely on different motor circuits. An important area of future study will be further exploration of the interaction between Hhex or Ctip2 manipulation and specific motor circuitry. It is also important to take a step back and view this through the lens of potential translational relevance. In the assessment of clinical

outcomes in human stroke patients, a greater than 10% increase in motor function may represent a clinically meaningful improvement in a patient's daily life (Gladstone et al., 2002). In this study, we observed a consistent 3 to 4-fold increase in motor function with Hhex treatment in the pasta matrix task, and both Ctip2 and Hhex treated mice showed an average of 50% improvement in the gridwalk test compared to stroke control. Taken together, these findings suggest a potential for either Hhex or Ctip2 to play a significant clinical role in promoting functional recovery following stroke to motor regions of the brain.

4.5 Figures

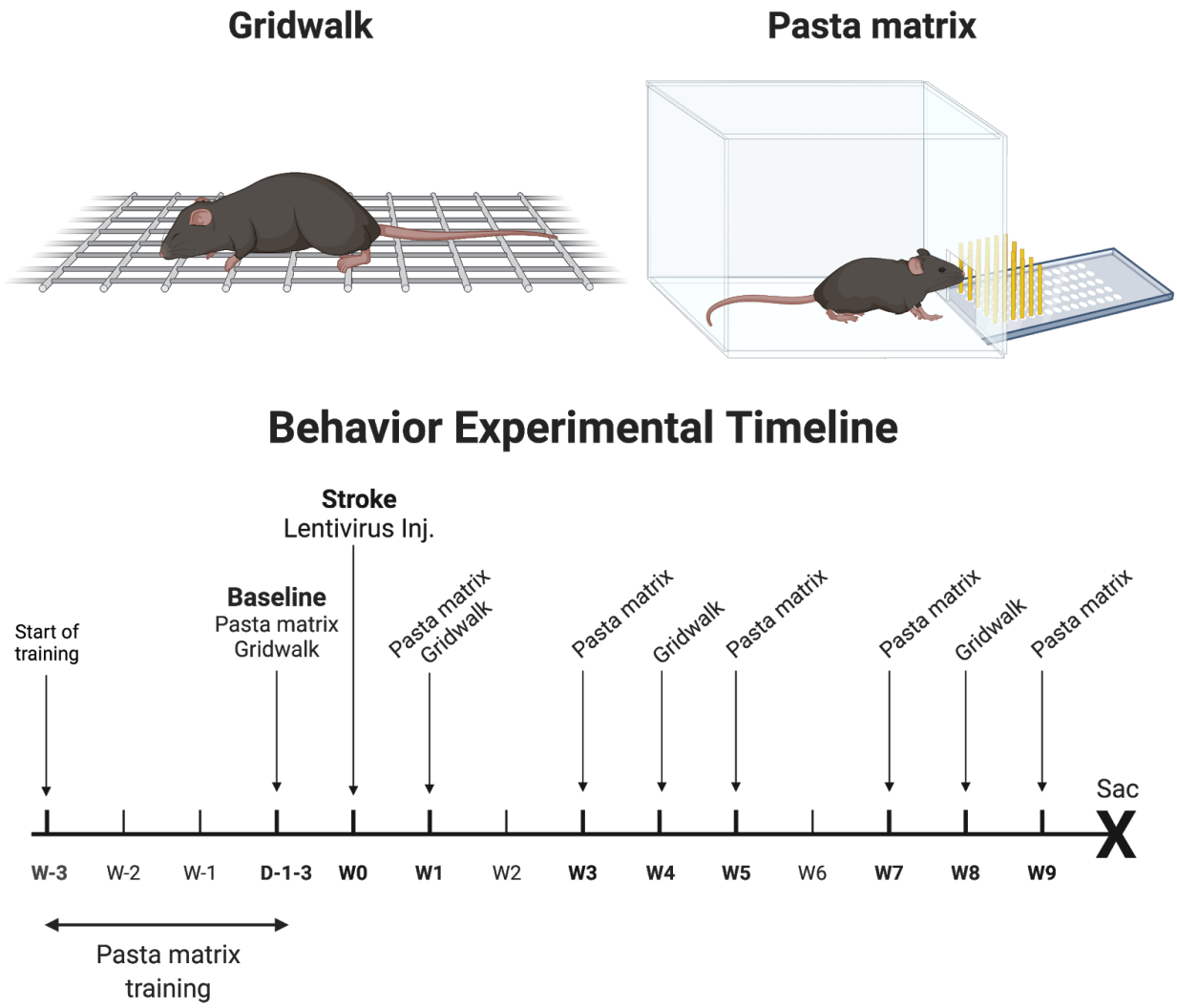

Figure 4-1. Behavior experimental timeline. 2-3-month-old food-deprived mice (n=12/group) were subjected to three weeks of training (6 days/week) prior to baseline assessment. Baseline behavior was assessed 1-3 days prior to stroke. Acute behavioral deficits induced by ischemia were assessed one week post stroke for gridwalk and pasta matrix tasks. Behavior was further assessed at 3, 5, 7, and 9 weeks post-stroke for the pasta matrix task and at 4 and 8 weeks following stroke for the gridwalk task. Created with BioRender.com.

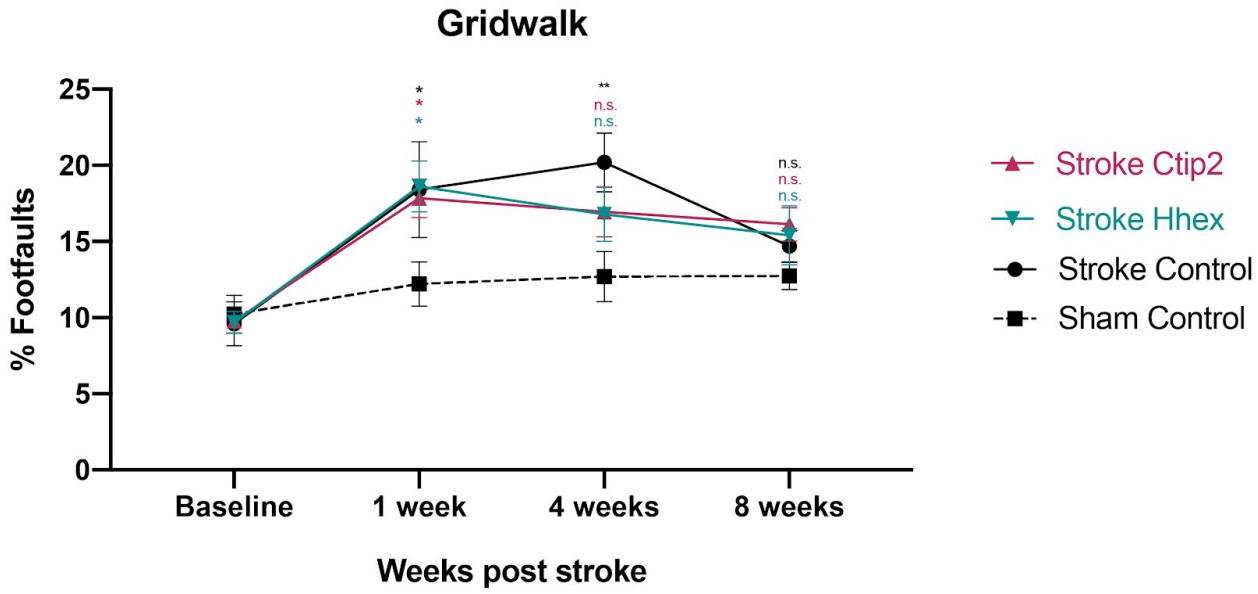

Figure 4-2. Gridwalk gait assessment. Gait performance was measured as percentage of footfaults [(number of footfaults / number of total steps) x 100]. Baseline gait performance was assessed 1-3 days prior to stroke. Acute behavioral deficits induced by ischemia were assessed 1 week post stroke, and gait was further assessed 4 and 8 weeks following stroke. Animals averaged about 10% footfaults at baseline. One week following surgery, all stroke groups nearly doubled their average percentage of footfaults (Baseline vs. 1 Week: Stroke Control p = 0.0004; Stroke Ctip2 p = 0.0007; Stroke Hhex p = 0.0009) and are significant impaired compared to sham mice (1 Week: Stroke Control vs Sham Control p = 0.0124; Stroke Ctip2 vs. Sham Control p = 0.0207; Stroke Hhex vs. Sham Control p = 0.0128). One month post stroke, Stroke Control mice continue to show impairment (avg. 20.2% footfaults) compared to Sham Control (p = 0.0018), but Hhex and Ctip2 treated mice show reduced footfaults that are not statistically different from sham control (4 Weeks: Stroke Ctip2 vs. Sham Control p = 0.1077; Stroke Hhex vs. Sham Control p = 0.1701). By two months post-stroke, all stroke animals demonstrated a degree of gait recovery. At this time point, all stroke groups return to performance that is statistically similar to sham control (8 Weeks: Stroke Control vs Sham Control p = 0.6980; Stroke Ctip2 vs. Sham Control p = 0.2487; Stroke Hhex vs. Sham Control p = 0.4998). All comparisons were conducted via two-way ANOVA followed by Dunnett's multiple comparisons test.

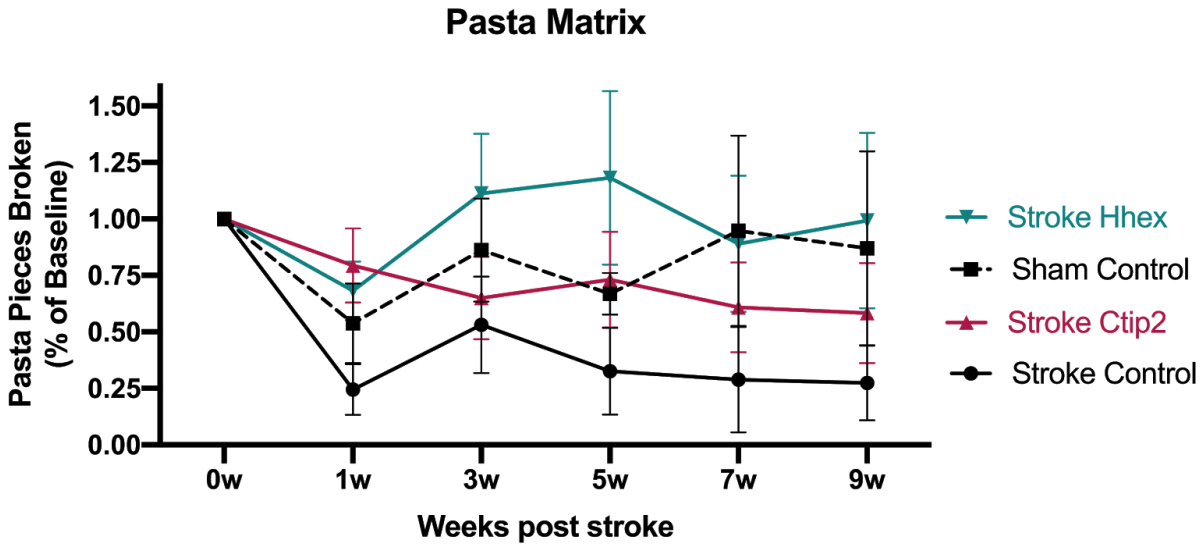

Figure 4-3. Pasta matrix assessment of reach. All mice domonstrated impairment in performance in this task following stroke, with the Stroke Control group showing the greatest decline in performance. Two-way ANOVA followed by Dunnett's multiple comparisons test revealed that Hhex-treated animals showed a statistically significant ($p = 0.0030$) elevation in overall performance compared to Stroke Control over the course of the study.

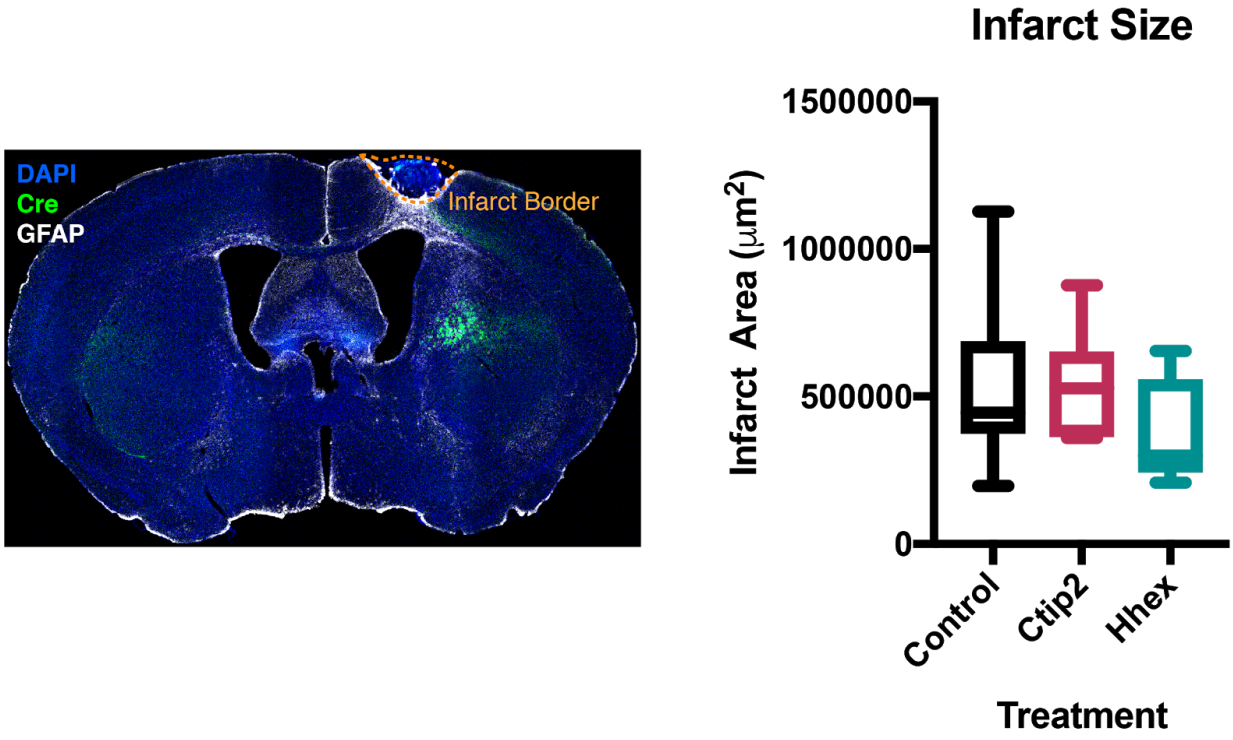

Figure 4-4. Infarct size analysis. Infarct border was defined by the GFAP+ astrocytic scar which was traced for area measurements in ImageJ (left). No significant differences in infarct size were observed across treatment groups as measured by ordinary one-way ANOVA and Dunnett's multiple comparisons test (right).

4.6 References

Ballermann M, Metz GAS, McKenna JE, Klassen F, Whishaw IQ (2001) The pasta matrix reaching task: a simple test for measuring skilled reaching distance, direction, and dexterity in rats. J Neurosci Meth 106:39–45.

Baskin YK, Dietrich WD, Green EJ (2003) Two effective behavioral tasks for evaluating sensorimotor dysfunction following traumatic brain injury in mice. J Neurosci Meth 129:87–93.

Carmichael ST, Kathirvelu B, Schweppe CA, Nie EH (2017) Molecular, cellular and functional events in axonal sprouting after stroke. Exp Neurol 287:384–394.

Dutta S, Sengupta P (2016) Men and mice: Relating their ages. Life Sci 152:244–248.

Gladstone DJ, Danells CJ, Black SE (2002) The Fugl-Meyer Assessment of Motor Recovery after Stroke: A Critical Review of Its Measurement Properties. Neurorehab Neural Re 16:232–240.

Oh SW et al. (2014) A mesoscale connectome of the mouse brain. Nature 508:207–214.

Overman JJ, Clarkson AN, Wanner IB, Overman WT, Eckstein I, Maguire JL, Dinov ID, Toga AW, Carmichael ST (2012) A role for ephrin-A5 in axonal sprouting, recovery, and activity-dependent plasticity after stroke. Proc National Acad Sci 109:E2230–E2239.

Tennant KA, Asay AL, Allred RP, Ozburn AR, Kleim JA, Jones TA (2010) The Vermicelli and Capellini Handling Tests: Simple quantitative measures of dexterous forepaw function in rats and mice. J Vis Exp Jove:2076.

Chapter 5

Transcriptional profiling of Hhex- and Ctip2-induced post-stroke axonal sprouting

5.1 Introduction

The preceding chapters have introduced a body of evidence for a role of the developmentally-associated transcription factors Ctip2 and Hhex in promoting axonal growth and functional recovery in the context of cortical ischemic stroke. One consistent finding has been, unsurprisingly, that there isn't clear consistency between these genes in their downstream effects. Ctip2 and Hhex showed differing effects on growth in neuronal culture: Ctip2 promoted growth only in early postnatal cultures, while Hhex demonstrated an ability to promote growth in both early postnatal and late postnatal cultures (**Chapter 2**). Ctip2 and Hhex showed differences in their impact on post-stroke axonal sprouting when overexpressed in the anterior premotor cortex following stroke to the forelimb motor cortex: both Ctip2 and Hhex demonstrated an ability to increase density of axon projections to the contralesional cortex, but only Hhex showed an ability to promote sprouting in the ipsilesional cortex (**Chapter 3**). In studies of motor recovery following stroke to the forelimb motor cortex, overexpression of these genes in the anterior premotor cortex also showed differing results: both Ctip2 and Hhex overexpression were linked to accelerated recovery of gait function, but Hhex overexpression showed a more defined effect on recovery of reach and fine motor manipulation (**Chapter 4**). Again, this is not surprising. Though Ctip2 and Hhex are both developmentally-associated transcription factors that have the ability to activate or repress gene expression directly or indirectly, that is where their similarities end. There is little overlap in their known downstream targets, so it remains a definite possibility that these genes are acting through different biological pathways to induce states of growth.

In order to better understand how these gene systems are acting in the post-stroke brain, a bulk RNA sequencing approach was selected. The goal of this study was to evaluate the canonical pathways and molecular systems associated with Ctip2 or Hhex overexpression in the context of stroke. Given the differences outlined above, it was hypothesized that though Ctip2 and Hhex both show effects on axon growth and functional recovery, these transcription factors are likely regulating different downstream signaling pathways. **Figure 5-1** outlines the experimental approach for the study detailed in this chapter. As in previous studies, Ctip2 and Hhex were virally overexpressed following photothrombotic stroke to the forelimb motor cortex. Ai9 mice were once again employed (as in Chapter 3) in order to achieve robust neuronal tdTomato labeling with Cre-containing lentiviruses. Neurons were isolated from the brain at one month post stroke via enzymatic dissociation followed by fluorescence-activated cell sorting (FACS), total RNA was extracted from cells, and RNA was library prepped followed by sequencing. Bioinformatic analyses were conducted in collaboration with the AMRF Functional Genomics Common Research Resource at UCLA. These analyses are currently ongoing to further probe these datasets, but preliminary findings are detailed in this chapter.

5.2 Methods

5.2.1 Mice

All animals used for the studies described in this chapter were Ai9 strain male mice (Madisen et al 2010) aged 2-4 months at the time of surgery (n = 16 total, n = 4/group). Mice were obtained from the Jackson Laboratory (JAX stock #007909). Mice were randomly assigned to one of four treatment groups such that there was one mouse representing each treatment group per surgery and FACS collection session (four sessions total). All experiments were performed in accordance with the National Institutes of Health animal protection guidelines and were approved by the University of California, Los Angeles Animal Research Committee (protocol #00-159).

5.2.2 Lentiviral vectors

Lentiviral vectors used in the studies outlined in this chapter were the same as described in Chapter 3.

5.2.3 Photothrombotic stroke and lentivirus injection

Ischemic stroke was produced in 2-4-month-old male Ai9 mice using a photothrombotic approach. Anesthesia was induced with 4% isoflurane supplied with 100% O_2 and maintained at 2% isoflurane for the duration of the procedure. Body temperature was maintained at 37.0 ˚C +/-0.5˚C by homeothermic heating pads. Under isoflurane anesthesia, mice were placed in a stereotactic apparatus (Model 900, David Kopf Instruments) with the skull exposed through a midline incision,

cleared of connective tissue, and dried. The photosensitive dye Rose Bengal (100 mg/kg in sterile PBS) was injected intraperitoneally (concentration 10 mg/ml) to enter the bloodstream. After 5 minutes, the skull was revealed and 520 nm wavelength laser light (laser light source CLD1010LP, ThorLabs; laser diode LP520-MF100, ThorLabs) at 10.5 mW output was targeted to the forelimb motor cortex (coordinates from Bregma: 1.5 mm medial, 0.0 mm anterior/posterior) for 10 minutes to activate the photosensitive dye and induce focal ischemia. When activated by light targeted through the skull to a precise area of the cortex, endothelial damage with platelet activation and thrombosis is induced, resulting in local blood flow disruption. This technique allows for precise targeting of ischemic infarct to the forelimb motor cortex. Immediately following stroke, mice received injections in the anterior intact peri-infarct forelimb motor cortex (coordinates from Bregma: 1.75 medial, 1.5 mm anterior, 0.7 mm ventral) with 500 nl lentivirus overexpressing Hhex or Ctip2, or control virus. A dental drill was used to create a small hole in the skull to allow for needle access, through which a 30-gauge Hamilton needle attached to a 25 ul syringe was lowered into the cortex. Virus was infused into the brain at 0.1 μl/min. After intracranial injection, the needle was allowed to remain in the brain for an additional 5 minutes, after which the needle was slowly removed from the brain, the wound was closed with Vetbond tissue adhesive (70200742529, 3M), and animals were returned to their home cage for recovery.

5.2.4 Isolation of virally transduced neurons

Virally transduced neurons were isolated from the brain for downstream FACS sorting and RNA sequencing at 28 days following stroke. A modified protocol for the Adult Brain Dissociation Kit (Miltenyi Biotec) was employed. Mice were deeply anesthetized with 5% isoflurane prior to sacrifice by cervical dislocation and decapitation. A midline incision of the scalp revealed the underlying skull which was carefully removed with forceps to allow access to the brain. The brain was quickly rinsed with ice-cold D-PBS (with added calcium and magnesium) and transferred to a petri dish for dissection in D-PBS. Cortices were separated from underlying white matter, hippocampal formations were removed, and tissue from the ischemic hemisphere was divided into 2 mm sagittal slices and collected in tubes containing D-PBS and proprietary dissociation enzymes (Miltenyi Biotec). Tissue was dissociated for 30 minutes at 37°C with heat and agitation provided by a GentleMACS Octo Dissociator with Heaters (Miltenyi Biotec). Following dissociation, tissue suspension was passed through a 70 μm cell strainer into a 50 mL conical tube with an additional 10 mL D-PBS and centrifuged at 300 x g for 10 min at 4°C. Supernatant was aspirated completely, and cell pellet was rinsed with 3100 μL D-PBS. 900 μL proprietary Debris Removal Solution (Miltenti Biotec) was added, and an additional 4 mL cold D-PBS was carefully overlayed on cell suspension. Cells were centrifuged at 3000 x g for 10 min at 4°C, forming three distinct phases. The top two phases were aspirated, and ~11 mL cold D-PBS was added to the remaining bottom phase for a total volume of 15 mL. Cell suspension was inverted 3-5 times then centrifuged at 1000 x g for 10 min at

4°C. Supernatant was discarded, and the pellet was resuspended in 1 mL Red Blood Cell Removal Solution (Miltenyi Biotec), incubated for 10 min at 4°C, then centrifuged at 300 x g for 10 min at 4°C. Supernatant was discarded, the cell pellet was resuspended in Hibernate A medium (BrainBits). One cortical hemisphere was dissociated for each FACS sample, for a total of 16 samples across 4 experimental groups.

5.2.5 FACS

Prior to flow cytometry, all cell suspensions were stained for live cell bodies using DRAQ5 and dead cell bodies using DAPI. Samples were maintained on ice before and during FACS isolation. Cy3 sorting gates were defined by a negative control of neuronal cells collected from an Ai9 mouse that had not received Cre lentiviral injection. The td-Tomato+ neurons were collected via FACS (FACSAria, BD Biosciences, UCLA Broad Stem Cell Research Center Flow Cytometry Core) into Hibernate medium on ice prior to RNA extraction.

5.2.6 RNA isolation

Total RNA was purified from 16 samples of FACS-isolated neurons using the *Quick*-RNA Microprep Kit (Zymo Research). RNA was eluted into 10 μl dd-H_2O and stored at -80° C prior to quality control analysis.

5.2.7 RNA library preparation and sequencing

Total RNA quality was verified via Bioanalyzer 2100 (Agilent Technologies), which provided an RNA integrity number (RIN) for each sample. A RIN reading of >5 ensured high-quality input RNA. Library preparation was conducted by the UCLA Neuroscience Genomics Core as previously described (Li et al., 2015; Nie, 2016). Total RNA was amplified and converted into double-stranded DNA. RNA libraries were prepared using a NuGen Ovation Ultra Low Mass kit for paired-end 2x75 RNA-sequencing (HiSeq2500, UCLA Neuroscience Genomics Core). After cDNA library preparation (Encore NGS Library System I, NuGen), amplified double-stranded cDNA was fragmented into 300 bp. DNA fragments were end-repaired to generate blunt ends with 59 phosphatase and 39 hydroxyls and adapters ligated. The purified cDNA library products were evaluated via Bioanalyzer 2100, quantified via Illumina Library Quantification Kit (KAPA Biosystems), and diluted to 10 nM for cluster generation in situ on the HiSeq paired-end flow cell using the CBot automated cluster generation system.

All libraries were sequenced using an Illumina HiSeq2500 sequencer (UCLA Neuroscience Genomics Core) across two lanes of 75-bp paired-end sequencing. After demultiplexing, between 37 and 51 million reads were obtained per sample.

5.2.9 Bioinformatics

Reads were aligned to the latest mouse mm10 reference genome using the STAR spliced read aligner (Dobin et al., 2013) (**Table 5-1**). Total counts of read-fragments aligned to known gene regions within the mouse mm10 refSeq reference annotation were used as the basis for the quantification of gene expression. QC analyses were conducted to assess the quality of the data and to identify potential outliers. Additional QC was performed after the alignment to examine: the level of mismatch rate, mapping rate to the whole genome, repeats, chromosomes, and key transcriptomic regions (exons, introns, UTRs, genes). Fragment counts were derived using the HTS-seq program with mm10 Ensembl transcripts as a model.

Differentially expressed genes were identified using three Bioconductor packages within the statistical environment R: edgeR, limma+voom, and limma, which were then considered and ranked based on False Discovery Rates (FDR, FDR Benjamini Hochberg adjusted p-values) of < 0.01 and simple p-values of ≤ 0.05. The results of DE genes from the three packages were also compared. DE genes were further analyzed for enriched canonical pathways and molecular signaling systems using Ingenuity Pathway Analysis (IPA, QIAGEN). For IPA analysis, differentially expressed genes were identified using EdgeR for Stroke Hhex vs Stroke Control and Stroke Ctip2 vs Stroke Control and filtered to only include genes with FDR < 0.01. These gene sets were then uploaded to IPA and compared to all genes known to be involved in a given canonical pathway or molecular signaling system in a large, manually curated database of molecular interactions within biological systems.

Benjamini Hochberg adjusted p-values were calculated by IPA to determine significant overlaps between these experimental datasets and the probed molecular pathways.

5.3 Results

5.3.1 FACS purification of adult cortical neurons

The experimental timeline for surgeries and isolation of transduced cortical neurons is presented in **Figure 5-1**. Neuronal cells from the ipsilesional cortex were isolated 28 days post-stroke and further sorted for virally transduced cells using flow cytometry. Representative plots from FACS runs for each experimental group are presented in **Figure 5-2**. On average, between 8,000 and 20,000 tdTomato+ cells were collected per sample.

5.3.2 Quality control analyses

Total RNA quality was verified via Bioanalyzer 2100, and resulting RIN values are presented in **Figure 5-3**. RIN values ranged from 5 to 9.5, and no samples were excluded from sequencing based on RIN values. Further quality control was carried out at the bioinformatics level prior to alignment. The number of total reads obtained from sequencing was 37.3 million to 50.6 million (average 43.7 million reads). No reads or samples were excluded based on Phred score (Cock et al., 2009). No read trimming was conducted with this dataset. Short reads were aligned using STAR to the latest mouse reference genome (mm10), with default parameters. The results of this alignment

are presented in **Table 5-1**. The percentage of uniquely mapped reads was 58.34% to 63.34% (average 60.76%). Uniquely aligned reads and transcript coverages were similar across samples. Read counts were normalized across samples using the approach described by Robinson and Oshlack (2010) prior to differential expression analysis.

Multiple clustering methods were used to examine the quality of replicates and to highlight possible outlier samples for potential exclusion. Hierarchical clustering, batch effect clustering, and multidimensional scaling were applied to normalized raw counts via variance stabilized transform (VST) normalized count expression values. At this point, it did not appear that samples were clustering together by condition with these methods, suggesting potential artifacts in the sequencing data. In order to overcome these artifacts, a remove unwanted variants (RUV) approach was taken (Risso et al., 2014). The resulting cluster analyses are presented in **Figure 5-4**. Differential expression analyses were subsequently performed on this cleaned data.

5.3.3 Differential expression analyses (preliminary)

Differentially expressed genes were identified using the Bioconductor EdgeR package. The EdgeR package models read count data using a negative binomial distribution in order to bypass the common type-I errors associated with overdispersed models (Anders and Huber, 2010). Data from Sham Control, Stroke Ctip2, or Stroke Hhex were compared to Stroke Control. Gene changes identified by simple p-value ($p < 0.01$, $p < 0.05$, or $p < 0.1$) and FDR (either FDR < 0.05 or no FDR) are presented in **Figure 5-5**. Notably, the number of differentially expressed genes between Stroke

Ctip2 or Stroke Hhex and Stroke Control was far greater than the number of differentially expressed genes between Sham Control and Stroke Control. With an FDR threshold of < 0.05 and a simple p value of $p < 0.05$, there were a total of 70 differentially expressed genes between Sham Control and Stroke Control, 698 differentially expressed genes between Stroke Hhex and Stroke Ctip2, and 1,026 differentially expressed genes between Stroke Ctip2 and Stroke Control (**Figure 5-5, top middle**).

Further inspection into the relationship of these genes and samples was visualized via clustering. In contrast to the previous clustering analyses in which expression levels of all genes were factored in, now a variance stabilization transform of scaled expression levels of the top-ranked DE genes was conducted. This transform can be understood as a moderated log transformation to quantify the data so it becomes approximately homoscedastic. By then applying a Euclidean distance function to it we can visualize the data in a heatmap to observe sample and gene clustering based on this distance function. This heatmap is presented in **Figure 5-6**.

Gene set enrichment analysis was performed using EnrichR, a web-based tool for analyzing gene sets. This enrichment analysis is a computational method for inferring knowledge about an input gene set by comparing it to gene ontology annotations sets representing prior biological knowledge (Chen et al., 2013; Kuleshov et al., 2016). Gene ontology biological processes, cellular components, and molecular functions were assessed. The results of the Stroke Ctip2 vs Stroke Control gene ontology enrichment analysis are presented in **Figure 5-7**. Significantly downregulated genes are associated with nervous system development, axonogenesis, regulation of

cell growth, myelination, and enrichment in the plasma membrane and main axon. Significantly upregulated genes are primarily associated with immune function and cytokine response. The results of the Stroke Hhex vs Stroke Control gene ontology enrichment analysis are presented in **Figure 5-8**. Significantly downregulated genes are associated with forebrain neuron differentiation. Significantly upregulated genes are largely associated with ATP generation, respiration, and mitochondrial function.

5.3.4 Ingenuity Pathway Analysis (preliminary)

For a more comprehensive evaluation of canonical pathways associated with overexpression of transcription factors Ctip2 or Hhex in the context of stroke, Ingenuity Pathway Analysis (IPA, Qiagen) was employed. Differentially expressed gene sets for Stroke Ctip2 vs Stroke Control and Stroke Hhex vs Stroke Control were filtered through an FDR threshold of < 0.1 for pathway analysis. The top 20 canonical pathways associated with Ctip2 overexpression following stroke were ranked based on Benjamini Hochberg adjusted p-values and are illustrated in **Figure 5-9**. These pathways include Tec kinase signaling, axonal guidance signaling, integrin signaling, CREB signaling in neurons, and synaptogenesis signaling pathway.

Canonical pathways associated with Hhex overexpression following stroke were ranked in the same manner and are illustrated in **Figure 5-10**. Similar to the gene ontology analysis detailed above, Hhex overexpression following stroke was associated with cellular metabolism: oxidative phosphorylation, mitochondrial dysfunction, and sirtuin signaling are three of the top five most

highly ranked pathways. The other two pathways rounding out the top five are associated with EIF2 Signaling and regulation of EIF4 and p70S6K signaling. Notably, Hhex overexpression is also associated with mTOR signaling, PTEN signaling, and (like Ctip2 overexpression) CREB signaling in neurons.

5.4 Discussion

Previous chapters have detailed studies implicating the overexpression of transcription factors Ctip2 and Hhex in the ability to promote axonal sprouting and functional recovery in the context of ischemic stroke. A number of studies have investigated the role of these genes in developmental contexts, but none have evaluated their function within neurons in the ischemic brain. The purpose of the studies in this chapter was to begin to evaluate the downstream signaling pathways associated with overexpression of either Ctip2 of Hhex in the premotor cortex following stroke to the forelimb motor cortex. For these studies, mice were sacrificed one month (28 days) following stroke and virus injection, and virally-transduced neurons were isolated via enzymatic dissociation followed by FACS. RNA was extracted from isolated neurons and underwent bulk RNA sequencing. Differential gene expression analysis was performed, revealing unique patterns of downstream signaling induced by either Ctip2 or Hhex compared to stroke control. These analyses are ongoing, but preliminary results are presented in this chapter.

Gene ontology and IPA analyses revealed a number of neuronal and axonal specific pathways enriched with overexpression of Ctip2 following stroke compared to stroke control. This

is not surprising, given the understood role of Ctip2 in guiding the extension of subcortical axonal projections in cortical development (Arlotta et al., 2005). Interestingly, these pathways appear to be associated with significantly downregulated genes in this dataset. Ctip2 is known to function in either an activating or regulatory capacity, so perhaps these downstream processes are associated with repressive activity.

The top canonical pathway associated with Ctip2 overexpression identified by IPA was the Tec kinase signaling pathway. This signaling pathway has an established immune function: members of the tec family of kinases are involved in leukocyte recruitment (Block and Zarbock, 2012), B-cell development (Horwood et al., 2012), and T-cell activation (August and Ragin, 2012). This finding in IPA also correlates with the high number of gene ontology annotations associated with immune functions that were found with Ctip2 overexpression. It is unclear if it is this pathway specifically that is driving axonal sprouting in post-stroke neurons, as there is not a clearly defined role for this system in neuronal development and function. Further investigation of the specific genes implicated in this pathway (**Figure 5-11**) is required to determine a causal role for this pathway in Ctip2-induced post-stroke axonal sprouting.

For Hhex, there was also a distinct overlap in gene ontology annotations associated with upregulated genes and IPA canonical pathways. In both the gene ontology and pathway analysis, metabolism was a recurring motif. Indeed, **Figure 5-12** highlights the top canonical pathway associated with Hhex overexpression following ischemic stroke: oxidative phosphorylation. The idea that mitochondria play a critical role in neuroplasticity and axonal remodeling is not new. The

development of mitochondrial-targeted therapies for neurodegenerative disorders and brain injury is an active area of research (Cunnane et al., 2020). Mitochondria are highly mobile organelles that have the ability to translocate throughout the cell to compartments critical for axonal wiring for local energy production (Cheng and Mattson, 2010). Additionally, the mechanism of CSPG inhibition of axonal sprouting has been linked to disruption of mitochondrial function (Sainath et al., 2017). Excitingly, there have been a number of studies implicating the sirtuin signaling pathway, one of the top 5 canonical signaling pathways associated with Hhex overexpression, specifically in promoting mitochondrial-mediated neuroprotection and recovery from stroke (He et al., 2020; Liang et al., 2020; Yang et al., 2020). Given this body of evidence, it appears likely that this effect of Hhex overexpression on mitochondrial function is playing an important role in its ability to promote axonal sprouting and functional recovery following cortical stroke.

The eIF2 signaling pathway also presents an interesting target for further exploration of Hhex's mechanism of action in the post-stroke brain. EIF2 signaling has long been understood for its role in the regulation of translation initiation (Haro et al., 1996). Recently, Cagnetta and colleagues (2019) reported a noncanonical modulation of the eIF2 pathway by Sema 3A that induces local translation that in turn phosphorylates eIF2α to initiate local protein translation. These findings suggest a novel pathway for targeted changes in axon translation required for neuronal wiring.

It is possible, even likely, that in the Hhex condition these mitochondrial-associated pathways are working in concert with local translation. Two recent studies identified separate

mechanisms of crosstalk between local translation and mitochondria in neurons (Rossoll and Bassell, 2019). Rangaraju et al. (2019) reported that local translation in neurons is powered by mitochondria, not glycolysis. In neuronal dendrites, mitochondria exist as stable compartments of single or multiple filaments. These localized mitochondria in turn supply local energy for mRNA translation at the synapse. In the same issue, Cioni et al. (2019) reported complementary findings that RNA granules associated with axonal endosomes in retinal ganglion cells. These endosomes in turn colocalize with ribosomes for protein synthesis. Furthermore, these RNA-bearing endosomes pause along mitochondria, creating a site for energy-supplied local translation in the axon. Taken together, these studies demonstrate the targeted interplay of mitochondria, endosomes, and local translation critical for axonal growth and synaptic plasticity. The gene ontology and canonical pathways associated with Hhex overexpression after stroke indicate that this axonal energetic niche may be the key to Hhex's ability to promote axonal growth both in vitro and in the context of ischemic injury.

As indicated above, these findings are preliminary. The study of proposed mechanisms of action for Ctip2 and Hhex overexpression following stroke remains an exciting area to be explored. These initial bioinformatic analyses provide us both with evidence and direction for future studies, hopefully leading to a deeper understanding of the molecular mechanisms associated with cortical development, axonal sprouting, and functional recovery following stroke.

5.5 Figures

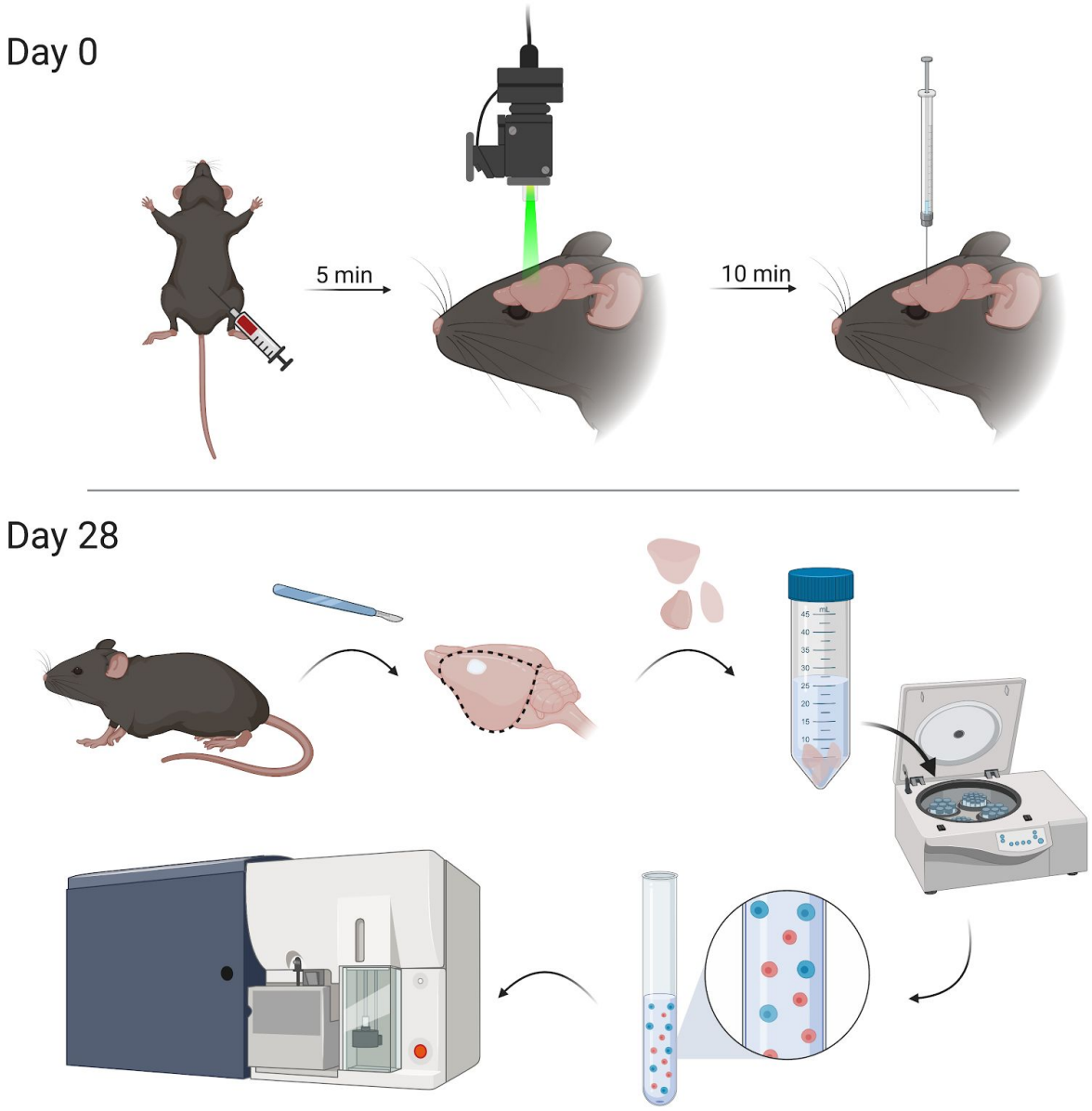

Figure 5-1. Experimental overview. Ai9 mice were subjected to photothrombotic stroke to forelimb motor cortex followed by premotor injection of Cre-expressing lentiviruses overexpressing genes of interest. After 28 days, mice were sacrificed and ipsilesional cortices were dissected from the brain. Tissue samples were dissociated to achieve a single-cell suspension prior to flow cytometry. TdTomato+ neurons were subsequently isolated from the cell suspension via flow cytometry.

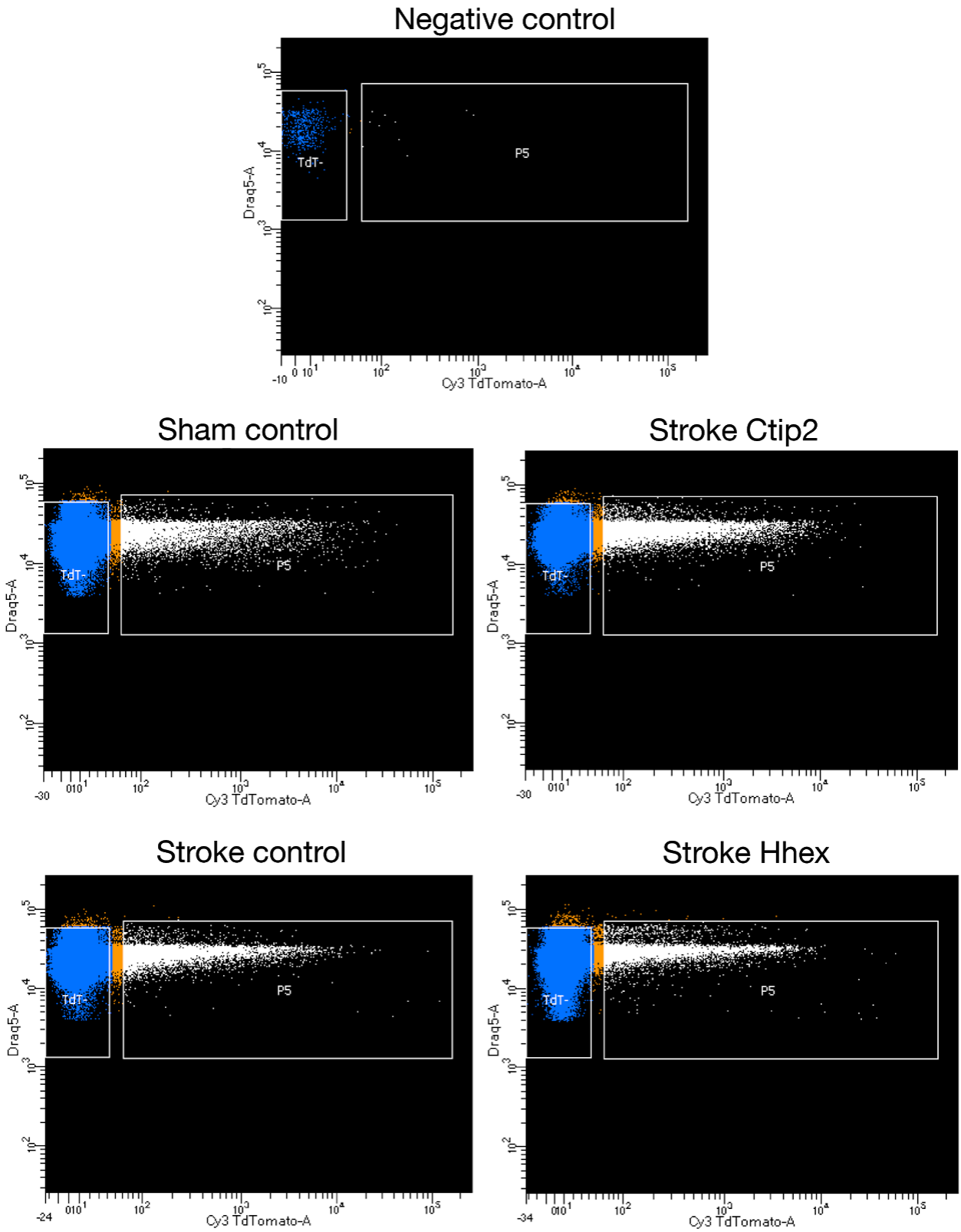

Figure 5-2. FACS of adult cortical neurons. TdTomato+ neurons were collected via FACS, with Cy3 TdTomato and DRAQ5 gates defined by negative control (top).

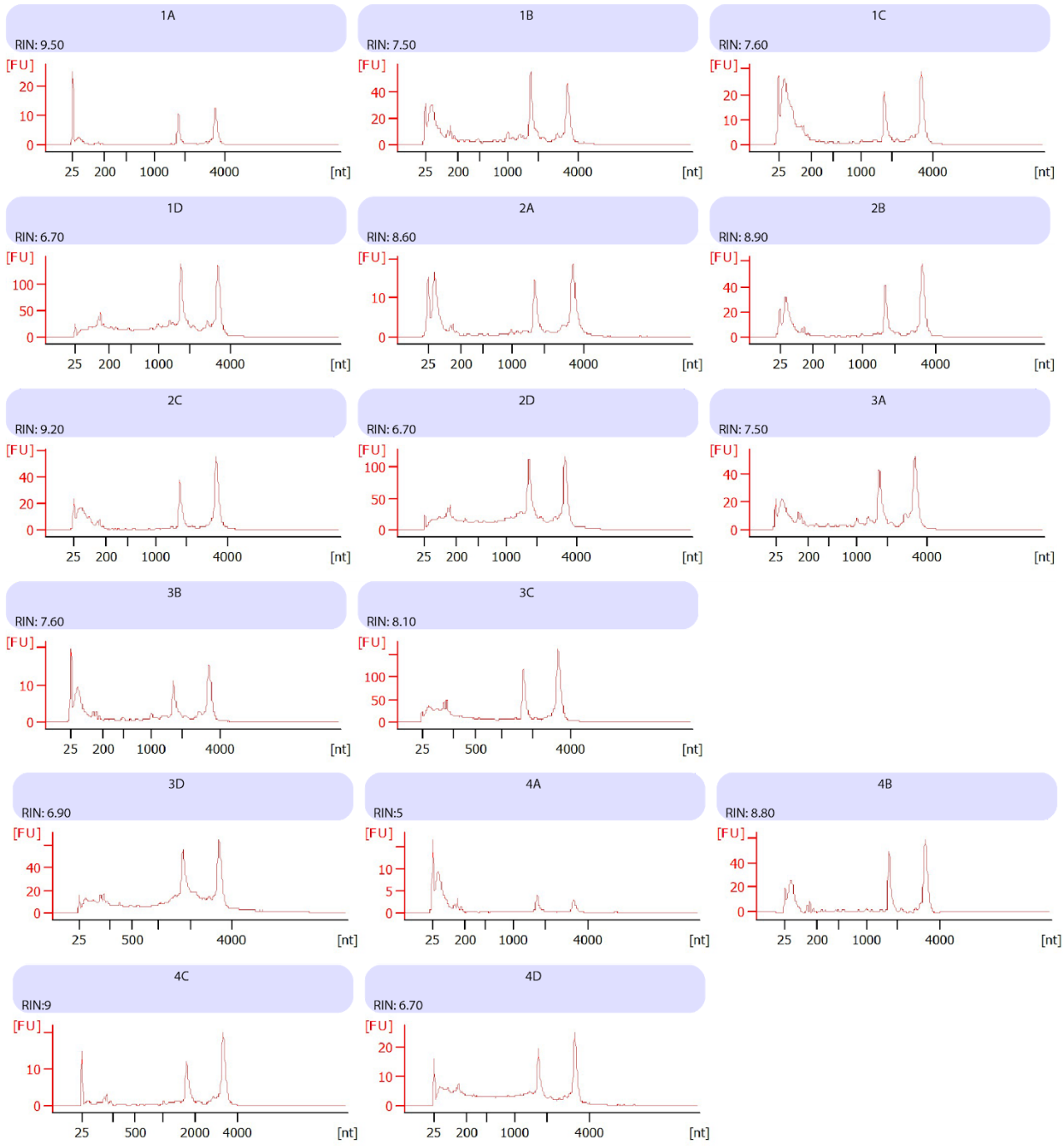

Figure 5-3. RNA quality control analysis. RNA integrity (RIN) values for each FACS sample, measured with Agilent Bioanalyzer 2100.

Multidimensional Scaling

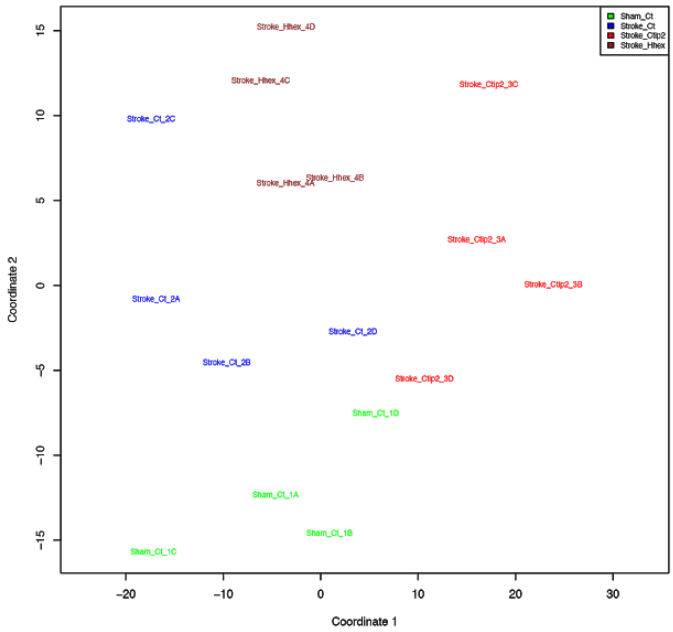

Sample Pearson Correlation

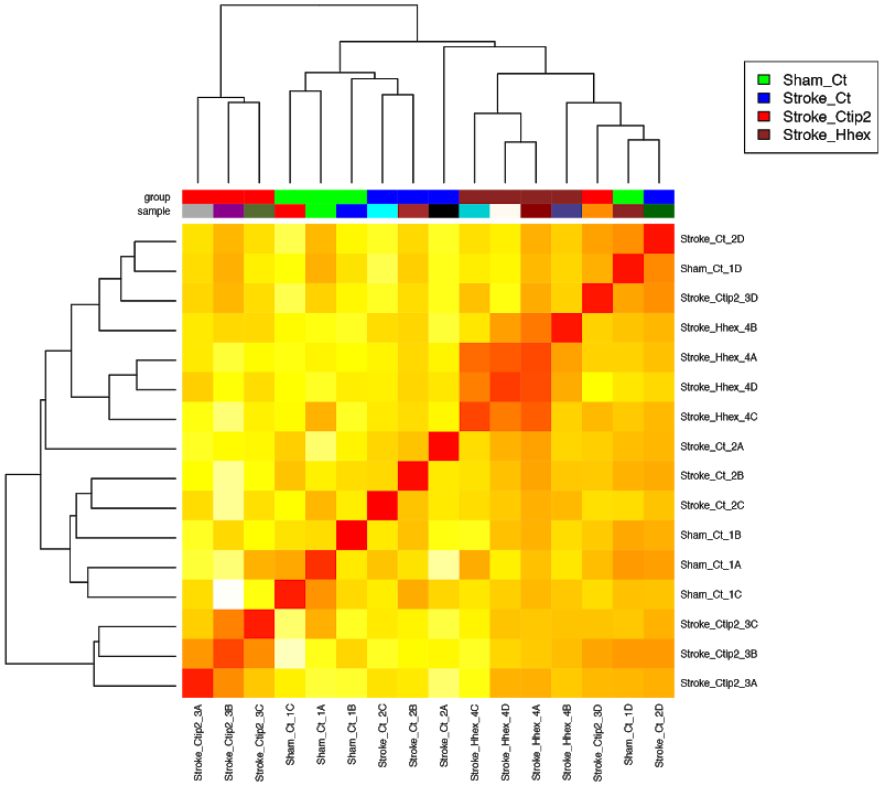

Figure 5-4. Clustering analysis. Expression levels of all genes were used for clustering analysis. Top: Multidimensional scaling is used to detect condition-specific sample relations. Bottom: Batch effect clustering with Pearson correlation metric as a means of identifying relationships between samples.

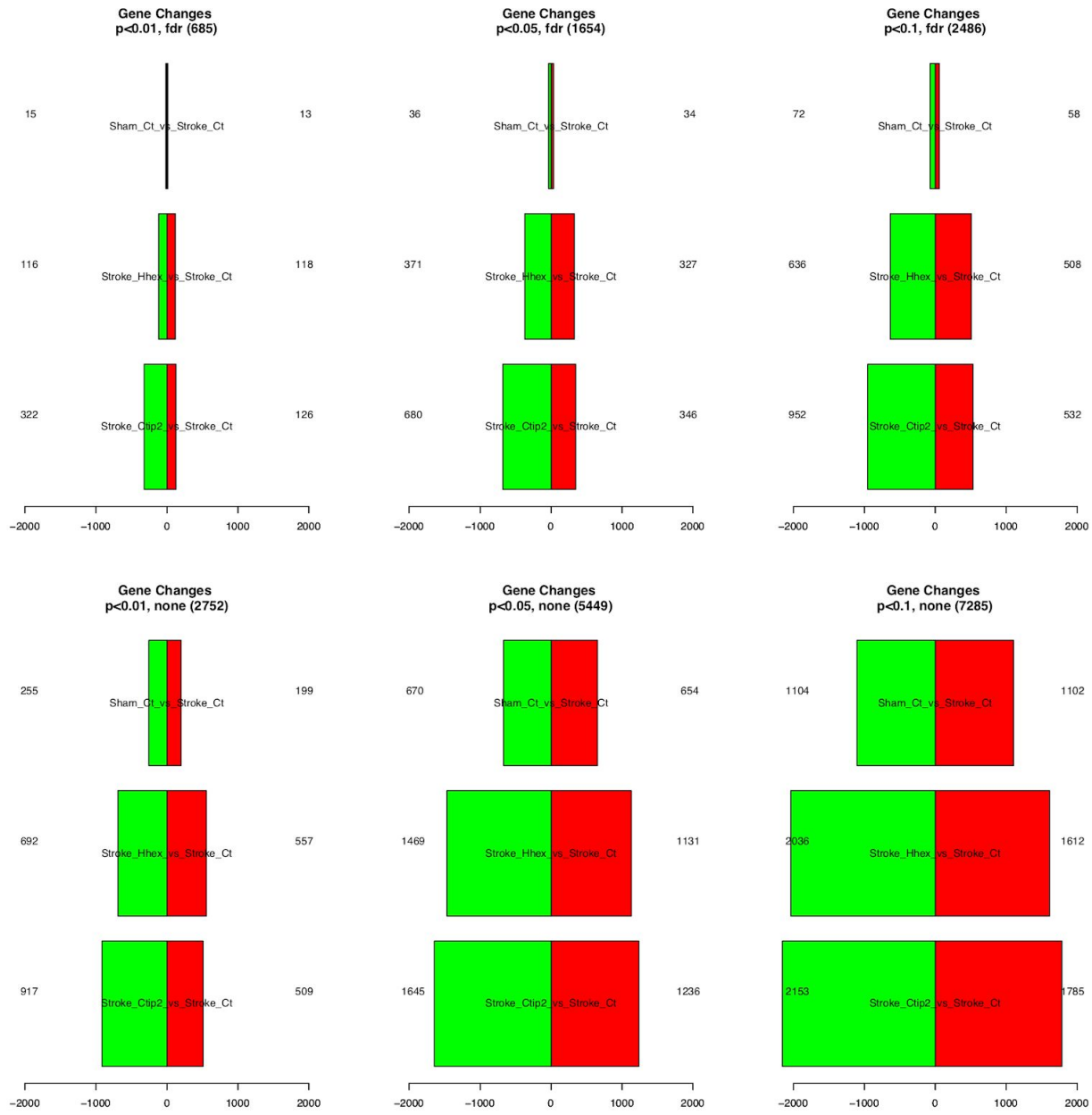

Figure 5-5. Threshold selection for differentially expressed genes using EdgeR. Sham Control, Stroke Ctip2, or Stroke Hhex are compared to Stroke Control. Gene changes are identified by simple p-value ($p < 0.01$, $p < 0.05$, or $p < 0.1$) and FDR (either FDR < 0.05, top; or no FDR, bottom).

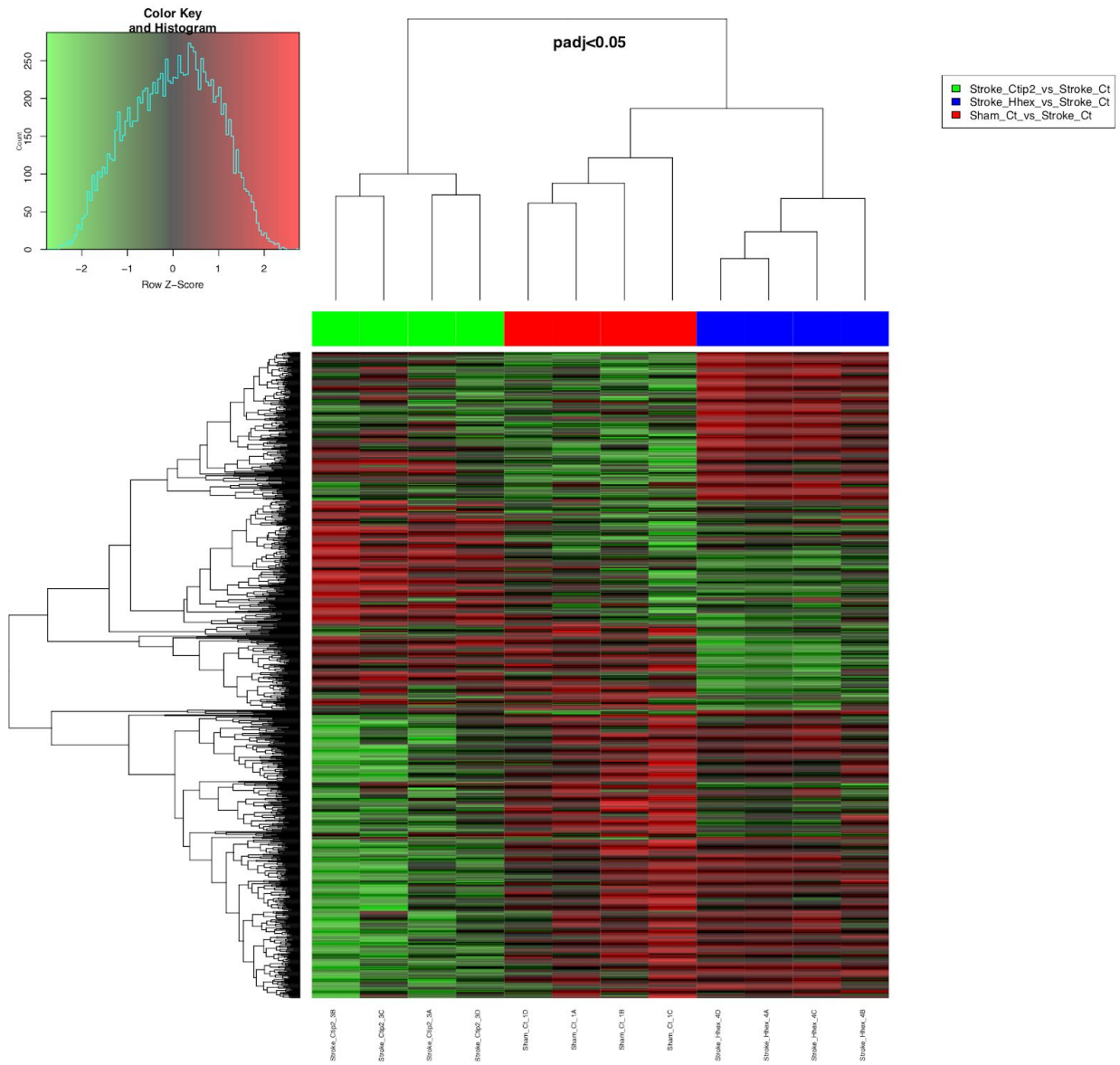

Figure 5-6. Heatmap of top DEG clustering. Clustering analysis based on top differentially expressed genes ($p < 0.05$) was conducted using Bioconductor/EdgeR. Left: Stroke Ctip2 vs. Stroke Control. Middle: Sham Control vs. Stroke Control. Right: Stroke Hhex vs. Stroke Control.

SigDownGene_Stroke_Ctip2_vs_Stroke_Ct_GO_Biological_Process_2018_enrichment.txt

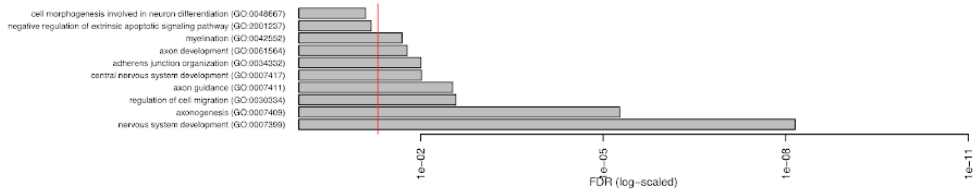

SigDownGene_Stroke_Ctip2_vs_Stroke_Ct_GO_Cellular_Component_2018_enrichment.txt

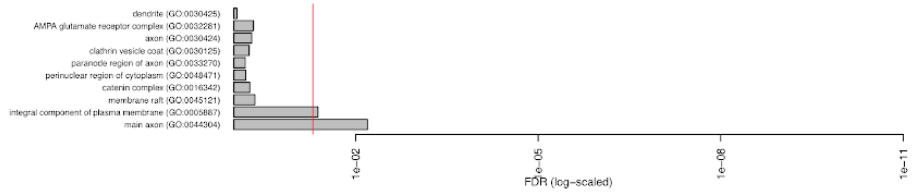

SigDownGene_Stroke_Ctip2_vs_Stroke_Ct_GO_Molecular_Function_2018_enrichment.txt

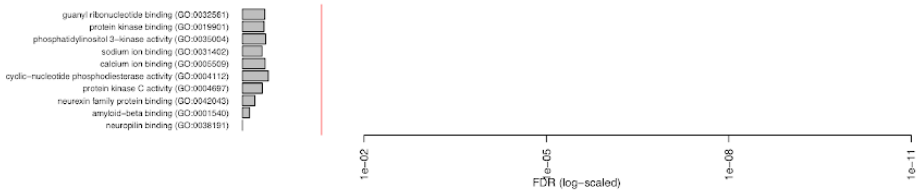

SigUpGene_Stroke_Ctip2_vs_Stroke_Ct_GO_Biological_Process_2018_enrichment.txt

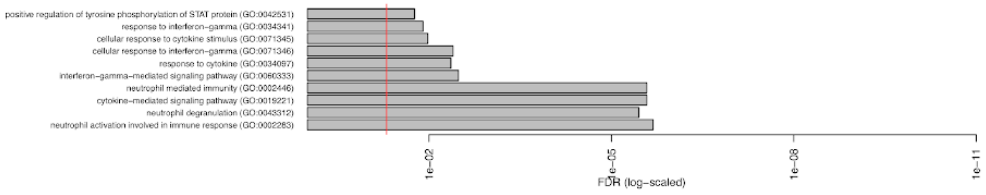

SigUpGene_Stroke_Ctip2_vs_Stroke_Ct_GO_Cellular_Component_2018_enrichment.txt

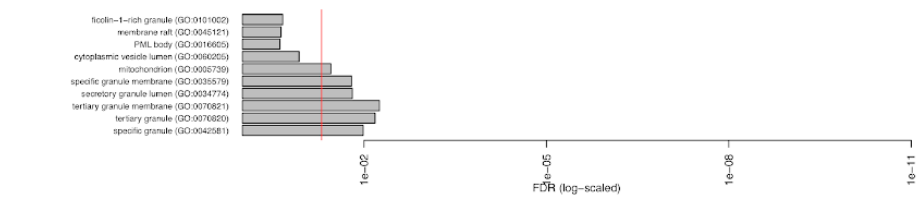

SigUpGene_Stroke_Ctip2_vs_Stroke_Ct_GO_Molecular_Function_2018_enrichment.txt

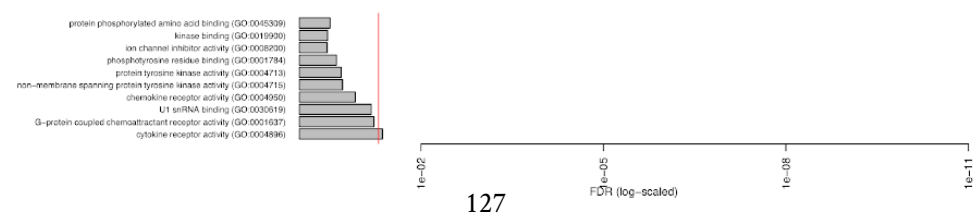

Figure 5-7. EnrichR gene ontology analysis of Stroke Ctip2 vs Stroke Control. Significantly downregulated genes are associated with nervous system development, axonogenesis, regulation of cell growth, myelination, and enrichment in the plasma membrane and main axon. Significantly upregulated genes are primarily associated with immune function and cytokine response. FDR threshold < 0.05.

SigDownGene_Stroke_Hhex_vs_Stroke_Ct_GO_Biological_Process_2018_enrichment.txt

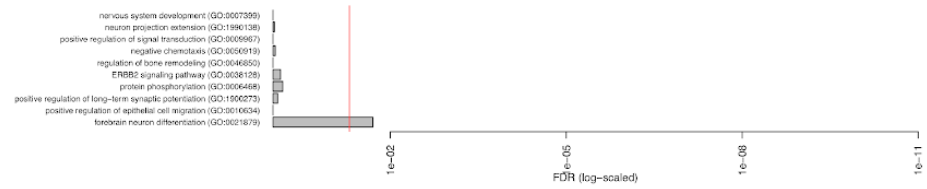

SigDownGene_Stroke_Hhex_vs_Stroke_Ct_GO_Cellular_Component_2018_enrichment.txt

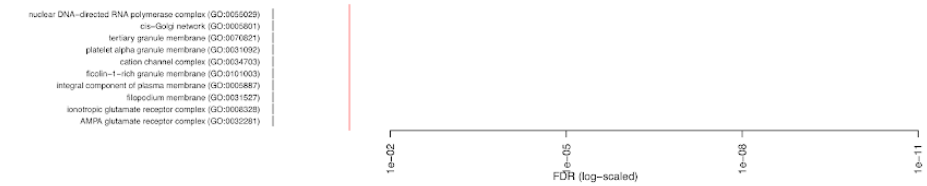

SigDownGene_Stroke_Hhex_vs_Stroke_Ct_GO_Molecular_Function_2018_enrichment.txt

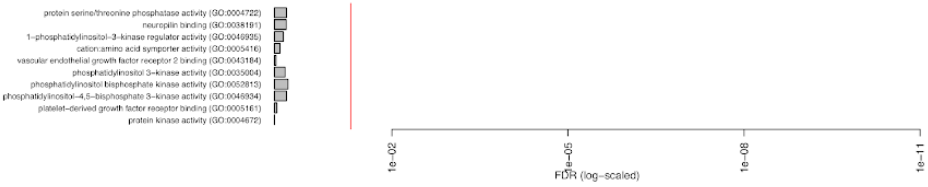

SigUpGene_Stroke_Hhex_vs_Stroke_Ct_GO_Biological_Process_2018_enrichment.txt

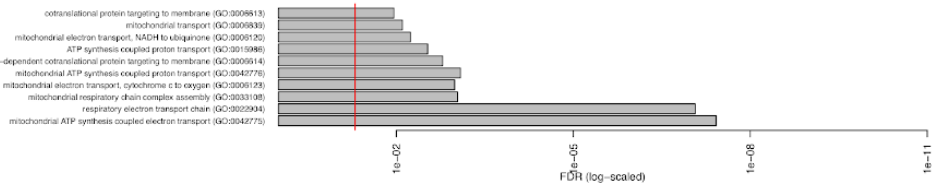

SigUpGene_Stroke_Hhex_vs_Stroke_Ct_GO_Cellular_Component_2018_enrichment.txt

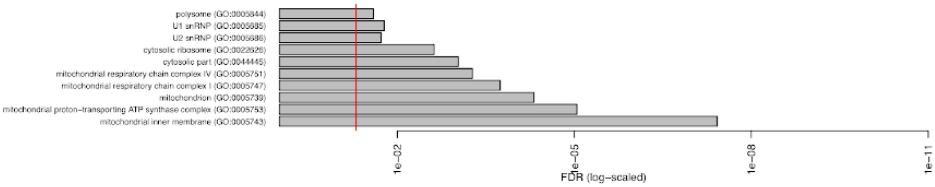

SigUpGene_Stroke_Hhex_vs_Stroke_Ct_GO_Molecular_Function_2018_enrichment.txt

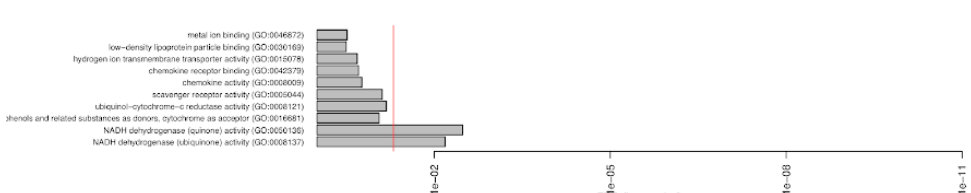

Figure 5-8. EnrichR gene ontology analysis of Stroke Hhex vs Stroke Control. Significantly downregulated genes are associated with forebrain neuron differentiation. Significantly upregulated genes are largely associated with ATP generation, respiration, and mitochondrial function. FDR threshold < 0.05.

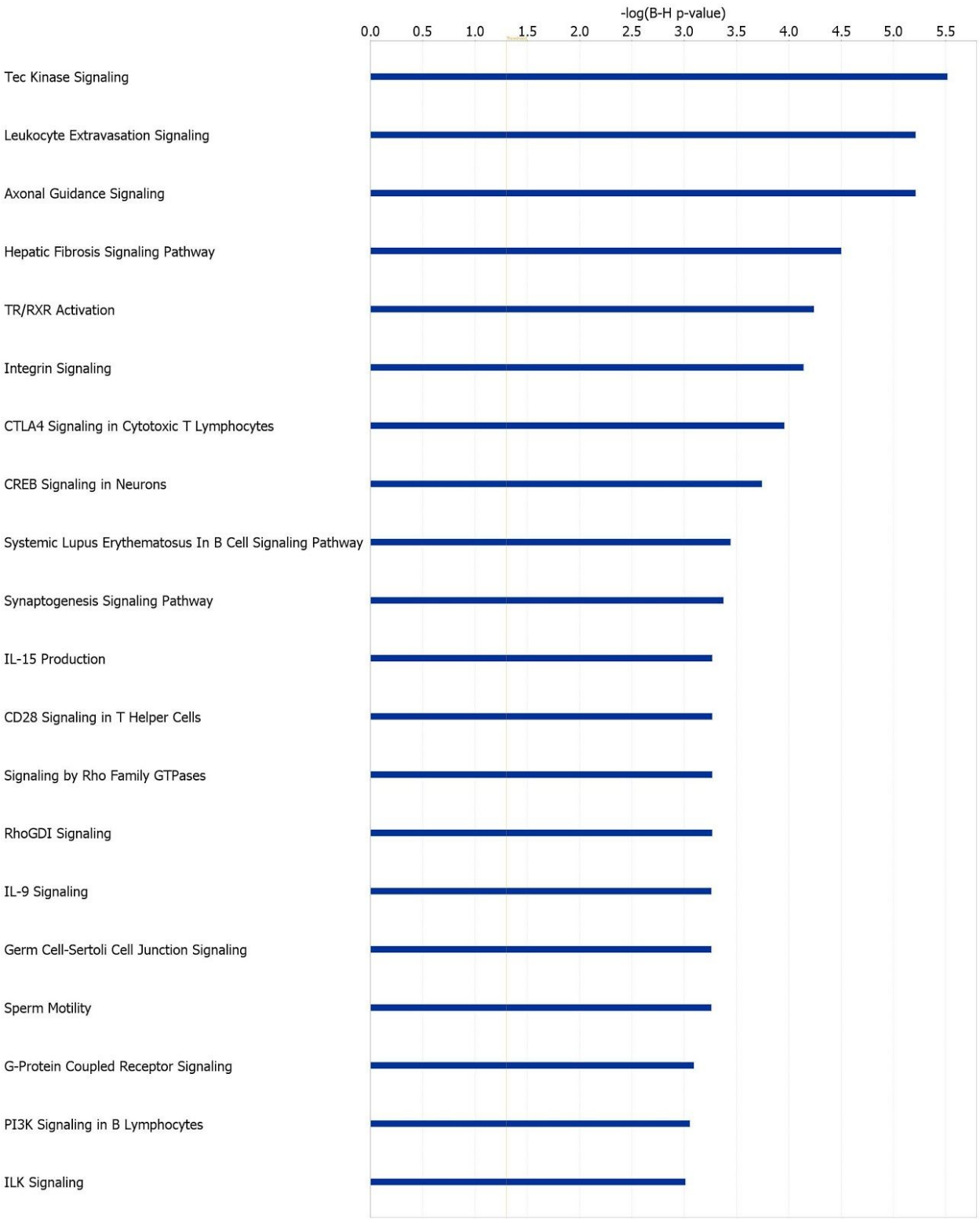

Figure 5-9. IPA top 20 canonical pathways associated with Stroke Ctip2 differentially expressed genes. Stroke Ctip2 vs Stroke Control DEGs with FDR < 0.1, ranking defined by Benjamini

Hochberg adjusted p-values, significance level of $p < 0.05$ indicated by orange line. Generated by Ingenuity Pathway Analysis (Qiagen).

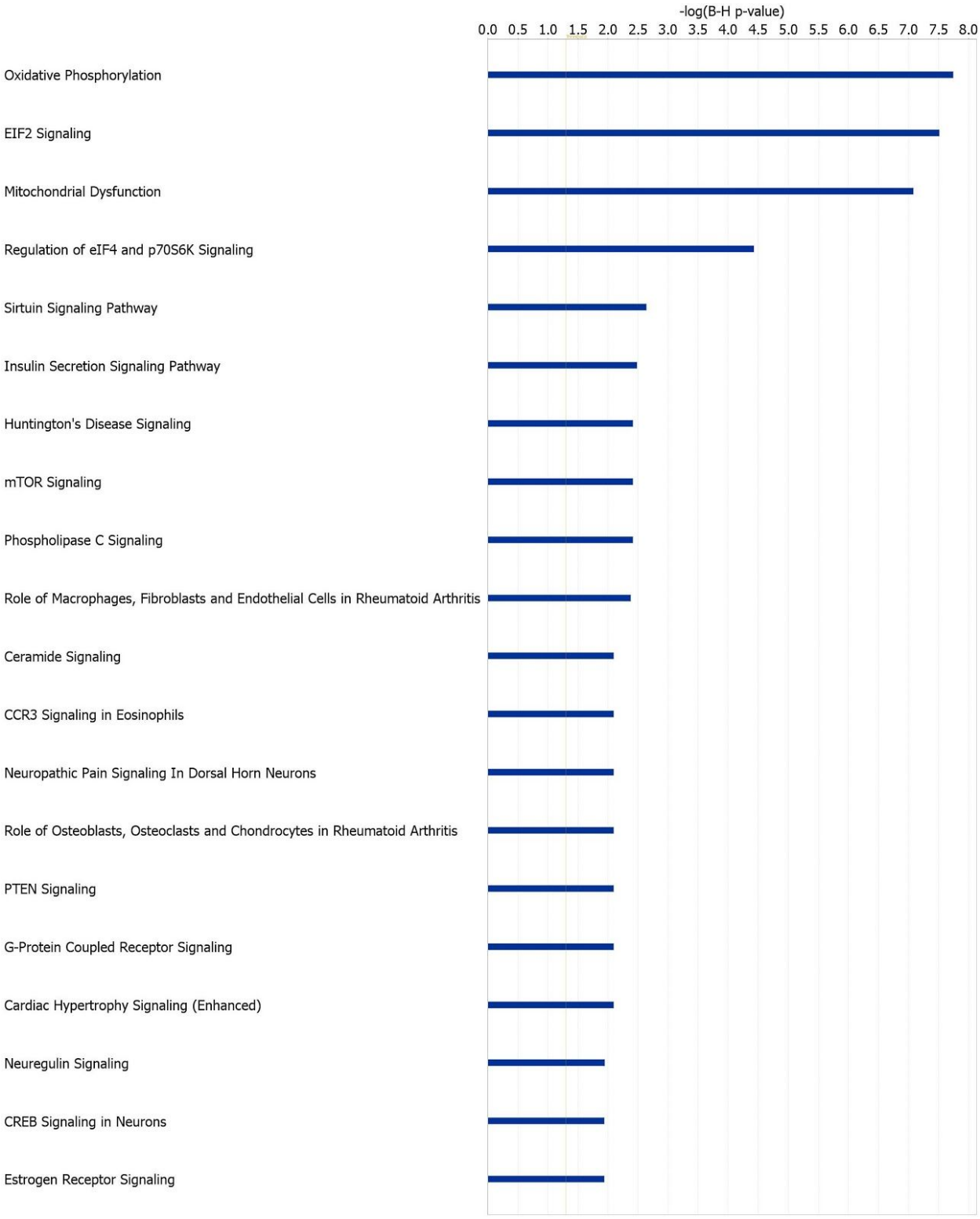

Figure 5-10. IPA top 20 canonical pathways associated with Stroke Hhex differentially expressed genes. Stroke Hhex vs Stroke Control DEGs with FDR < 0.1, ranking defined by Benjamini

Hochberg adjusted p-values, significance level of $p < 0.05$ indicated by orange line. Generated by Ingenuity Pathway Analysis (Qiagen).

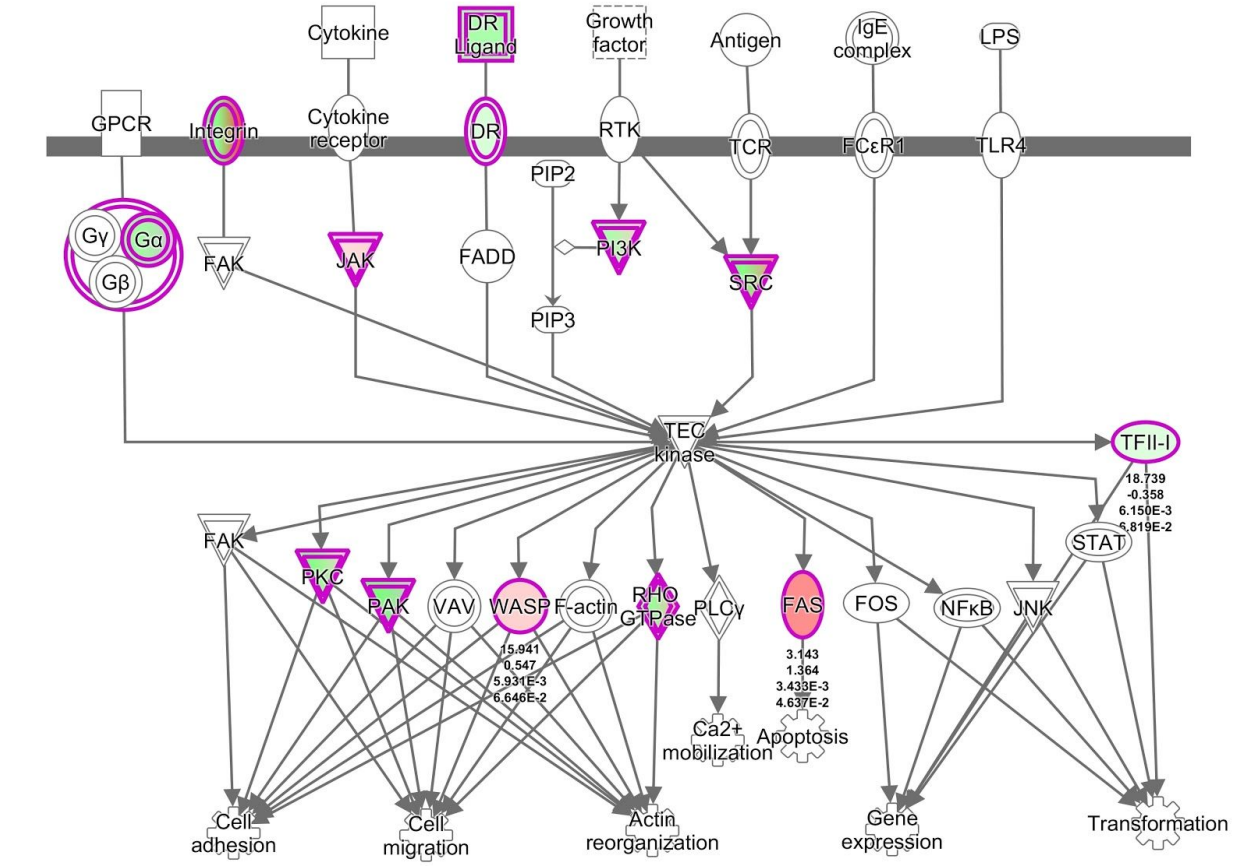

Figure 5-11. Tec Kinase Signaling and Ctip2 transcriptome. The tec kinase signaling pathway is represented above with Ctip2-associated genes highlighted in green or red. Green indicates gene downregulation and red indicates gene upregulation in the Stroke Ctip2 vs Stroke Control transcriptome. FDR > 0.1. Generated by Ingenuity Pathway Analysis (Qiagen).

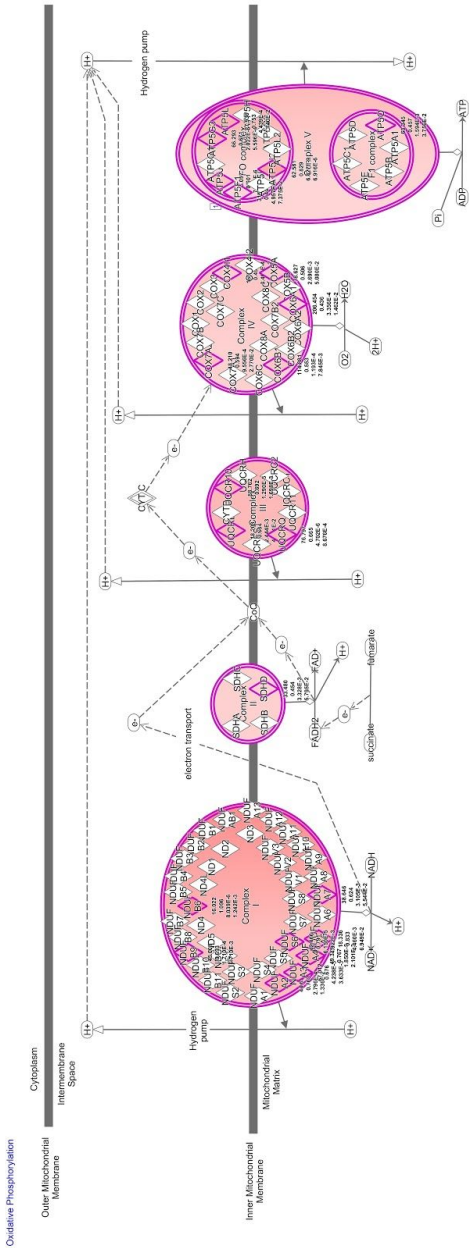

Figure 5-12. Oxidative phosphorylation canonical pathway and Hhex transcriptome. The tec kinase signaling pathway is represented above with Hhex-associated genes highlighted in green or red. Green indicates gene downregulation and red indicates gene upregulation in the Stroke Hhex vs Stroke Control transcriptome. FDR > 0.1. Generated by Ingenuity Pathway Analysis (Qiagen).

info	Number of input reads	Average input read length	Uniquely mapped reads number	Uniquely mapped reads %	Average mapped length	Number of splices: Total	Number of splices: Annotated (sjdb)	Number of splices: GT/AG	Number of splices: GC/AG	Number of splices: AT/AC	Number of splices: Non-canonical	Mismatch rate per base %	Deletion rate per base	Deletion average length	Insertion rate per base	Number of reads mapped to multiple loci	% of reads mapped to multiple loci	Number of reads mapped to too many loci	% of reads unmapped: too many mismatches
Sham_Ct_1A	37324065	150	22187858	59.45%	142.98	3098816	3021530	3037384	30778	2809	27845	0.75%	0.03%	4.09	0.04%	2810232	7.55%	68333	0.00%
Sham_Ct_1B	39313894	150	23627571	60.09%	143.19	2886556	2813801	2829801	26140	2206	28209	0.75%	0.03%	4.04	0.03%	2767317	7.04%	76194	0.00%
Sham_Ct_1C	44392283	150	27555796	62.07%	143.17	3206766	3117746	3137214	34347	2711	32494	0.68%	0.03%	4.04	0.03%	3134785	7.06%	98717	0.00%
Sham_Ct_1D	50575146	150	31156346	61.60%	142.99	3312512	3218269	3233559	33359	2616	58268	0.65%	0.02%	3.26	0.02%	3278221	6.48%	266036	0.00%
Stroke_Ct_2A	42197534	150	25256850	59.85%	142.94	2989854	2902448	2920279	30552	2657	36366	0.70%	0.03%	3.93	0.03%	2919275	6.92%	125020	0.00%
Stroke_Ct_2B	46696369	150	28576664	61.20%	143.11	3712070	3618473	3638344	36531	2995	34200	0.74%	0.03%	3.94	0.03%	3240230	6.94%	85723	0.00%
Stroke_Ct_2C	40595862	150	24933898	61.42%	143.06	3425213	3333359	3354066	32310	2903	35934	0.77%	0.03%	3.93	0.03%	2882869	7.10%	78488	0.00%
Stroke_Ct_2D	45048849	150	27855604	61.83%	143.22	3047308	2932400	2963019	29469	2470	52350	0.66%	0.02%	3.27	0.02%	2868341	6.37%	257688	0.00%
Stroke_Clip2_3A	46542625	150	27853963	59.85%	142.83	3015250	2931441	2947473	30346	2663	34768	0.75%	0.04%	4.19	0.04%	3385740	7.27%	91626	0.00%
Stroke_Clip2_3B	46343522	150	27306856	58.92%	142.52	2703851	2618704	2638964	26858	2728	35301	0.80%	0.04%	4.27	0.04%	3607152	7.78%	80673	0.00%
Stroke_Clip2_3C	38991866	150	23816411	61.08%	143.64	4001708	3922859	3935974	35666	2891	27177	0.69%	0.03%	3.87	0.03%	2864342	7.35%	102076	0.00%
Stroke_Clip2_3D	38862587	150	24614671	63.34%	143.49	2022212	1911706	1944081	22439	1879	53813	0.63%	0.01%	2.58	0.01%	2383142	6.13%	334091	0.00%
Stroke_Hhex_4A	44606973	150	27978277	62.72%	143.32	3988205	3896589	3911065	38879	3860	34401	0.67%	0.03%	4.03	0.03%	3188267	7.15%	101707	0.00%
Stroke_Hhex_4B	43097542	150	25672639	59.57%	143.32	3859351	3777932	3793654	34115	3427	28155	0.72%	0.03%	4.15	0.03%	3130508	7.26%	86683	0.00%
Stroke_Hhex_4C	50397843	150	30681087	60.88%	142.84	3659397	3559101	3579678	37207	3588	38924	0.75%	0.03%	4.12	0.04%	3770844	7.48%	94388	0.00%
Stroke_Hhex_4D	44982891	150	26244009	58.34%	142.58	2460786	2348437	2377604	25498	2603	55081	0.70%	0.03%	3.46	0.03%	2923671	6.50%	255919	0.00%

Table 5-1. Summary of alignments by STAR program.

5.6 References

Anders S, Huber W (2010) Differential expression analysis for sequence count data. Genome Biol 11:R106.

Arlotta P, Molyneaux BJ, Chen J, Inoue J, Kominami R, Macklis JD (2005) Neuronal Subtype-Specific Genes that Control Corticospinal Motor Neuron Development In Vivo. Neuron 45:207–221.

August A, Ragin MJ (2012) Regulation of T-cell Responses and Disease by Tec Kinase Itk. Int Rev Immunol 31:155–165.

Block H, Zarbock A (2012) The Role of the Tec Kinase Bruton's Tyrosine Kinase (Btk) in Leukocyte Recruitment. Int Rev Immunol 31:104–118.

Chen EY, Tan CM, Kou Y, Duan Q, Wang Z, Meirelles GV, Clark NR, Ma'ayan A (2013) Enrichr: interactive and collaborative HTML5 gene list enrichment analysis tool. Bmc Bioinformatics 14:128.

Cheng A, Hou Y, Mattson MP (2010) Mitochondria and neuroplasticity. Asn Neuro 2:e00045.

Cioni J-M, Lin JQ, Holtermann AV, Koppers M, Jakobs MAH, Azizi A, Turner-Bridger B, Shigeoka T, Franze K, Harris WA, Holt CE (2019) Late Endosomes Act as mRNA Translation Platforms and Sustain Mitochondria in Axons. Cell 176:56-72.e15.

Cock PJA, Fields CJ, Goto N, Heuer ML, Rice PM (2010) The Sanger FASTQ file format for sequences with quality scores, and the Solexa/Illumina FASTQ variants. Nucleic Acids Res 38:1767–1771.

Cunnane SC et al. (2020) Brain energy rescue: an emerging therapeutic concept for neurodegenerative disorders of ageing. Nat Rev Drug Discov 19:609–633.

Dobin A, Davis CA, Schlesinger F, Drenkow J, Zaleski C, Jha S, Batut P, Chaisson M, Gingeras TR (2013) STAR: ultrafast universal RNA-seq aligner. Bioinformatics 29:15–21.

Haro CD, Méndez R, Santoyo J (1996) The eIF-2α kinases and the control of protein synthesis1. Faseb J 10:1378–1387.

He W, Wang H, Zhao C, Tian X, Li L, Wang H (2020) Role of liraglutide in brain repair promotion through Sirt1-mediated mitochondrial improvement in stroke. J Cell Physiol 235:2986–3001.

Horwood NJ, Urbaniak AM, Danks L (2012) Tec Family Kinases in Inflammation and Disease. Int Rev Immunol 31:87–103.

Kuleshov MV, Jones MR, Rouillard AD, Fernandez NF, Duan Q, Wang Z, Koplev S, Jenkins SL, Jagodnik KM, Lachmann A, McDermott MG, Monteiro CD, Gundersen GW, Ma'ayan A (2016) Enrichr: a comprehensive gene set enrichment analysis web server 2016 update. Nucleic Acids Res 44:W90–W97.

Li S, Nie EH, Yin Y, Benowitz LI, Tung S, Vinters HV, Bahjat FR, Stenzel-Poore MP, Kawaguchi R, Coppola G, Carmichael ST (2015) GDF10 is a signal for axonal sprouting and functional recovery after stroke. Nature neuroscience 18:1737–1745.

Liang H, Matei N, McBride DW, Xu Y, Tang J, Luo B, Zhang JH (2020) Activation of TGR5 protects blood brain barrier via the BRCA1/Sirt1 pathway after middle cerebral artery occlusion in rats. J Biomed Sci 27:61.

Nie, E. H. (2016). Axonal sprouting in a novel intracortical connection formed upon limb overuse after stroke: a circuit-specific transcriptomic study. *UCLA*. ProQuest ID: Nie_ucla_0031D_14527. Merritt ID: ark:/13030/m5jx32hb. Retrieved from https://escholarship.org/uc/item/9w5976qh

Rangaraju V, Lauterbach M, Schuman EM (2019) Spatially Stable Mitochondrial Compartments Fuel Local Translation during Plasticity. Cell 176:73-84.e15.

Risso D, Ngai J, Speed TP, Dudoit S (2014) Normalization of RNA-seq data using factor analysis of control genes or samples. Nat Biotechnol 32:896–902.

Robinson MD, Oshlack A (2010) A scaling normalization method for differential expression analysis of RNA-seq data. Genome Biol 11:R25.

Rossoll W, Bassell GJ (2019) Crosstalk of Local Translation and Mitochondria: Powering Plasticity in Axons and Dendrites. Neuron 101:204–206.

Sainath R, Ketschek A, Grandi L, Gallo G (2017) CSPGs inhibit axon branching by impairing mitochondria-dependent regulation of actin dynamics and axonal translation. Dev Neurobiol 77:454–473.

Yang X, Zhang Y, Geng K, Yang K, Shao J, Xia W (2020) Sirt3 Protects Against Ischemic Stroke Injury by Regulating HIF-1α/VEGF Signaling and Blood–Brain Barrier Integrity. Cell Mol Neurobiol:1–13.